Aus dem Deutschen Zentrum für Neurodegenerative Erkrankungen (DZNE)



AAV-Mediated Anti-GA Antibody Therapy in C9orf72 ALS/FTD Mouse Models

Dissertation

zum Erwerb des Doktorgrades der Medizin
an der Medizinischen Fakultät der

Ludwig-Maximilians-Universität München

vorgelegt von

Mikołaj Leszek Cygan

aus

Lublin

Jahr

2025

Mit Genehmigung der Medizinischen Fakultät der Ludwig-Maximilians-Universität München

Erster Gutachter: Prof. Dr. Dieter Edbauer

Zweiter Gutachter: Prof. Dr. Dr. Sabine Liebscher

Dritter Gutachter: Prof. Dr. Jochen Herms

Mitbetreuung durch den

promovierten Mitarbeiter: Dr. Qihui Zhou

Dekan: Prof. Dr. med. Thomas Gudermann

Tag der mündlichen Prüfung: 06.10.2025

Abstract

Neurodegenerative diseases present a significant personal and economic challenge within today's aging societies. Unfortunately, curative therapeutic options are largely absent. Amyotrophic lateral sclerosis (ALS) and frontotemporal dementia (FTD) are no exception. Genetic, pathophysiological and clinical parallels of ALS and FTD suggest that they represent two ends of a disease spectrum. C9orf72 mutation is the most common genetic cause of both diseases and is characterized by a massive expansion of a GGGGCC repeat in the non-coding part of this gene. One of the pathophysiological mechanisms of the C9orf72 mutation is the translation of the expanded repeat into dipeptide repeat (DPR) proteins. DPR proteins form aggregates inside neurons that impair neuronal function and may ultimately lead to neurodegeneration. The most abundant DPR protein, poly-GA, likely plays a major role in pathogenesis, because it promotes cytoplasmic mislocalization of TDP-43, a key feature of both sporadic and genetic ALS/FTD. Various therapy approaches have been attempted to tackle the DPR protein aggregation. Use of antibodies against DPR-aggregates is one of the most promising therapy strategies against the C9-ALS/FTD and constitutes the focus of this thesis. I used a monocistronic transgene to express an anti-GA antibody of IgG1 isotype utilizing adeno-associated virus (AAV) inside the CNS to avoid poor delivery of systemically administered antibodies across the blood-brain barrier. In in vitro experiments I was able to show that neuronal AAV 2/9 transduction resulted in expression of functional antibodies. Moreover, the use of monocistronic vector resulted in functional antibody expression as shown by antigen binding. In vivo, the recombinant AAV was injected into the ventricular system of pups on the first postnatal day via ultrasound-guided intracerebroventricular (ICV) injection. The therapy was tested on two poly-GA expressing mouse models. In the fast-progressing GA-Nestin mouse model the rapid weight-loss and the level of poly-GA aggregates were measured at 4 weeks of age. In the less severe GA-Camk2A mouse model memory deficits were examined using the Barnes Maze at 16 weeks of age. Unfortunately, the AAV-mediated anti-GA therapy neither inhibited the weight loss and poly-GA aggregation in GA-Nestin mice nor did it improve Barnes Maze performance of GA-Camk2A mice. These findings suggest that AAV-mediated anti-GA expression could not slow down disease progression in the two poly-GA mouse models. However, different experimental designs, like longer observation period of GA-Nestin or testing of the therapy in a less severe mouse model might show beneficial effects. The vectorized antibody expression system presented in this thesis could also be used to screen other monoclonal antibodies with higher affinity or other antibody isotypes to engage other

effector functions. Thus, these findings provide additional insight to the realm of treatment possibilities in C9-ALS/FTD.

Zusammenfassung (Deutsch)

Neurodegenerative Erkrankungen stellen in den heutigen alternden Gesellschaften eine erhebliche persönliche und wirtschaftliche Herausforderung dar. Weitgehend fehlen leider therapeutische Möglichkeiten. Amyotrophe Lateralsklerose kurative (ALS) Frontotemporale Demenz (FTD) sind dabei keine Genetische, Ausnahmen. pathophysiologische und klinische Überlappungen zwischen ALS und FTD deuten darauf hin, dass sie eigentlich zwei Enden eines Krankheitsspektrums darstellen. Die C9orf72-Mutation ist die häufigste genetische Ursache beider Erkrankungen und zeichnet sich durch eine massive Expansion eines GGGGCC-Repeats im nicht-codierenden Teil dieses Gens aus. Ein wichtiger pathophysiologischer Mechanismus der C9orf72-Mutation ist die Translation des expandierten Repeats in Dipeptid-Repeat (DPR)-Proteine. DPR-Proteine bilden Aggregate in Neuronen, die die neuronale Funktion beeinträchtigen und letztlich zur Neurodegeneration führen können. Das am häufigsten vorkommende DPR-Protein, Poly-GA, spielt wahrscheinlich eine entscheidende Rolle in der Pathogenese, da es eine zytoplasmatische Fehlverteilung von TDP-43 fördert, ein zentrales Merkmal sowohl sporadischer als auch genetischer ALS/FTD. Verschiedene Therapieansätze wurden versucht, um die Aggregation von DPR-Proteinen zu bekämpfen. Der Einsatz von Antikörpern gegen DPR-Aggregate ist eine der vielversprechendsten Therapieansätze gegen C9-ALS/FTD und stellt den Schwerpunkt dieser Arbeit dar. Ich verwendete ein monozistronisches Transgen, um einen Anti-GA-Antikörper des IgG1-Isotyps unter Nutzung von adeno-assoziertem Virus (AAV) im zentralen Nervensystem (ZNS) auszudrücken, um eine schlechte Verteilung systemisch verabreichter Antikörper wegen der Blut-Hirn-Schranke zu vermeiden. In in-vitro Experimenten konnte ich zeigen, dass die neuronale AAV 2/9 Transduktion zur Expression funktionaler Antikörper führte. Darüber hinaus führte der Einsatz des monozistronischen Vektors zur funktionalen Antikörperexpression, was durch Antigenbindung gezeigt wurde. In vivo wurde das rekombinante AAV ersten postnatalen Tag mittels ultraschallgeführter intrazerebroventrikulärer (ICV) Injektion in das Ventrikelsystem von Mäusewelpen injiziert. Die Therapie wurde an zwei Poly-GA-exprimierenden Mausmodellen getestet. Im schnell fortschreitenden GA-Nestin-Mausmodell wurden der schnelle Gewichtsverlust und das Niveau der Poly-GA-Aggregate im Alter von 4 Wochen gemessen. Im weniger schweren GA-Camk2A-Mausmodell wurden Gedächtnisdefizite im Barnes Maze-Test im Alter von 16 Wochen untersucht. Leider verhinderte die AAV-vermittelte Anti-GA-Therapie weder den Gewichtsverlust noch die Poly-GA-Aggregation bei GA-Nestin-Mäusen, noch verbesserte sie die Leistung der GA-Camk2A-Mäuse im Barnes Maze. Diese Ergebnisse deuten darauf hin, dass die AAV-vermittelte Anti-GA-Expression das Fortschreiten der Krankheit in den beiden Poly-GA-Mausmodellen nicht verlangsamen konnte. Allerdings es ist nicht ausgeschloßen, dass andere experimentelle Designs, wie eine längere Beobachtungszeit des GA-Nestin-Modells oder die Prüfung der Therapie in einem weniger belasteten Mausmodell, positive Effekte erzeugen könnte. Das in dieser Arbeit vorgestellte System zur Vektorisierung der Antikörperexpression könnte auch verwendet werden, um andere monoklonale Antikörper mit höherer Affinität oder andere Antikörper-Isotypen mit anderen Effektorfunktionen zu testen. Diese Ergebnisse liefern somit zusätzliche Erkenntnisse über die Behandlungsmöglichkeiten bei C9-ALS/FTD.

Table of Contents

Figure	es	<i>IV</i>
Table	s	<i>v</i>
Abbre	viation	s
1	Introd	uction 8
	1.1	Burden of neurodegenerative diseases8
	1.2	Clinical picture of ALS and FTD8
	1.3	ALS/FTD spectrum disease
	1.4	C9orf72 mutation and C9-ALS/FTD
	1.5	Current therapy strategies against ALS/FTD
	1.6	Adeno-associated virus – a vector for genetic therapy15
	1.7	Established AAV-based drugs
2	Research question	
3	Metho	ods22
	3.1	The study design
	3.2	Therapeutic rAAV – transgene cassette design
	3.3	Animal models and <i>in vivo</i> therapy testing design23
	3.4	Material
	3.5	In house AAV packaging32
	3.6	Antibody visualization after AAV transduction and expression in cell culture 33
	3.7	Visualization of antibody-DPR complexes in immunoblot34
	3.8	Intracerebroventricular AAV injection36
	3.9	Standardized mouse scoring
	3.10	Tissue collection
	3.11	Staining of animal sections

	3.12	ELISA44		
	3.13	Barnes maze45		
	3.14	Genotyping47		
4	Result	s 49		
	4.1	AAV-transduced primary rat neurons expressed functional anti-GA and anti-PR		
	antibo	dies		
	4.2	AAV injection in newborn pups led to widespread transgene expression in the		
	nervou	ıs system54		
	4.3	Antibody expression was exclusive to neurons using the hSynapsin promoter 55		
	4.4	GA-Nestin therapy – study design57		
	4.5	Slower rate of weight gain of GA-Nes⁺ was not mitigated by the AAV-mediated		
	anti-G	A antibody therapy58		
	4.6	Antibody expression after ICV AAV injection was the most profound for anti-GA in		
	the forebrain			
	4.7	The AAV-mediated anti-GA therapy did not reduce neurodegeneration and		
	inflam	mation in the hippocampus of GA-Nestin mice60		
	4.8	The AAV-mediated anti-GA antibody therapy did not reduce poly-GA levels in GA-		
	Nestin	mice		
	4.9	Anti-GA expressing GA-Nestin mice showed no signs of muscle denervation at 4		
	weeks of age			
	4.10	Study design in the GA-Camk2A mouse model		
	4.11	The therapy did not attenuate memory impairment in GA-Camk2A67		
5	Discussion			
	5.1	The AAV system allows for successful antibody expression in neurons70		
	5.2	Rationale for AAV-mediated anti-GA therapy70		
	5.3	Potential reasons for lack of therapeutical effect		
	5.4	Possible improvements and follow-up experiments:		
	5.5	Choice of the mouse model		

	5.6	AAV-mediated anti-DPR antibody therapy compared to ASO therapy	. 76
	5.7	Outlook for AAV-mediated antibody therapy in C9-ALS/FTD and final words	. 78
6	Refer	ences	80
Ackno	wledge	ements	96
Affida	ıvit		97
Confir	mation	of congruency	98
Public	ations.		99

Figures

Figure 1: Three mechanisms responsible for C9-ALS/FTD pathology
Figure 2: Schematic representation of AAV genome for wildtype and recombinant AAV 1
Figure 3: Genetic therapy with use of rAAV vector – transduction on cellular level
Figure 4: AAV transgene cassette used for the AAV-mediated anti-GA antibody therapy 23
Figure 5: Mouse breeding for experiments and CRE-Recombinase system23
Figure 6: rAAV production by HEK293 triple transfection
Figure 7: Visualization of antibody-DPR complexes in immunoblot
Figure 8: Setup and ultrasound images from the ultrasound-guided ICV injection38
Figure 9: Filled ventricular system after ICV injection with dyed solution38
Figure 10: Sample collection from GA-Nestin
Figure 11: Automated quantification of the poly-GA aggregates from the green channel o
immunofluorescent nervous tissue stains
Figure 12:Barnes maze setup40
Figure 13: Example of genotyping done for GA-Nestin and GA-Camk2A mice48
Figure 14: Immunofluorescent stains of primary rat neurons transduced with AAV 2/DJ
showed antibody expression50
Figure 15: Immunoblots: anti-GA and anti-PR antibodies secreted from AAV2/DJ8 transduced
neurons bound to corresponding DPRs5
Figure 16: Immunofluorescent stains of primary rat neurons transduced with AAV 2/9 revealed
antibody expression52
Figure 17: Immunoblots: anti-GA and anti-PR antibodies secreted from AAV 2/9 transduced
neurons bound to corresponding DPRs53
Figure 18: Immunohistochemistry stains of Cre-GFP in brains and spinal cords of 21-days old
C57/BL6 mice after AAV injections done 1 and 3 days after birth55
Figure 19:Anti-GA and anti-PR antibodies were expressed exclusively in neurons after AAV
2/9 ICV injection
Figure 20: Experimental design for AAV therapy in GA-Nestin mouse line5
Figure 21: AAV-mediated antibody therapy did not prevent weight loss in GA-Nestin mice 59
Figure 22: Antibody expression in different brain regions measured by ELISA60
Figure 23: Neurodegeneration, poly-GA aggregation, and inflammation were not reduced by
AAV-mediated anti-GA antibody expression.

Figure 24: Poly-GA aggregation was not reduced by neonatal antibody expression in 4-w	reek-
old GA-Nestin mice	64
Figure 25: GA-Nestin mice did not show muscle denervation at 4 weeks of age	65
Figure 26: Experimental design for GA-Camk2A	67
$Figure\ 27:\ Barnes\ maze:\ 4\text{-}day\ learning\ period\ and\ 5^{th}\ day\ measurements-anti-GA\ antillar anti-GA\ antillar anti-GA$	body
therapy did not improve GA-Camk2A's cognitive function	69
Tables	
Table 1: PCR setup for genotyping	47
Table 2: Experimental groups in GA-Nestin mouse line experiments	57
Table 3: Experimental groups in GA-Camk2A mouse line experiments	66

Abbreviations

(r)AAV	(recombinant) Adeno-associated virus
ALS	Amyotrophic lateral sclerosis
ASO	Antisense oligonucleotide
BAC	Bacterial artificial chromosome
BB	Blocking buffer
BBB	Blood-brain barrier
BCA	Bicinchoninic acid
BSA	Bovine Serum Albumin
bvFTD	Behavioural variant frontotemporal dementia
CA	Cornu ammonis
CMV	Cytomegalovirus
CNS	Central nervous system
CSF	Cerebrospinal fluid
DPR	Dipeptide-repeat
DTT	Dithiothreitol
ECL	Enhanced chemiluminescence solution
EDTA	Ethylenediaminetetraacetic acid
ELISA	enzyme-linked immunosorbent assay
FCS	Fetal Calf Serum
FTD	Frontotemporal dementia
GFP	Green fluorescent protein
GST	Glutathione S-Transferase
HE	Hematoxylin-eosin
ICV	intracerebroventricular
IgG	Immunoglobulin G
ITR	Inverted terminal repeat
L2K	Lipofectamine 2000
LMN	Lower motor neuron
LPL	Lipoprotein lipase
	•

LPLD	Lipoprotein lipase deficiency
MEM	Minimum Essential Medium
MND	Motor neuron disease
NBM	Neurobasal medium
NMJ	neuromuscular junction
P1	Postnatal day 1
PBS	Phosphate Buffered Saline
PCR	Polymerase chain reaction
PFA	Paraformaldehyde
PPA	Primary progressive aphasia
PVDF	Polyvinylidene fluoride
RAN	Repeat associated non-ATG
SMA	Spinal muscular atrophy
SMN1	Survival motor neuron 1
ssDNA	Single stranded DNA
TDP-43	Transactive response DNA binding protein-43
TMB	3,3',5,5'-Tetramethylbenzidine Liquid Substrate
TUDCA	Tauroursodeoxycholic acid
UMN	Upper motor neuron
VA RNA	virus-associated RNA

1 Introduction

1.1 Burden of neurodegenerative diseases

Neurodegenerative diseases such as Alzheimer's disease, Parkinson's disease, amyotrophic lateral sclerosis and frontotemporal dementia start in different cell types and brain regions and lead to progressive impairment of cognitive and/or motor domains. Since age is a very important risk factor for neurodegenerative diseases, their prevalence continually rises in the aging population of today (Checkoway et al., 2011). Recent strides in research have yielded groundbreaking therapies, such as two recently approved antibody drugs targeting β -amyloid plaques in Alzheimer's disease (Dhillon, 2021; Hoy, 2023). This achievement has ignited a profound sense of optimism, particularly for antibody-based therapy. Nevertheless, for the vast majority of patients suffering from neurodegenerative disorders no curative therapy is attainable. That is why, it is crucial to urgently conduct research aiming at finding novel therapy approaches to attenuate the burden of these debilitating diseases.

1.2 Clinical picture of ALS and FTD

Amyotrophic lateral sclerosis (ALS) and frontotemporal dementia (FTD) are two insidious neurodegenerative diseases. Like all neurodegenerative diseases they are characterized by progressive functional impairment and eventual death of affected neuron populations.

ALS is the most common motor neuron disease (MND) (Tiryaki & Horak, 2014). Disorders among this group are classified according to the degree of upper and lower motor neuron damage (Statland et al., 2015). In contrast to other MNDs like spinal muscular atrophy or primary lateral sclerosis, where either upper (UMN) or lower motor neurons (LMN) of the pyramidal pathway are affected, ALS is defined by simultaneous degeneration of both of these types of neurons (Shababi et al., 2014; Statland et al., 2015). UMN pathology commonly presents itself with spasticity and hyperreflexia, whereas LMN pathology leads to fasciculations and muscle atrophy (Brotman et al., 2022). Degeneration in upper and lower motor neurons typically observed in ALS patients leads to a complex clinical manifestation which combines symptoms typical for UMN and LMN disease.

Depending on the symptoms at early stage of the disease ALS is categorized into limb-onset and bulbar-onset forms. In the limb-onset ALS, muscle weakness and atrophy of limbs can be observed, which may be preceded by fasciculations, cramps and substantial weight loss

(Masrori & Van Damme, 2020). In the slightly less prevalent bulbar-onset form the symptoms include spastic or flaccid dysarthria, enhanced gag and jaw reflexes, tongue wasting, facial weakness and facial fasciculations (Kiernan et al., 2011). Limb wasting and other symptoms rather associated with limb-onset ALS develop as the disease progresses (Zarei et al., 2015). In advanced stages of both types of ALS dysphagia leading to pathological weight loss and severely decreased body endurance set in (Brent et al., 2020; Ramirez et al., 2008). The progression of ALS is rapid, with 50% of patients dying within 3 years of onset (Mitchell & Borasio, 2007). The cause of death is usually associated with respiratory failure often augmented by respiratory infection (Lyall et al., 2001; Sorenson et al., 2007). Reported incidence rate of ALS ranges from 0.6 and 3.8 per 100 000 person-years, while the prevalence rate ranges from 4.1 to 8.4 in 100 000 (Longinetti & Fang, 2019). About 5 % of ALS cases are familial and follow the pattern of mendelian inheritance (Byrne et al., 2011). The most common, known genetic mutations responsible for familial ALS are C9orf72, SOD1, TARDBP and FUS mutations with variable prevalence in different ethnical groups (Kwiatkowski et al., 2009; Mathis et al., 2019; Renton et al., 2011; Rosen et al., 1993; Sreedharan et al., 2008). In FTD the neurodegeneration afflicts cognitive function. Unlike in ALS, where motor neurons are primarily affected, in FTD the neurons of frontal and temporal lobe degenerate. There are two types of FTD: behavioural variant FTD (bvFTD) and slightly less common form – primary progressive aphasia (PPA) (Kirshner, 2014; Onyike & Diehl-Schmid, 2013). In case of bvFTD patients experience change in personality and stop complying to social norms. Characteristic for bvFTD are disinhibition, apathy, compulsive behaviours, hyperorality and a dysexecutive neuropsychological profile (Rascovsky et al., 2011). On the other hand, PPA is characterized by isolated progressive impairment of language function which includes word-finding trouble, dissolution of grammatical structure and problems with comprehension of language (Mesulam, 2001). Depending on the extent of these symptoms, PPA can be further categorized into: logopenic, nonfluent/agrammatic and semantic variants (Gorno-Tempini et al., 2011). Language deficit remains the primary impairment throughout the progression of PPA, while in some patients cognitive and behavioural anomalies develop as the disease progresses (Mesulam et al., 2014).

FTD stands out among other types of dementia with its relatively early onset with usual age of onset between 45 and 65 years of age (Khan & De Jesus, 2022). It is estimated to be either second or third most common type of dementia (with Alzheimer's disease and according to some studies vascular dementia being ranked above it) among patients younger than 65 years of age (Vieira et al., 2013). Incidence rate of FTD lies between 1.6 and 4.1 per 100 000 person-

years (Olney et al., 2017). Its prevalence is estimated to be between 15 and 22 per 100 000 persons (Onyike & Diehl-Schmid, 2013). 20 to 50 % of FTD cases are familial (Olszewska et al., 2016). The most common genetic mutations responsible for these cases are C9orf72, MAPT and GRN, with C9orf72 being the most common and accounting for 25% of familial cases in people of European descent (Olszewska et al., 2016).

1.3 ALS/FTD spectrum disease

ALS and FTD have a strong genetic, pathophysiological and clinical overlap. Often patients develop symptoms typical for both ALS and FTD. More than 10 % of FTD patients have ALS comorbidity and about 30% show mild symptoms of MND such as fasciculations, wasting and weakness (Burrell et al., 2011; Lomen-Hoerth et al., 2002). Among patients primarily suffering from ALS, comorbid FTD can be diagnosed in approximately 30% of cases. (Lomen-Hoerth et al., 2002). It has been shown that mutations of some genes can lead to either ALS or FTD. The most common of these genes are: C9orf72, SQSTM1, VCP, TBK1, CHCHD10, TDP-43, (Abramzon et al., 2020). On the cellular level ALS and FTD share a characteristic hallmark, which is formation of cytoplasmic aggregates containing Transactive response DNA binding protein-43 (TDP-43) (Neumann et al., 2006). Misfolded TDP-43 protein aggregates can be found in about 95% of ALS and 45% FTD patients (Cairns et al., 2007; Smethurst et al., 2020). Physiologically TDP-43 is found mainly in cell nucleus (Winton et al., 2008). It plays an important role in nuclear transport, regulation of splicing and monitoring of the stability of RNA (Scotter et al., 2015). In ALS and FTD the abnormally phosphorylated and aggregated TDP-43 is found mainly in the cytoplasm of affected neurons and the extent of its aggregation correlates with the extent of neurodegeneration (Afroz et al., 2017).

These genetic, pathophysiological and clinical parallels have recently led to a consensus that ALS and FTD can be seen as opposite ends of a spectrum of one underlying disease (McCauley & Baloh, 2019; Van Langenhove et al., 2012). The most common single-gene mutation responsible for both ALS and FTD is C9orf72 gene mutation.

It is common to refer to the ALS/FTD spectrum disease caused by an expansion mutation in the C9orf72 gene as *C9-ALS/FTD*. The same terminology has been adopted in this thesis.

1.4 C9orf72 mutation and C9-ALS/FTD

The C9orf72 protein is encoded by a gene of the same name located on the short arm of chromosome 9 in the open reading frame 72 (DeJesus-Hernandez et al., 2011). Physiologically,

C9orf72 protein plays an important role in autophagy and lysosome homeostasis (Shao et al., 2020; Webster et al., 2016).

As firstly reported by DeJesus-Hernandez (2011) a repeat expansion mutation of a noncoding hexanucleotide GGGGCC in *C9orf72* gene is responsible for C9-ALS/FTD. The mutation is localized in the first intron of the *C9orf72* gene (Renton et al., 2011). It is responsible for about every fifth familial ALS and about every tenth familial FTD case, making it the most common mutation from all known ALS/FTD causing genes (DeJesus-Hernandez et al., 2011). While a healthy individual carries from 0 to 23 repeats of GGGGCC in *C9orf72* gene, a C9-ALS/FTD patient typically carries several hundred to several thousand repeats (DeJesus-Hernandez et al., 2011; Renton et al., 2011). The prevalence of the *C9orf72* mutation varies greatly between regions arguing for a founder effect, which is also supported by a common haplotype in expansion carriers. While it is the most common ALS/FTD cause in Europe and America, it is relatively rare in Asia and Middle East (Majounie et al., 2012).

Three pathomechanisms have been proposed for *C9orf72* ALS/FTD and synergistic effects are likely. Firstly, sense and antisense transcripts from the *C9orf72* repeat form RNA foci, which appear to be toxic through sequestration of RNA binding proteins and disruption of RNA processing (Lee et al., 2013). Therapy approaches targeting RNA transcripts successfully mitigate RNA toxicity and halt neurodegeneration in cell culture and in mice (Donnelly et al., 2013; Jiang et al., 2016; Sareen et al., 2013).

Secondly, sense and antisense transcripts are translated into aggregating Dipeptide Repeat (DPR) proteins: poly-GA, -GP, -GR, -PA, and -PR (Ash et al., 2013; Mori et al., 2013; Zu et al., 2013) by a non-canonical mechanism. It occurs although the repeat expansion in C9orf72 is intronic and does not contain the ATG start codon. Nevertheless, harpin-formations of long repeat sequences seem to support the initiation of translation in a mechanism known as repeat associated non-ATG (RAN) translation (Zu et al., 2011). RAN translation plays a critical role in pathophysiology of other diseases, like Huntington disease, where CAGCTG expansion mutation is found on Huntingtin gene (Bañez-Coronel et al., 2015). The DPR proteins in C9-ALS/FTD form neuronal cytoplasmic inclusions are positive for ubiquitin and ubiquitin-binding proteins but usually negative for TDP-43 (Al-Sarraj et al., 2011; Bieniek et al., 2013; Mori et al., 2013). In cells, which express DPR proteins, cytoplasmic mislocalization of TDP-43 – a hallmark of ALS/FTD, can be observed (Ryan et al., 2022). Among all DPR proteins, poly-GA is the most prevalent in C9-ALS/FTD patients, appearing about 2,5 times more often than the second most common poly-GP (Mackenzie et al., 2015). The relative toxicity of DPR proteins is still under debate. Individually expressed, only poly-GA forms abundant

cytoplasmic inclusions (May et al., 2014), while synthetic poly-GR and poly-PR typically accumulate in the nucleolus and inhibit translation (Hartmann et al., 2018; Zhang et al., 2018). At least one study suggests that poly-GA is the most toxic of all DPR proteins in vivo (Lee et al., 2017). Schludi et al (2017) showed that mice expressing codon-modified poly-GA develop motor deficits and inflammation in the nervous system. Moreover, presence of poly-GA aggregates has led to formation of phosphorylated TDP-43 in these mice (Schludi et al., 2017). This suggests that the presence of this DPR alone is sufficient to induce neurodegeneration. Furthermore, it has been demonstrated that poly-GA aggregates sequester physiological proteins involved in proteasomal degradation and nucleocytoplasmic transport (Guo et al., 2018; Zhang et al., 2016). Poly-GA also inhibits transport of TDP-43 into the nucleus leading to cytoplasmic TDP-43 mislocalization and aggregation (Khosravi et al., 2017). While poly-GA plays a notable role in C9orf72 pathogenesis, it is important to point out that other dipeptide repeat proteins, particularly the arginine-rich ones: poly-GR and poly-PR, are also considered to be neurotoxic (Kwon et al., 2014; Lee et al., 2017; Mizielinska et al., 2014). The high toxicity of arginine rich DPRs is correlated with their tendency to undergo liquid-liquid phase separation (Boeynaems et al., 2017), a process linked to formation of membrane-less organelles, like nucleoli, in eucaryotic cells. Interaction with poly-GR/PR alters phase separation properties of other proteins and impairs formation of membrane-less organelles. Finally, the third postulated mechanism responsible for C9-ALS/FTD is reduced expression of C9orf72 protein, because the $(G_4C_2)_n$ repeat expansion inhibits expression of the mutant allele. Reduced C9orf72 expression in human induced motor neurons triggered neurodegeneration by insufficient clearance of the DPR proteins, which links the previously described mechanisms with the C9orf72 haploinsufficiency (Shi et al., 2018). Shi (2018) shows that restoration of physiological C9orf72 protein level mitigates neurodegeneration in patient induced motor neurons. On the other hand, complete knock-out of C9orf72 protein in a different mouse model results in splenomegaly and enlarged lymph nodes but does not affect motor nervous system (Jiang et al., 2016).

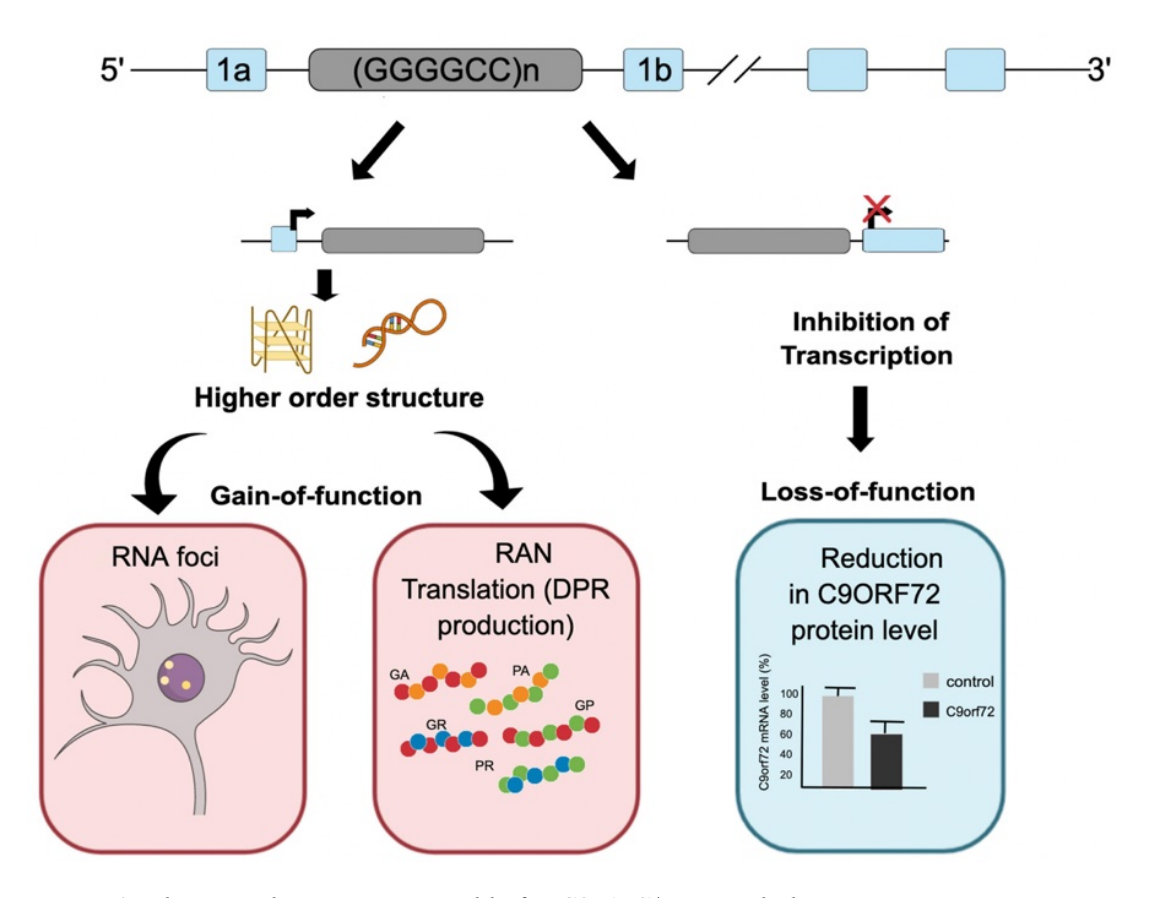


Figure 1: Three mechanisms responsible for C9-ALS/FTD pathology.

The GGGGCC repeat mutation located in the first intron of C9orf72 gene leads to C9-ALS/FTD. RNA-toxicity and DPR-protein aggregation represent two gain-of-function mechanisms responsible for the pathophysiology of this disease. Both the RNA transcripts forming intracellular foci as well as the DPR protein aggregates, which are a result of the RAN translation are toxic to the neurons and contribute to neurodegeneration. In addition, in a sense of a loss-of-function mechanism, the lack of physiological levels of functional C9orf72 protein can also be considered as a contributing factor to the C9-ALS/FTD. Source: modification of a figure from (Schmitz et al., 2021).

1.5 Current therapy strategies against ALS/FTD

Currently, therapy options for patients suffering from ALS or/and FTD are very limited. For a long time two substances were available for ALS therapy: Riluzole, and in some countries, Edaravone (Bensimon et al., 1994; Corcia et al., 2021; Hardiman & van den Berg, 2017). Both substances increase survival only by a few months (Corcia et al., 2021). Riluzole appears to be the most effective in patients having bulbar onset ALS (Bensimon et al., 1994). In case of FTD only off-label use of drugs for symptomatic relieve is practiced (Tsai & Boxer, 2014). As of September 2022 a combination drug of taurursodiol and sodium phenylbutyrate (Relyvrio) has

been approved by FDA for ALS therapy (Benedetto Tiz et al., 2022), but the company withdrew it from the market in 2024. Taurursodiol, is a close relative of tauroursodeoxycholic acid (TUDCA), which is a taurine-conjugated form of UDCA. It is well-established in treatment of cholestatic syndromes. TUDCA has antiapoptotic properties and is investigated not only for ALS/FTD but also for therapy of other neurodegenerative diseases (Amaral et al., 2009; Kusaczuk, 2019). Sodium phenylbutyrate plays an important role in expression of antiapoptotic genes and leads to prolonged survival when administered to ALS mouse models (Ryu et al., 2005).

Since these three drugs have rather small effects on ALS/FTD, other approaches are being explored. One of them involves genetic therapy with antisense oligonucleotides (ASO). ASOs are usually complexly designed molecules of about 20 modified DNA and RNA nucleotides, which either target mRNA for degradation by RNase H or alter pre-mRNA splicing process by interfering with pre-mRNA binding to splicing factors (Crooke, 2004). An ASO targeting the repeat-containing *C9orf72* transcript leads to reduction of RNA foci, inhibits DPR protein expression and improves behavioural deficits in transgenic mouse models (Jiang et al., 2016). Similar findings were reported for a different, independently created ASO, targeting the same *C9orf72* transcripts (Liu et al., 2022).

Another very promising approach for C9-ALS/FTD treatment is immunotherapy directed against DPR proteins. Anti-GA antibodies show very promising effects in cell culture (Khosravi et al., 2020; Nguyen et al., 2020; Zhou et al., 2017). Recently conducted *in vivo* experiments also emphasize the viability of antibody therapy against DPR proteins. Work of Nguyen et al. (2020) shows that systemic anti-GA antibody administration leads to reduction of poly-GA, poly-GP and poly-GR in nervous tissue, mitigates behavioural changes associated with neurodegeneration, reduces inflammation in nervous tissue and increases survival in a transgenic mouse model. Zhou et al. (2020) were able to show that vaccination of a poly-GA expressing mouse model with (GA)₁₀ conjugated to ovalbumin as an immunogenic carrier leads to expression of anti-GA antibody in the mouse organism. The mice in the study of Zhou et al. (2020) showed decreased levels of poly-GA in nervous tissue and their motor deficits were largely rescued. Moreover, the active immunization led to decreased neuroinflammation, reduced TDP-43 mislocalization and reduced neuroaxonal damage marker in CSF (Zhou et al., 2020).

On the other hand, a recent attempt at passive vaccination using an anti-GA antibody, conducted by Jambeau et al. (2022), demonstrated only minimal efficacy in two other mouse models. Poly-GA levels remained unchanged or even increased, depending on the mouse

model tested, following the anti-GA antibody treatment. In addition, only minimal improvement in the behavioural phenotype was observed in one mouse model, while the disease progression remained unaltered in another (Jambeau et al., 2022).

Furthermore, there are a few substances, which are already established in treatment of different diseases, which deserve to be mentioned when debating future therapy concepts in ALS/FTD. Tamoxifen is a well-known antiestrogenic drug used in treatment of breast cancer (Jordan, 1992). It was found to slow down TDP-43 aggregation in mice (Wang et al., 2012). In humans it has shown promising, though statistically insignificant results. (Chen et al., 2020). Considering small sample size (10 tamoxifen patients, 8 placebo), larger studies on Tamoxifen are needed to better evaluate its effect on ALS patients. Tyrosine kinase inhibitor Masitinib is approved for the treatment of mastocytosis in dogs (Dubreuil et al., 2009) and has prolonged life of ALS patients to up to two years (Mora et al., 2021). It probably is the most effective when introduced early before severe symptoms set in. Deferiprone is an iron chelator and is explored for its neuroprotective effect through attenuation of iron excess in CNS (Zampatti et al., 2022). Finally, Metformin, which is an approved drug for management of type 2 diabetes mellitus, has been reported to inhibit RAN-translation in a C9orf72 mouse model (Zu et al., 2020).

1.6 Adeno-associated virus – a vector for genetic therapy

Adeno-associated virus (AAV) was discovered in 1965 during electron microscopy as a contaminant of adenovirus sample, hence its name (Atchison et al., 1965). AAV is an unenveloped virus of the genus dependoparvovirus belonging to parvovirus family (Cotmore et al., 2014). Wildtype AAV goes through a bi-phasic cycle. It exists either in a latent state, where integration of viral DNA to host genome happens or in a lytic state, where it replicates in the presence of a helper virus like adenovirus or herpesvirus, which provides essential proteins for replication (McLaughlin et al., 1988; Meier et al., 2020). AAV constitutes of capsid and single stranded DNA (ssDNA) genome (Agbandje-McKenna & Kleinschmidt, 2011; Rose et al., 1969). Its genome is only 4.7 kilobases long and contains three genes: Rep, Cap and Aap (Wu et al., 2010). Rep encodes for proteins used in replication and viron packaging, Cap encodes for capsid proteins and Aap provides a protein playing a vital role in capsid assembly (Naso et al., 2017; Naumer et al., 2012). A distinctive part of AAV's genome are the inverted terminal repeats (ITR), which take over the role of primers during DNA replication (Hastie & Samulski, 2015). Moreover ITRs enable the DNA of AAV to integrate to the host cell's genome

(Cheung et al., 1980). In humans this integration takes place preferentially on the long arm of chromosome 19 (Samulski et al., 1991). ITRs are the only wildtype AAV DNA sequence required for encapsidation of a DNA strand (Xiao et al., 1997). Thus, when creating a recombinant AAV (rAAV) for genetic therapy purposes, only the gene of interest, which is flanked by ITRs is required for an assembly of a functional rAAV vector. In case of AAV 2, the most established serotype in AAV genetic therapy research, ITR sequences are built of 145 nucleotides from which the first 125 are capable of self-base pairing into hairpin structures which allow self-priming for replication (Lusby et al., 1980).

There exist different variants of AAV, which are referred to as serotypes (e.g., the AAV 2). They contain distinct capsid proteins which interact in a specific way with a receptor on a target cell (Gao et al., 2003; Pillay et al., 2017). Each serotype possesses a unique tissue-binding ability – a characteristic referred to as tropism. (Liu et al., 2015; Zhang et al., 2022). Some serotypes have evolved naturally, while others were artificially designed to enhance the desired tissue tropism (Wang et al., 2019). In gene therapy, capsid proteins of different AAV serotypes can be used to package a viral vector which contains just the ITRs of the ssDNA genome of the AAV 2. This approach is particularly effective due to the well-studied and safe integration site in the human genome determined by the AAV 2 ITRs. ITR sequences from AAV 2 along with capsid proteins that are well-suited for the targeted tissue are combined to construct an rAAV vector for genetic therapy purposes (Wilmott et al., 2019). This practice is also highlighted in rAAV nomenclature. For example, if AAV 2 genome is packaged into AAV 9 capsid such rAAV is denoted as AAV 2/9.

Recombinant AAV vectors have gained much popularity in gene therapy context. AAV drugs are already approved, and AAV technology is increasingly being employed in drug development.

Adeno-Associated Virus

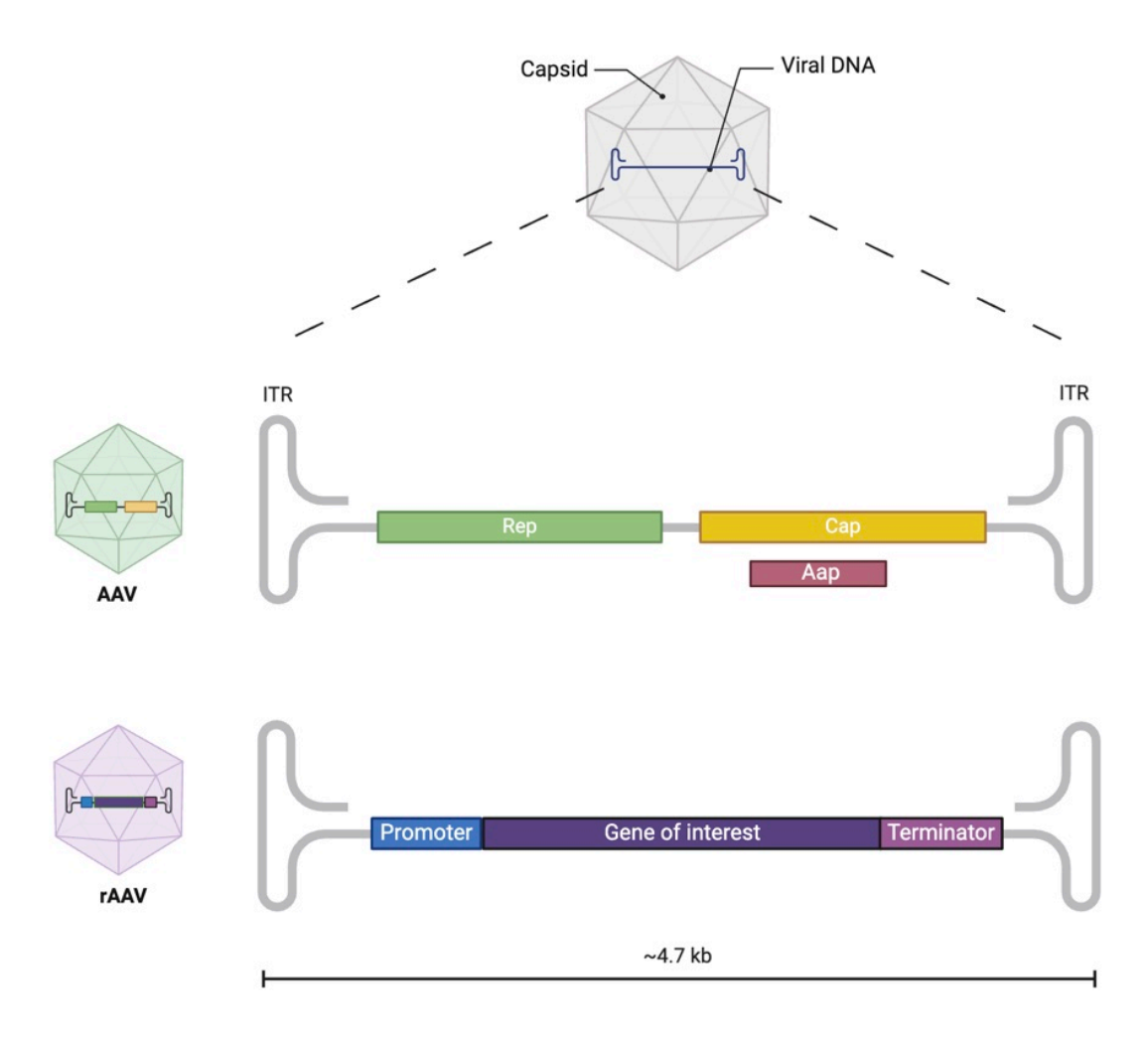


Figure 2: Schematic representation of AAV genome for wildtype and recombinant AAV

Recombinant AAV (rAAV) is created by replacing all genes in the AAV genome between the inverted terminal repeats (ITRs) with a transgene. Rep and Cap genes are components of wildtype AAV genome. Aap is encoded by an alternative reading frame on the Cap gene (Naumer et al., 2012). The genome of AAV is 4.7 kilobases long and longer sequences cannot be efficiently packaged into the capsid. Adapted from "Adeno-Associated Virus with Callout (Layout)" and "Adeno-Associated Virus (AAV) Genome", by BioRender.com (2022). Retrieved from: https://app.biorender.com/biorendertemplates.

The process by which rAAV DNA is integrated into host cells, followed by the expression of the transgene enabling this therapeutic approach, is known as transduction. It starts with endocytic internalization of the virus (Bartlett et al., 2000). The endosomal rAAV is then trafficked using the microtubule system of the host cell in perinuclear direction where the virus escapes the endosome (Xiao & Samulski, 2012). The rAAV with an intact capsid enters the cell nucleus through a nuclear pore complex (Johnson et al., 2010; Kelich et al., 2015; Sonntag et al., 2006). In the nucleus the rAAV capsid is either ruptured or the ssDNA slips out of it without damaging the capsid, which leaves free ssDNA in the nucleus of the cell (Bernaud et al., 2018). Thanks to self-priming, made possible by folded into hairpins ITRs, viral ssDNA undergoes a host-cell mediated replication in the cell nucleus to form double-stranded DNA (Berns & Linden, 1995). This double-stranded DNA persists within the cell by adopting an episomal state forming a circular or concatemeric structure or it can also potentially integrate into the genome of the host cell (McCarty et al., 2004). The recombinant DNA can be then transcribed to mRNA which subsequently will be used as a matrix for translation resulting in the expression of the encoded transgene.

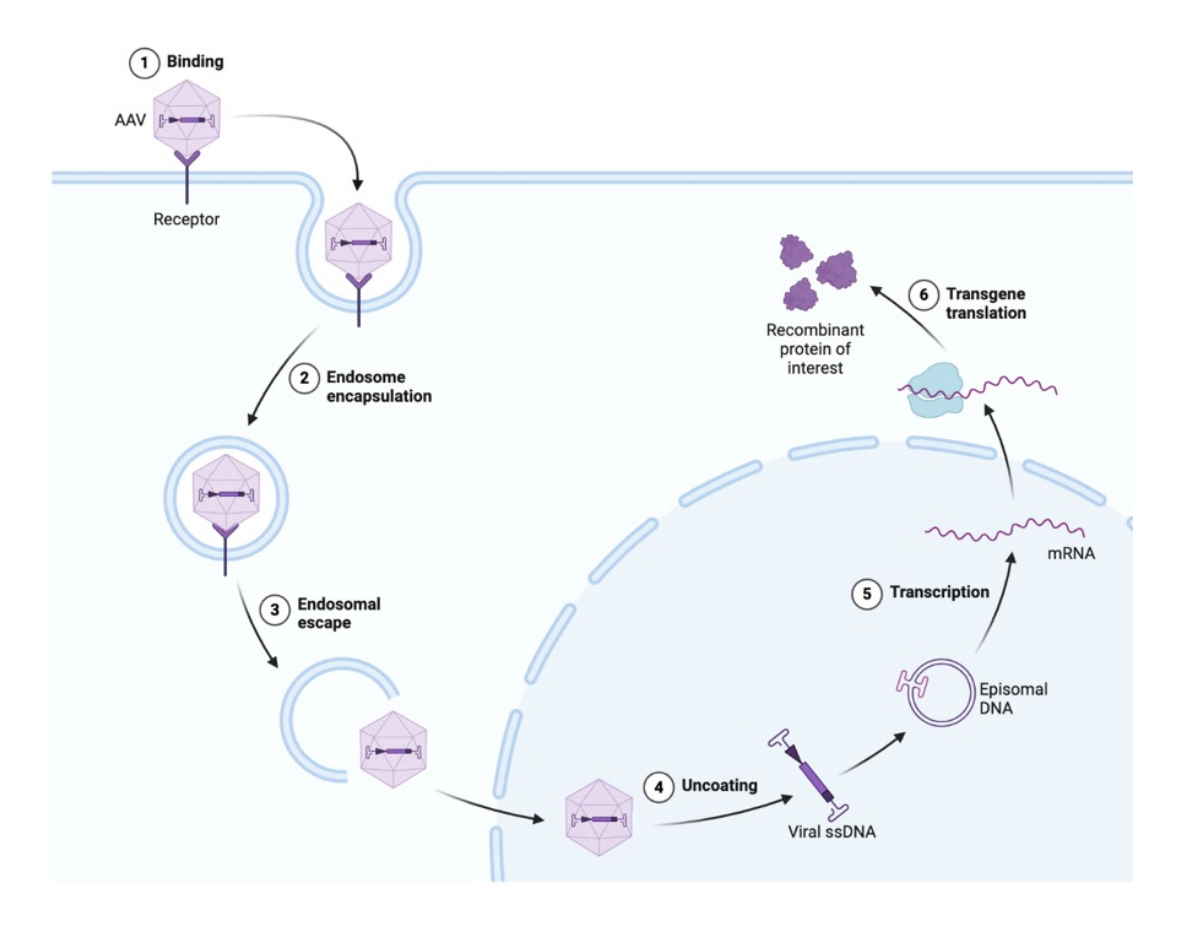


Figure 3: Genetic therapy with use of rAAV vector – transduction on cellular level

After binding to its specific receptor rAAV is internalized via endocytosis. The endosomal rAAV travels to the nucleus. Close to the nucleus an intact rAAV virion escapes the endosome and enters the nucleus through nuclear pore. Viral ssDNA is released and either formation of stable episomal molecule (exemplarily presented in the figure) or integration into the host cell genome takes place. Newly introduced transgene can be transcribed and translated resulting in creation of the protein of interest. Reprinted from "AAV Vector Infection", by BioRender.com (2022). Retrieved from: https://app.biorender.com/biorender-templates

1.7 Established AAV-based drugs

To date, there are four drugs designed with AAV vector technology, which have been approved by regulatory agencies worldwide. The first AAV drug Glybera, approved in 2012 in Europe, was directed against the rare familial lipoprotein lipase deficiency (LPLD) (Bryant et al., 2013). In LPLD, patients carry a loss of function mutation in lipoprotein lipase (LPL) resulting in extremely high triglyceride levels with severe complications (Burnett et al., 1993). Glybera allowed integration of LPL gene into the patient's cells' genome via intramuscular injection (Bryant et al., 2013). In this case AAV ITR sequences flanking the LPL gene were from AAV 2, while the capsid protein came from AAV 1 (Rip et al., 2005). Glybera was taken off market in 2017 due to economic reasons (Keeler & Flotte, 2019).

Luxturna was approved for inherited retinal dystrophy (IRD) caused by mutation in RPE 65 gene (Russell et al., 2017). Functional RPE 65 isomerase is essential for physiological retinoid cycle in the eye, so the mutation in RPE 65 gene results in congenital blindness, also known as Leber congenital amaurosis (Cideciyan et al., 2008). Luxturna was approved in 2017 in USA and in 2018 in Europe (Keeler & Flotte, 2019). In Luxturna, a vector is constructed using both the capsid and the ITRs of AAV 2. This vector is administered through subretinal injection and transduces retinal cells with a functional RPE 65 gene (Keeler & Flotte, 2019; Russell et al., 2017).

Zolgensma was approved in 2019 in the USA (Hoy, 2019) for gene therapy of spinal muscular atrophy (SMA). In this relatively common autosomal recessive neurological disease (about 1:10 000 births), a genetic deletion or mutation of survival motor neuron 1 (SMN1) gene results in motor neuron degeneration leading to progressive muscle weakness, atrophy and premature death (Kolb & Kissel, 2015; Sugarman et al., 2012). Zolgensma is an rAAV encoding functional SMN1 to restore expression of SMN1 in neurons of SMA patients (Stevens et al., 2020). In this case the AAV 9 capsid was employed because of its ability to pass blood-brain barrier thereby enabling intravenous administration (Foust et al., 2009). Therapy with Zolgensma in form of one-time intravenous injection is now approved for children below 2 years of age with biallelic mutations in SMN1 gene (Blair, 2022; Hoy, 2019).

Most recently, AAV-based gene therapy drug against haemophilia B, Hemgenix, has been approved in both United States and in Europe. One-time intravenous injection of AAV 5 vector carrying a gene for clotting Factor IX, which is defect in haemophilia B, decreases bleeding rate, increases Factor IX activity and reduces necessity of Factor IX concentrate administration in patients (Pipe et al., 2023).

2 Research question

Despite many efforts to develop a curative therapy for C9-ALS/FTD, this objective has not been accomplished yet. It is crucial to explore various therapy strategies which in their own ways would help alleviate the burden of this disease. Recent research shows that immunotherapies against DPR proteins have big potential to achieve this goal. Poly-GA is the most abundant DPR protein, and it directly links the mutation to TDP-43 pathology by sequestering and inhibiting proteasomes (Guo et al., 2018; Khosravi et al., 2020). Antibodies against poly-GA alleviate the DPR aggregation and rescue phenotypes of C9-ALS/FTD mouse models. Passive immunization with anti-GA antibodies leads to partial degradation of poly-GA inside the cell (Nguyen et al., 2020). Also, active immunization against poly-GA showed remarkable benefits (Zhou et al., 2020). Moreover, poly-GA can be transmitted from one neuron to another causing TDP-43 aggregation in the receiving cell and thus potentially propagate the causes of neurodegeneration (Khosravi et al., 2020). This seeding behaviour of poly-GA can be ameliorated with antibodies in cell culture (Zhou et al., 2017). Results of Zhou et al. (2020), also indicate effective antibody interception of poly-GA during cell-to-cell transmission in vivo. However, conventional antibody therapy for CNS diseases requires very high antibody doses, as less than 1% of antibody crosses the blood-brain barrier (Kouhi et al., 2021). This inefficiency can be mitigated through AAV technology, which facilitates transgene expression in the transduced tissue, allowing for accurate and site-specific antibody production. Intracerebroventricular (ICV) AAV injection in neonatal mice enables diffusion of AAV from the cerebrospinal fluid to the brain parenchyma and transduction of the constituting cells (Kim et al., 2014). Antibody expression directly in the brain utilizing the ICV injection of AAV has already been successfully implemented in treatment of alpha-synuclein pathology in mice (Chatterjee et al., 2018). The aim of this work was to investigate whether high concentrations of anti-GA antibody, expressed after AAV2/9 injected into the lateral ventricles of neonatal mice, could interfere with the cell-to-cell poly-GA transfer in the nervous system and so slow the neurodegeneration in poly-GA-expressing mouse models. The choice of a fast-progressing mouse model could facilitate rapid screening of several anti-GA clones and variants designed to improve affinity or remove liabilities for drug manufacturing such as deamidation sites. The therapeutic effect of the antibody was compared with a negative control of an anti-PR antibody. Answering this research question provided an important insight into realm of possibilities in C9-ALS/FTD therapy strategies and supported further research to develop drugs against this currently uncurable disease.

3 Methods

3.1 The study design

The study design incorporated both in vitro and in vivo methods. Firstly, the AAV antibody expression and functionality was tested on primary rat neurons. Afterwards the intracerebroventricular injection (ICV) was done on C57BL/6 mice to establish the best timepoint for injection and to prove the selective expression of antibodies in neurons accomplished with hSynpasin promoter. For in vivo therapy experiments, GA-Nestin mouse model and GA-Camk2A mouse model were compared with their unaffected littermates after injections of therapeutic anti-GA antibody AAV and a control anti-PR antibody AAV. GA-Nestin mice were harvested at 4 weeks of age. The outcome of the therapy was investigated with multiple methods. Firstly, the effect of the therapy on weight of the mice was measured. Secondly, expression pattern of the antibody in the nervous system was investigated. Moreover, immunohistochemistry stains with focus on hippocampal region were done to estimate and compare the extent of neurodegeneration and neuroinflammation between experimental and control groups. Poly-GA aggregation was also quantified on immunofluorescence (IF). Lastly, anatomical state of neuromuscular junction was investigated with IF. The effect of the therapy on behavior of GA-Camk2A at 16 weeks of age was measured by means of modified Barnes Maze.

3.2 Therapeutic rAAV – transgene cassette design

Two antibodies were used in the experiments: the tested, therapy antibody – anti-GA (1A12) (Zhou et al., 2020) and the control antibody – anti-PR (32B3) (Schludi et al., 2015). Both were modified to be of murine IgG1 class to reduce effector functions. The mouse and human antibodies consist of heavy and light chains, which are assembled in the endoplasmic reticulum prior to secretion. For an antibody to take a functional tertiary protein structure, both the heavy and light chain must be expressed. To avoid transduction of heavy and light chains using two separate AAVs, a Furin-P2A system was implemented in designing the AAV transgene cassette driven by a single promoter, which is barely within the limiting packaging capacity of AAV (strategy implemented thanks to valuable input of David M. Holtzman, MD). The P2A self-cleaving peptide triggers ribosomal "skipping" rather than actual proteolytic cleavage. After translation and release of the heavy chain, the ribosomes continue translation of the remaining mRNA of the light chain located after the P2A sequence (Doronina et al., 2008). To remove

these leftover amino acids from P2A (Fang et al., 2007) a furin recognition sequence was included between the heavy chain and P2A sequence, as also demonstrated by Fang (2007). This way, it was possible to place sequences for both the heavy and the light chain in one rAAV construct. The transcription was driven by a single human synapsin (hSynapsin) promoter. Combination of hSynapsin promoter transcription and use of AAV 2/9 were shown to be highly effective in neuronal tissue (McLean et al., 2014).

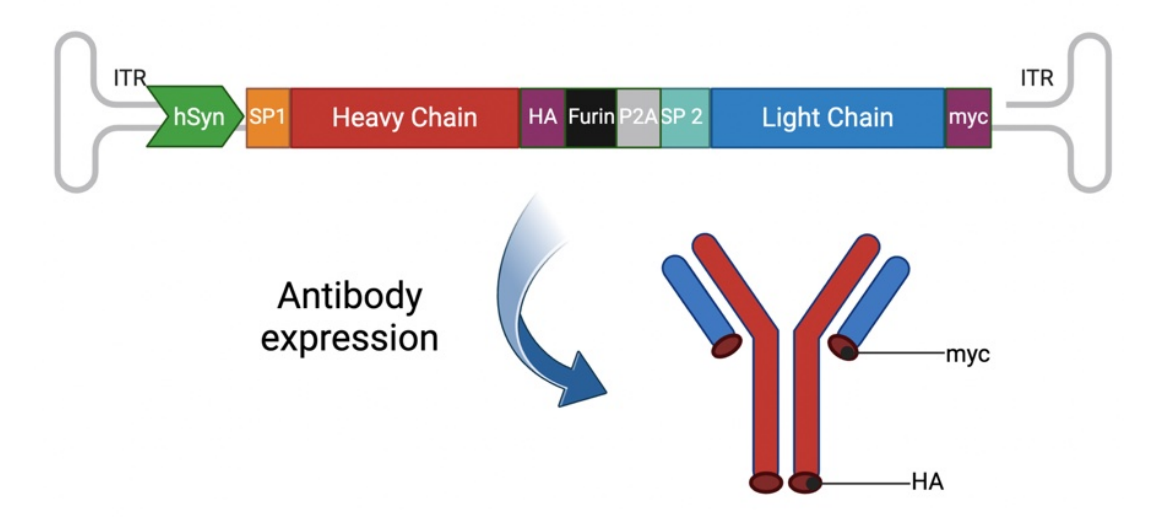


Figure 4: AAV transgene cassette used for the AAV-mediated anti-GA antibody therapy

The coding sequence for heavy and light chains of the antibody were placed on the same AAV genome. Both chains were guided for endoplasmic reticulum and for secretion thanks to signal peptide sequences (SP1, SP2). The heavy and light chains were tagged by HA and myc, respectively. The P2A self-cleaving peptide triggered ribosomal skipping resulting in expression of equal amounts of heavy and light antibody chains as separate polypeptides. The furin recognition site (black box) helped to remove the P2A residues through the protease furin. The transcription was dependent on hSynapsin promoter (green arrow). The whole sequence was flanked by inverted terminal repeat sequences (ITR), essential for AAV packaging. Created with BioRender.com.

3.3 Animal models and *in vivo* therapy testing design

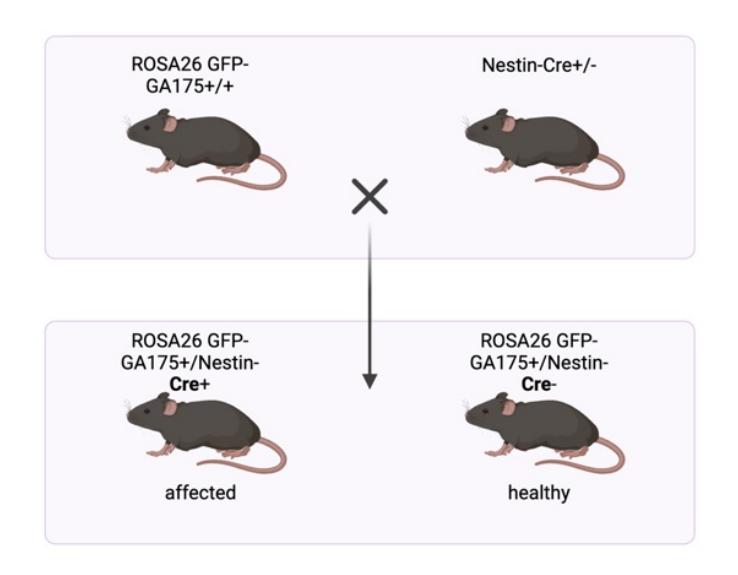
The AAV-mediated anti-GA antibody therapy efficacy was tested on two C9-ALS/FTD mouse models. The GA-Nestin model was previously described by LaClair et al. (2020). This mouse line expressed GFP-(GA)₁₇₅, which displays a high poly-GA aggregation without (G₄C₂)_n RNA foci toxicity or C9orf72 haploinsufficiency. GA-Nestin mice are characterized by wasting, selective neuron loss, inflammation, and muscle denervation. Due to a rapid development of severe phenotype, they require euthanasia before reaching 7 weeks of age when they reach the humane endpoint due to weight loss or muscle weakness (LaClair et al., 2020). Another mouse model used was the unpublished GA-Camk2A line. GA-Camk2A mice express poly-GA

predominantly in excitatory neurons without the other pathological features of C9-ALS/FTD. This line initially shows impaired memory function, but slowly progressing weight loss requires termination at humane end point at around 30 weeks of age according to predefined scoring criteria (manuscript in preparation). The expression of poly-GA in GA-Nestin and GA-Camk2A is based on genetic modification technique, a Cre-Recombinase system, which involves removal of a STOP cassette flanked by loxP sequences by Cre-Recombinase enzyme (Cox et al., 2012). The difference in the phenotypes of the 2 models can be attributed to the promoter used for Cre recombination, which drives poly-GA expression. Nestin-Cre leads to ubiquitous expression and aggregation of poly-GA in the nervous system whereas Camk2A-Cre leads to aggregation of poly-GA mostly in the hippocampus.

Crossing mice homozygous for poly-GA gene located at ROSA26 position with mice heterozygous for Cre gene with Nestin or Camk2A promoter, resulted in birth of animals which all had one allele of the poly-GA gene, but only half of them were heterozygous for Cre and expressed Cre-Recombinase. In these animals the STOP cassette, located just after the poly-GA gene promoter, was excised by the Cre-recombinase and poly-GA expression was enabled. In consequence poly-GA aggregate formation took place and these mice developed disease symptoms. Littermates, which did not inherit the Cre gene, also possessed the poly-GA gene however presence of the STOP cassette did not allow for its expression. These littermates were healthy.

In both GA-Nestin and GA-Camk2A groups affected and healthy mice were born in 1:1 ratio. Both affected and healthy mice were injected with blindly picked for injection of either anti-GA antibody AAV or the control anti-PR antibody AAV consequently resulting in four groups per each mouse model. The healthy mice were pooled together to form one control group. The methods used to investigate the therapy effect were picked to match the symptoms that were characteristic for the mouse lines. Thus, GA-Nestin mouse model was investigated thoroughly on the cellular level for poly-GA expression and GA-Camk2A mouse model was analysed with a memory test.

All mice were kept in a pathogen-free animal facility in a 12-hour light/dark cycle with ad libitum food and water access in accordance with the German animal welfare law.



STOP-cassette excision by Cre-Recombinase

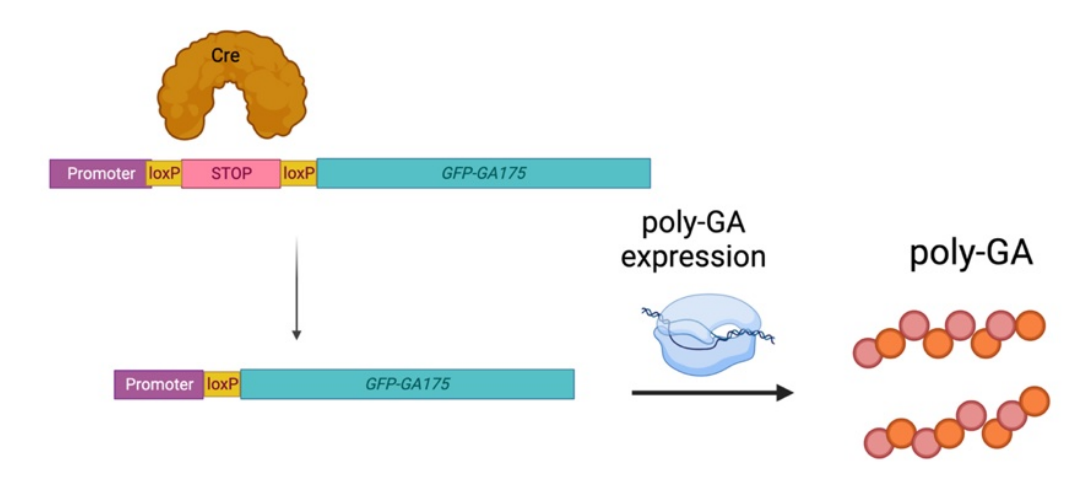


Figure 5: Mouse breeding for experiments and Cre-Recombinase system.

Top: Breading of mice homozygous for GFP-GA175 at ROSA26 locus and mice heterozygous for Nestin-Cre created offspring showing two genotypes – both littermate types possessed the poly-GA gene, but only half of them possessed the Nestin-Cre gene. Consequently, half of the litter was affected and the other half healthy. Analogous breeding process was implemented for GA-Camk2A. Adapted from "Mouse Breeding Chart (Layout)" by BioRender.com (2022). Retrieved from: https://app.biorender.com/biorender-templates.

Bottom: Expression of Cre-Recombinase in animals possessing the Cre gene, allowed enzymatic excision of the STOP cassette by the Cre-Recombinase. The result was expression of poly-GA. Created with BioRender.com.

3.4 Material

Plasmids:

For in house-AAV packaging:

- pAAV-RC DJ8 capsid plasmid 7.3 kb (Cell Biolabs)
- pHelper plasmid 11.6 kb (Cell Biolabs)
- 1A12 (Anti-GA) antibody plasmid 6.9 kb (own stock)
- 32B3 (Anti-PR) antibody plasmid 6.9kb (own stock)

Own stock DPR-protein plasmids for HEK293-cell transfection:

- 175xGA-GFP plasmid (AD793)
- 175xPR-GFP plasmid (AD797)
- GFP plasmid (MM167)

Cells:

- Human embryonic kidney (HEK293 FT) cells (Thermo Fisher Scientific)
- Primary hippocampal rat neurons

Ready-made AAV:

- AAV 2/9 with 1A12 antibody transgene
- AAV 2/9 with 32B3 antibody transgene
- AAV with GFP transgene

Ready AAV samples were obtained from TUM Institute for Pharmacology and Toxicology and had a concentration of 10^{12} viral copies/µl in Ringer solution.

Primers for genotyping:

- GA-GFP primer mix-MS125/MS126 (TCCAGGAGCGTACCATCTTC / GTGCTCAGGTAGTGGTTGTC)
- Cre primer mix pCre1/pCre2
 (ATGCCCAAGAAGAAGAGGAAGGT / GAAATCAGTGCGTTCGAACGCTAGA)

Antibodies:

For stains:

Alexa Fluor 488 Mouse anti-rat (Life Technologies); Alexa Fluor 488 Mouse anti-streptavidin (Life Technologies); Alexa Fluor 555 Mouse anti-rabbit (Life Technologies); Alexa Fluor 555 Mouse anti-β-Tubulin III (BD Pharmingen); Alexa Fluor 647 Mouse Bungarotoxin (Thermo Fisher Scientific); Anti-GFAP (Dako); Anti-GFP (Sigma-Aldrich); Anti-myc from rat (Abcam); Anti-HA from rabbit (Sigma-Aldrich); Anti-NeuN, from rabbit (Abcam); Anti-Iba1 from rabbit (Wako); Biotinylated anti-GA (own stock)

For immunoblotting:

Anti-mouse HRP conjugated (Promega); Anti-rabbit HRP conjugated (Promega); Anti-Calnexin from rabbit (Enzo Life Science); Anti-GA (1A12, hybridoma supernatant); Anti-GA (1A12, purified); Anti-PR (32B3, hybridoma supernatant); Anti-PR (32B3, purified)

For ELISA:

Anti-mouse HRP conjugated (Promega)

Kits:

- BCA Protein Assay (Thermo Fisher Scientific)
- DCS Detection Kit 2 PD000

Buffers:

- 1M Dithiothreitol (DTT) (Sigma-Aldrich)
- 20x SB Buffer: 38.17 g sodium borate decahydrate (Borax) and 33 g boric acid in 1L dH2O, pH 8.0
- Blocking Buffer (BB): 0.2% I-Block in TBSTx
- Cathode buffer: 0.1 M Tris-HCl 0.1 M Tricine 0.1 % SDS
- GDB: 0.1% gelatine, 0.3% Triton X-100, 450 mM NaCl, 16 mM sodium phosphate, pH 7.4
- Mouse tail lysis buffer: 100 mM Tris-Cl, 5 mM EDTA, 200 mM NaCl, 0.2% (w/v)
 SDS
- PCR reaction buffer 5x Green GoTaq (Promega)
- Permeabilization and Blocking Buffer 5% FCS, 0.1 % Triton X in PBS
- Phosphate Buffered Saline (PBS): 0.14 M NaCl, 10 mM Na2HPO4, 2.8 mM KH2PO4,
 2.7 mM KCl, pH 7.4

- RIPA Buffer: 137 mM NaCl, 20 mM Tris pH 7.5, 0.1 % SDS, 10 % glycerol, 1 % Triton-X-100, 0.5 % sodium deoxycholate, 2 mM EDTA
- Running buffer: 1.5 M Tris, 0.4 % SDS, pH 8.8
- Transfer buffer: 1.5 M Tris, pH 8.8
- Tris-buffered saline with Triton-X (TBSTx): 20 mM Tris, 0.14 M NaCl, 0.2 % Triton-X-100, pH 7.6
- Washing buffer 0.05 % Tween20 in PBS

Media:

- Fluoromount G Mounting Medium (Thermo Fisher Scientific)
- Hardening mounting medium (Merck, EUKIT)
- Minimum Essential Medium (MEM) (Life Technologies)
- Neurobasal medium (NBM) (Life Technologies)
- Opti-MEM (Life Technologies)

Other reagents:

- 3,3',5,5'-Tetramethylbenzidine Liquid Substrate (TMB) (Sigma-Aldrich)
- Agarose
- Alcoholic eosin
- Bovine Serum Albumine (BSA) (Sigma-Aldrich)
- Citric acid
- Cresyl violet
- dNTP nucleotides for PCR (Thermo Fisher Scientific)
- EDTA 0.5 M (Thermo Fisher Scientific)
- Enhanced chemiluminescence solution (ECL) (Thermo Fisher Scientific)
- Eosin (Sigma HT 110-1128)
- Ethanol
- Ethylenediaminetetraacetic acid (EDTA)
- Fetal Calf Serum (FCS) (Capricorn Scientific)
- Fluorescent nucleic acid stain GelRed (Merck)
- Formic acid 5%
- GA-GST and PR-GST for plate coating in ELISA

- Glacial acetic acid
- Hematoxylin (Waldeck 2E-038)
- Hydrogen peroxide
- I-Block Protein Based Blocking Reagent (Thermo Fisher Scientific)
- Isopropanol
- Ketamine/Xylazine
- Lipofectamine 2000 (L2K) (Life Technologies)
- Marker for DNA electrophoresis DirectLoad 1kb DNA Ladder (Merck)
- Methanol
- Natrium citrate
- Paraformaldehyde (PFA) (Carl Roth, ROTI Histofix 4%)
- Penicillin-Streptomycin 10.000 U/ml (Gibco)
- Poly-D-Lysine (PDL) (Merck)
- Protease Inhibitor Cocktail (Merck)
- Protease/Phosphatase Inhibitor Cocktail (Cell Signaling Technology)
- Protein Standard for Immunoblot SeeBlue Plus 2 (Thermo Fisher Scientific)
- Proteinase K (Carl Roth)
- RNase Free H₂O (Thermo Fisher Scientific)
- Sucrose
- Taq DNA Polymerase (Sigma-Aldrich)
- Trypan Blue Stain 0.4% (Thermo Fisher Scientific)
- Xylol

Laboratory Equipment:

For ICV injection:

- Glass capillaries fire polished, 3.5 inches long, inner/outer diameter: 0.530/1.14mm (World Precision Instruments)
- Immersion oil (Sigma-Aldrich)
- Isoflurane Isofluran CP (CP-Pharm)
- Isoflurane pump Tec3 Selectatec Vaporiser (Hugo Sachs Elektronik)
- Micropipette Puller P1000 (Sutter Instruments)

- Nanoliter Injector NL2010MC2T with SMARTouch controller (World Precision Instruments)
- Ultrasound gel Aquasonic (Parker)
- Ultrasound system VEVO 3100 (Fujifilm VisualSonics)

For Barnes maze:

- Camera (Sony)
- Maze for Barnes Maze (Maze Engineers)

For tissue harvesting:

- Needles Sterican 23G, 25 mm (Braun)
- Peristaltic pump PeriStar Pro (World Precision Instruments)
- Scalpel, scissors, tweezers (Saleem Chir. Instrumente)

Bench equipment:

- 1 ml Syringes Injekt-F (Brown)
- 1, 2, 200, 1000 μl Pipettes Pipetman classic (Gilson)
- 10 cm Petri dish (Thermo Fisher Scientific)
- 15 ml sterile tubes (Merck)
- 50 ml sterile tubes (Merck)
- Automatic Cell profiler Countess II FL Automated Cell Counter (Invitrogen)
- Automatic multichannel pipette Pipet-Lite Pipette Multi L12-1200XLS+ (Renin)
- Blotting chamber Mini Gel Tank (Thermo Fisher Scientific)
- Cell culture incubator D180 CO2 Incubator (RWD Life Science)
- Centrifuge 5427 R (Eppendorf)
- Centrifuge (for 15 ml sterile tubes) 75004525 Sorvall ST 40R (Thermo Fisher Scientific)
- Combs for electrophoresis
- Confocal microscope LSM800 (Carl Zeiss)
- Coverslips DIV 7 (Pearl)
- Electrophoresis chamber
- Electrophoresis Power Supply PowerPack® (Bio-Rad)
- Embedding cassettes Histosette (Sigma-Aldrich)
- Freezer -80° C

- GE cassette foam sponges (Merck)
- Gel System (Peq Lab)
- Hard tissue tube MK28 (Bertin)
- Leica Microscope Fluorescent Camera DFC9000 GT (Leica)
- Light and fluorescent microscope Dmi8 (Leica)
- Liquid repellent pen Pap Pen (Sigma-Aldrich)
- Metal matrix for Brain and Spine (World Precision Instruments)
- Microplate photometer Synergy H4 (Biotek)
- Microscope slides SuperFrost Plus (Thermo Fisher Scientific)
- Microwave Oven R20CT (Sharp)
- Multichannel pipette 0.5-10, 10-100 µl (Eppendorf)
- PCR Thermal Cycler Nexus (Eppendorf)
- Pipette-boy Accu-jet Pro (Avantor)
- Plastic ice block
- Polyvinylidene fluoride (PVDF) Membrane
- Shaker KL 2 (Edmund Bühler GmbH)
- Soft tissue tube CK14 (Bertin)
- Spectrophotometer NP-80 (Implen)
- Thermoblock Thermomixer comfort 5355 (Eppendorf)
- Tissue homogenizer Percellys Evolution (Bertin)
- Transfer chamber mini trans blot cell package (Bio-Rad)
- Tricine Protein Gel Polyacrylamide concentration 10-20% (Thermo Fisher Scientific)
- UV-Transilluminator (INTAS, UVT 2020)
- Vibratome VT 1200 (Leica)
- Vortex Mixer (Thermo Fisher Scientific, Vortex-Genie 2)
- Weighing scale (Sartorius, BP 3100)
- X-Ray Development Cassette (IP Cassette 20x40 cm)
- X-ray film processor (CAWO, Cawomat 2000IR)
- X-Ray Films (Fuji, Super RX)

Software:

• Barnes Maze Tracking Software (ANY-maze)

- Fiji
- Excel (Microsoft)
- myassays.com
- Python (libraries: Matplotlib, NumPy, pandas, SciPy, scikit-image, seaborn, statsmodels)

3.5 In house AAV packaging

AAV with DJ8 capsid (Grimm et al., 2008) with anti-GA or anti-PR antibody transgene were produced to test the transduction effectiveness and to assess the functionality of the expressed antibody in vitro. The AAV packaging was done by transfecting HEK293 FT cells. AAV can enter a lytic state, in which functional virions are assembled, only in the presence of viral helper genes. These genes are: E1a, E1b, E2a, E4, and virus-associated RNA (VA RNA) (Daya & Berns, 2008; Vachon & Conn, 2016). HEK293 cells already express the E1a and E1b genes what makes them suitable for rAAV production (Tan et al., 2021). In addition, Rep and Cap genes, which normally are a part of the wildtype AAV genome, and the transgene of interest flanked between ITR sequences must be transfected in form of plasmids to produce desired rAAV. To create the rAAV 10 ml of 500,000 cells/ml HEK293 cells in MEM were seeded on a 10 cm Petri dish and cultured in 37° C, 5% CO₂, 95% humidity incubator to 80% confluency. Automatic cell profiler was used to determine the cell concentration. Cells were then transfected with 3 plasmids: pAAV-RC plasmid with Rep and Cap genes for DJ8 capsid, pHelper plasmid with E2a, E4 and VA RNA genes and either anti-GA clone 1A12 or anti-PR clone 32B3 encoding plasmids. 4.55µg of pAAV-RC, 5.8µg of pHelper and 3.45 µg of either 1A12 or 32B3 plasmid were added to 1.5 ml Opti-MEM. The obtained solution was then mixed with 36 μl of Lipofectamine 2000 (L2K) preincubated in 1.5 ml Opti-MEM for 5 minutes at room temperature. The final solution was again incubated for 20 minutes at room temperature. Next, 5 ml of Opti-MEM with 10% fetal calf serum (FCS) with 1% Penicillin/Streptomycin and 3 ml plasmid and L2K Opti-MEM solution prepared beforehand was added to the Petri dish with HEK293 cells. After 72 hour-incubation period at 37° C, 5% CO₂ and 95% humidity, 160 µl of 0.5 M EDTA was added to the Petri dish with the HEK293 cells, to get 10mM EDTA concentration, and the dish was left for 3 minutes at room temperature to allow the cells to detach from the bottom of the dish. The contents were then moved into a 15ml sterile tube and centrifuged for 5 minutes at 3000 rpm at room temperature. The cell pellet was then resuspended in 250 µl of Neurobasal Medium (NBM). The cell suspension was then subjected to four rounds of freeze/thaw cycles with two-minute phases of dry ice-ethanol bath and 37° C water bath. Finally, the suspension was centrifuged at 10 000 g for 10 minutes and the supernatant with AAV 2/DJ8 virions was collected. Ready AAV solution was stored at -80°C.

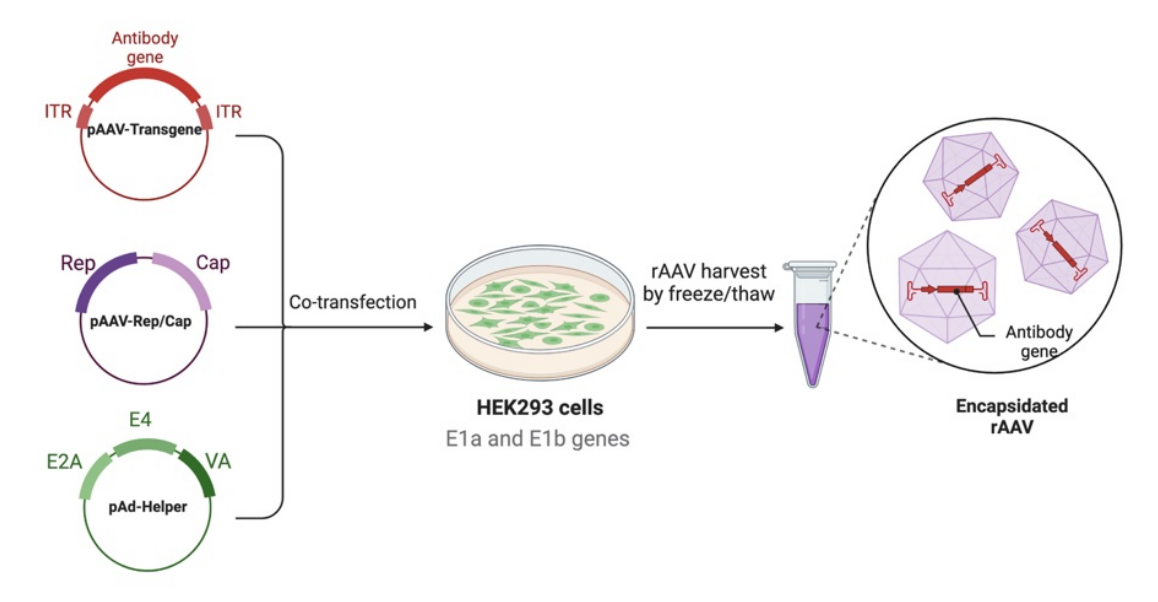


Figure 6: rAAV production by HEK293 triple transfection

AAV 2/DJ8 was created by transfecting HEK293 cells with 3 plasmids – plasmid with the antibody transgene flanked by ITR sequences, pAAV-RC plasmid with Rep and Cap genes and pHelper plasmid with the E2A E4 and VA RNA helper genes. The remaining two helper genes E1a and E1b were present in HEK293 cells' genome. After 72-hour incubation period the rAAV was harvested by freeze/thaw cycles and ready rAAV solution was stored in -80° C. Adapted from "AAV Production by Triple Transfection" by BioRender.com (2022). Retrieved from: https://app.biorender.com/biorender-templates.

3.6 Antibody visualization after AAV transduction and expression in cell culture

Primary hippocampal rat neurons grown on coverslips for 7 days *in vitro* (DIV 7) in NBM (Riemenschneider et al., 2022) were transduced with 5 µl of the in house packaged AAV 2/DJ8 and in a later test with the imported AAV 2/9 solution. After 5 days of 37° C, 5% CO₂, 95% humidity the medium was collected and stored at 4° C for immunoblotting (see 3.7). The coverslips were carefully washed with PBS and fixated with 1 ml of 4% Paraformaldehyde (PFA) with 4% sucrose for 15 minutes at room temperature. Next, the coverslips were again washed with PBS and incubated overnight at 4° C on a 200 µl droplet of 1:500 primary antimyc and anti-HA antibody in GDB buffer solution. Afterwards, the coverslips were washed with PBS and were incubated on a 120µl droplet of 1:250 secondary Alexa Fluor 488 Mouse

anti-rat and Alexa Fluor 555 Mouse anti-rabbit antibody in GDB for 1 hour at room temperature. After careful PBS washing, the coverslips were mounted with Fluoromount G mounting medium on a microscope slide and left for 30 minutes at room temperature and later overnight at 4° C. Imaging was done with a confocal microscope with a 20x magnification objective.

3.7 Visualization of antibody-DPR complexes in immunoblot

To show that the anti-GA and anti-PR antibodies are expressed after rAAV transduction in neurons and that they bind to their corresponding DPR target immunoblot visualizations were done. The supernatant from AAV transduced primary rat neurons was used as a primary anti-GA and anti-PR antibody source. The supernatant was used to bind to DPR protein aggregate samples which were placed in the wells of the gel. The antibody-DPR complex was visualized with help of anti-mouse-HRP secondary antibody.

3.7.1 Preparation of aggregate samples

The DPR aggregate samples were expressed in HEK293 cells. Firstly, transfection with poly-GA (AD793), poly-PR (AD797) or GFP (MM167) (for negative control) plasmids was done. 170 000 HEK293 cells per well, counted with automatic cell profiler, were seeded in wells of a 12-well plate, and incubated at 37° C, 5% CO₂, 95% humidity overnight. 1µg of poly-GA, poly-PR or GFP plasmid was diluted in 125µl of Opti-MEM. 2,5µl of L2K was diluted in 125µl Opti-MEM in a separate tube. After incubation for 5 minutes at room temperature the two solutions were mixed and left for 20 minutes at room temperature. For the transfection, 250 µl of the mixture solution was added to each well and incubated at 37° C, 5% CO₂, 95% humidity for 4 days. For the harvest, the cells were carefully washed with PBS and then incubated on ice in 200 µl RIPA buffer for 20 minutes. The obtained lysate was then transferred to a 1.5 ml tube and centrifuged in 1000 g for 10 minutes at 4° C. 1000 g allowed the cell debris to form a pellet while keeping the aggregates in the supernatant fraction. The protein amount of the supernatant was determined with a bicinchoninic acid (BCA) assay. 150µl of the supernatant was finally mixed with 50 µl of 3xDTT buffer and boiled on the Thermoblock at 95° C for 10 minutes.

3.7.2 BCA assay

To determine the protein concentration of RIPA lysates BCA assay was performed in a 96-well plate using a BCA Protein Assay kit according to supplied protocol. Bovine serum albumin

(BSA) solutions of increasing concentrations in RIPA were used to develop a standard protein concentration curve. After adding BCA developing solution to the wells, the plate was incubated for 30 minutes at room temperature and the absorbance of 562 nm wavelength was measured by with a photometer. The protein concentrations were determined with a linear regression model using MS Excel.

3.7.3 Immunoblotting

15μg of ready poly-GA or poly-PR boiled DTT sample was loaded into a 10-20% Tricine Protein gel. Protein separation was done by standard SDS-PAGE. 5µl of protein standard was loaded as well to be able to determine the size of the separated proteins. The gels were run first for 30 minutes at 80 V and then for 1 hour at 110V in the running buffer. The proteins from the gel were then blotted on a Polyvinylidene fluoride (PVDF) membrane which was beforehand tanked in 100% isopropanol for 2 minutes and washed with transfer buffer. The transfer took place at 400 mA in a transfer chamber filled with transfer buffer. A plasticcovered ice block was used to keep the chamber temperature low for 1 hour transfer. Afterwards, the PVDF membrane was incubated in a blocking buffer (BB) for 1 hour to block unspecific binding sites. It was then incubated in a neuronal supernatant primary antibody solution diluted 1:5 in BB. Anti-GA 1A12 and anti-PR 32B3 hybridoma supernatant antibodies in respectively 1:100 and 1:50 dilutions in BB were prepared as positive controls. The incubation took place overnight at 4° C. Afterwards, the membrane was extensively washed with TBSTx and incubated in an anti-mouse-HRP antibody solution diluted 1:5000 in BB for one hour. The membrane was again extensively washed with TBSTx before development. The washed membrane was dried and incubated for 1 minute in ECL solution from DCS Detection Kit at room temperature. The membrane together with an X-Ray film were then placed into an X-Ray cassette in absence of light. The film was then developed with an X-ray film processor. Finally, the same membrane was again extensively washed with TBSTx, and calnexin blotting was done in an analogous manner. Anti-calnexin antibody in 1:3000 dilution in BB was used as primary antibody and anti-rabbit-HRP in 1:500 dilution in BB was used as secondary antibody.

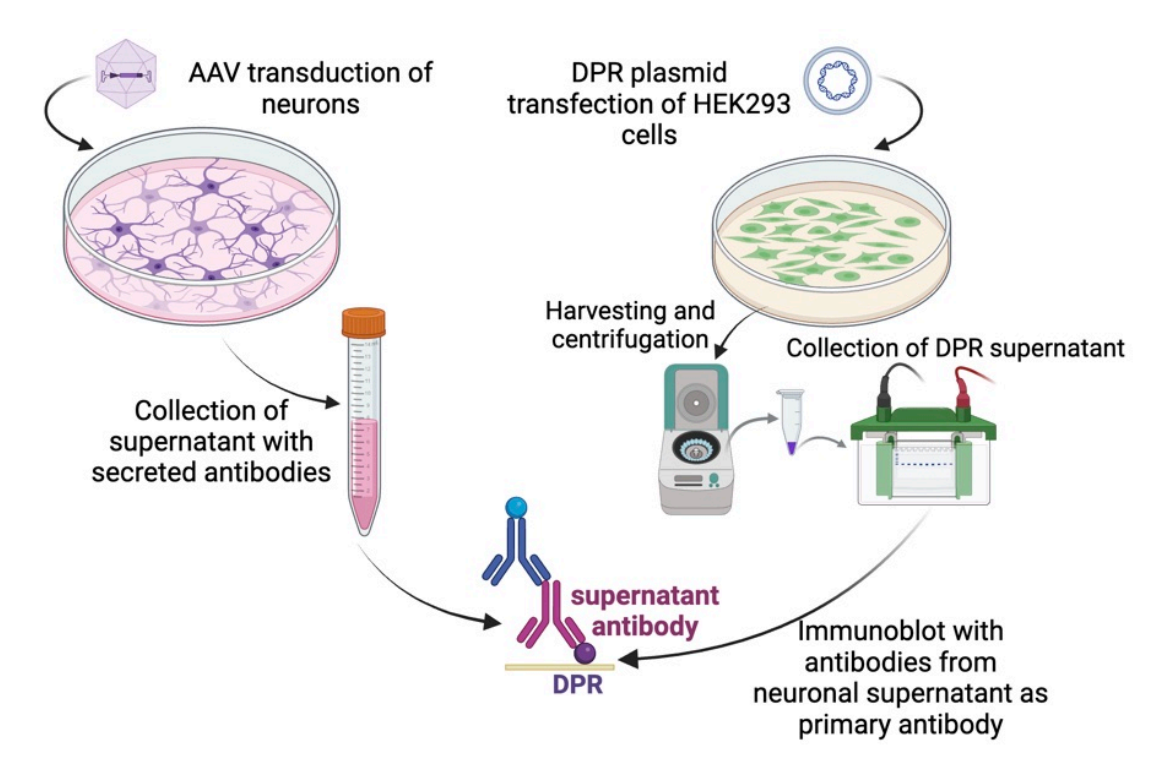


Figure 7: Visualization of antibody-DPR complexes in immunoblot

To show that AAV transduced neurons secrete antibodies supernatant of the neurons was collected and used as a primary antibody source in immunoblotting experiment. The antibody would bind to the aggregates which were collected after transfection, harvesting and specific centrifugation of HEK293 cells. Created with BioRender.com.

3.8 Intracerebroventricular AAV injection

The AAV-mediated anti-GA therapy was tested on two poly-GA expressing C9-ALS/FTD mouse models. The application of AAV into the central nervous system was achieved by means of ultrasound-guided intracerebroventricular (ICV) injection according to an already established protocol (Wang et al., 2022).

3.8.1 **Setup**

Prior to injection, P1 pups and their mother were habituated 15 minutes to the room in which ICV injections were performed. In addition, a drop of ultrasound gel was placed inside their cage to let the mother adapt to the unfamiliar smell of ultrasound gel.

3.8.2 Injector setup

A Nanoliter injector was used to perform the ultrasound-guided ICV injection. At first, 15 μ l of AAV solution was dyed with 0.5 μ l of 0.4% Trypan blue, to later verify a correct liquid uptake by the injector. A sharp, heat-pulled capillary was filled through the blunt end with

immersion oil with a 1 ml syringe. The capillary was then placed on the injector and 4 μ l of immersion oil was ejected out and 4 μ l of dyed AAV solution was taken up.

3.8.3 Preparation of a glass capillary:

A micropipette puller was used to sharpen the tip of the glass capillary. The puller was set up with the following parameters: Cycles = 1; Heat = 580; Pull = 230; Velocity = 70; Delay = 40; Pressure = 500; Ramp = 536. The heat-pulled tip was then cut at length of 0.5 cm.

3.8.4 Injection

An acclimatized pup was taken out of the cage and anesthetized in a 50 ml sterile tube filled with paper towels lightly soaked in isoflurane. The pup was taken out of the tube after its movements seized. It was placed on the left body side facing away from the experimenter with its mouth placed in a tube with a constant 2% isoflurane flow from an isoflurane pump. Ultrasound gel was placed on top of the pup's head. The capillary filled with AAV solution and the head of ultrasound transducer were aligned so that both the ventricles and the tip of the glass capillary were visible on the screen. The capillary was first inserted into the right then into the left ventricle. Per ventricle, $2\mu l$ of AAV solution was injected at a speed of 30 nl/minute. 30 seconds after the end of the injection, the capillary was slowly retracted. Slow injection speed and delayed retraction were supposed to prevent a build-up of intraventricular pressure in the brain and minimize the risk of leakage from the injection site. As the injections on both sides were completed, the pup was allowed to recover from anaesthesia, received a paw tattoo for later identification, and was returned to the cage, where it could recuperate with its mother and other littermates. The procedure was repeated for all littermates.

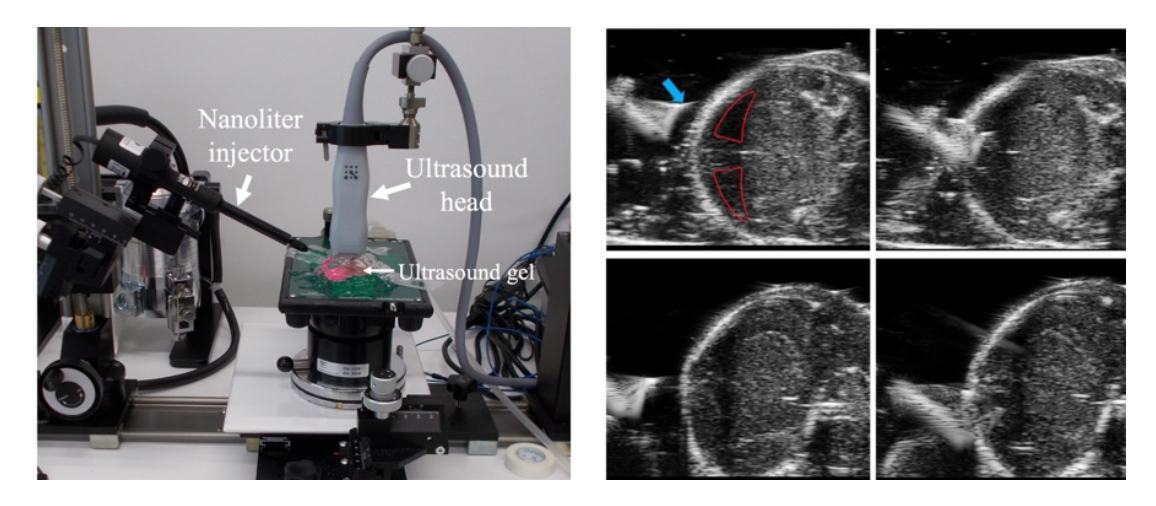


Figure 8: Setup and ultrasound images from the ultrasound-guided ICV injection

Intracerebroventricular (ICV) injection with help of ultrasound imaging was established to administer AAV into the ventricular system of the brain of neonatal mice.

On the left: procedural setup with the pup placed under the gel with the injector and the ultrasound head surrounding the pup.

On the right: ultrasound images taken during the procedure. In the upper left image, the tip of the AAV solution filled glass capillary attached to the injector is marked with a blue arrow and the ventricular system is marked as red area (right lateral ventricle on the top and left lateral ventricle on the bottom. The upper left image represents how the capillary was aimed at the right lateral ventricle and the injection was performed as seen in the upper right image. Following the injection to the right ventricle the injection was performed to the left ventricle with the same volume of $2 \mu l$ of AAV as seen in the bottom images.



Figure 9: Filled ventricular system after ICV injection with dyed solution.

Representative image showing how the ventricles fill up with the blue-tainted injected solution. In this case a solution with high dye concentration was used to visualize fluid distribution inside the ventricular system. The red arrow points to the center of the ventricular system of the brain.

3.9 Standardized mouse scoring

The weight, wound healing and the health status of mice was closely monitored after the ICV injection. All mice were weighed weekly to make sure that they gain weight properly. In total 3 mice had to be killed due to lack of weight gain during first week after birth and 2 developed signs of hydrocephalus and had to be excluded and sacrificed. All properly developing mice of GA-Nesting mouse line were sacrificed at 4 weeks of age, about 3 weeks before they would reach the humane endpoint according to a standardized score sheet (LaClair et al., 2020).

3.10 Tissue collection

At 4 weeks of age brain and spinal cord samples of GA-Nestin mice were collected to compare whether antibody expression was able to delay disease progress. Transcardiac perfusion was used in order to clear the blood out of the nervous tissue, as described in (Wu et al., 2021). The procedure was performed in deep anaesthesia using intraperitoneal Ketamine/Xylazine (50 mg/kg - 5 mg/kg). Narcotic sufficiency was examined by testing the loss of the back-paw withdrawal reflex. Preparation was started with a vertical cut of thoracic and abdominal cavities to secure a clear access to mouse's heart. A needle connected to a perfusing pump was inserted into the left ventricle of the heart and a perfusion with 4° C PBS was carried out for 10 minutes at a rate of 6.5 ml/min. Right atrium of the heart was cut open just as the perfusion started, to allow the blood to leak out. After the perfusion, left brain hemisphere, cervical/thoracic spinal cord (C3-T3) and lumbar spinal cord (L1-L4) were taken out and frozen on dry ice for later biochemical investigation. Additionally, in some instances the quadriceps femoris muscle was also harvested and used for neuromuscular junction (NMJ) staining. The right brain hemisphere and thoracic spine of the segments T4-T13 were fixed in 4% PFA overnight at 4° C and, if needed, stored in PBS solution at 4° C. Spinal cord samples were additionally decalcified in 4% formic acid for 72 hours at 4° C after PFA fixation. Finally, samples were embedded in paraffin wax and cut for immunohistochemical and immunofluorescent staining.

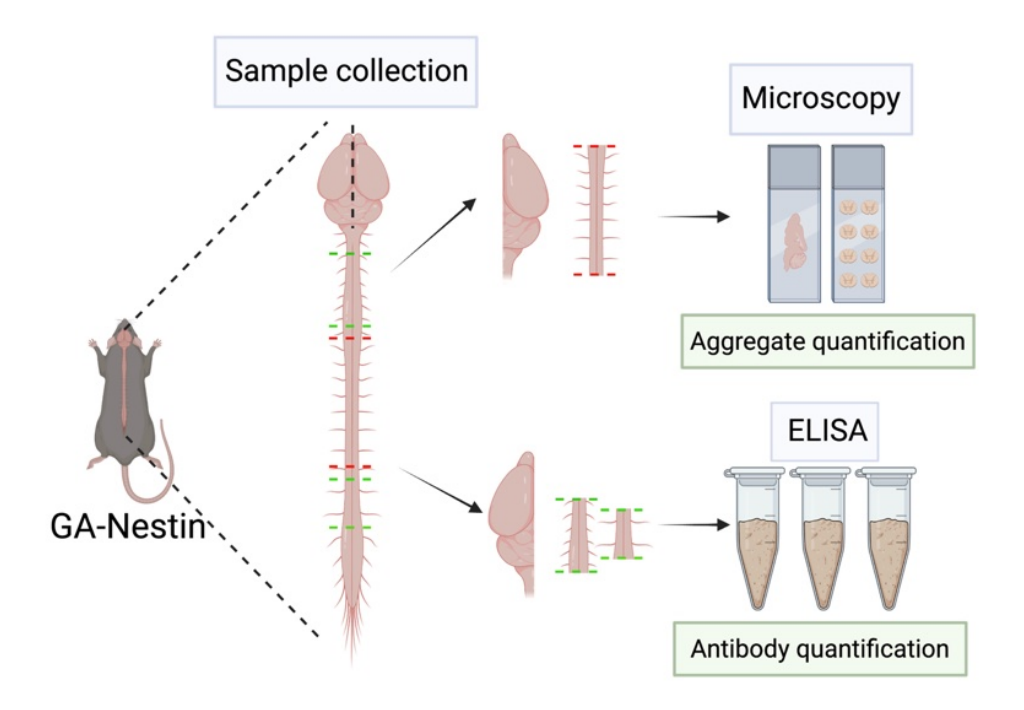


Figure 10: Sample collection from GA-Nestin

Nervous tissue from the right hemisphere and from the thoracic spine (T4-T13) was collected for aggregate quantification by microscopy and the left brain hemisphere cervical/thoracic spinal cord (C3-T3) and lumbar spinal cord (L1-L4) parts were used for antibody quantification with ELISA. Created with BioRender.com.

3.11 Staining of animal sections

The right brain hemisphere and thoracic part of spinal cord were stained for visualizations of the antibody distribution after ICV injection, for visualizations of exclusively neuronal expression and for comparison of the extent of poly-GA aggregation between the treatment and the control groups. The right brain hemisphere was cut in half sagittally. The spinal cord was cut transversally to 1 mm thick pieces. Afterwards both sample types were embedded in paraffin to create blocks for cutting. The blocks were cut with a microtome in 5 μ m thick tissue samples and were rested on a glass slide. The sections underwent a deparaffinization in the following order:

- 1. Xylol 100%. Rinsing and 15 minutes incubation.
- 2. Xylol 100%. Rinsing.
- 3. Ethanol 100%. Rinsing.
- 4. Ethanol 100%. Rinsing and 5 minutes incubation.
- 5. Ethanol 96%. Rinsing.

- 6. Ethanol 70%. Rinsing.
- 7. Ethanol 70%. Rinsing.

Sections were then heated up in citrate buffer for 15 minutes in microwave oven and left to cool down at room temperature for 20 minutes.

3.11.1 Immunohistochemistry of nervous tissue

For immunohistochemistry staining, sections were placed for 15 minutes in 5% H₂O₂/MeOH solution at room temperature in order to inhibit the endogenous peroxidase and prevent targetless staining after citric buffer incubation. Sections were then washed under running cold water for 5 minutes. Next, sections were incubated for 60 minutes in permeabilization and blocking buffer at room temperature. Afterwards they were incubated in primary antibody solution diluted in 10% BS in PBS at 4° C. To present the AAV transgene expression in different parts of nervous system and to establish the most effective injection timepoint anti-GFP antibody in 1:500 dilution was used. To visualize the microglial response and poly-GA aggregation at the hippocampus site anti-Iba1 (1:500) and biotinylated anti-GA (1:500) primary antibodies were used. The sections were afterwards carefully washed with washing buffer. DCS Detection Kit 2, implementing a 3'-3'-Diaminobenzidine (DAB) reaction with Horseradish peroxidase, was used for staining. Afterwards, the sections were stained with hematoxylin to visualize the nuclei. The slides were carefully rinsed in a row of alcohol solutions in opposite direction to deparaffinization step in order to get rid of water residues on the slides. The slides were than covered with a cover glass with Eukitt mounting medium.

3.11.2 Immunofluorescence of nervous tissue

In immunofluorescent stains of animal nervous tissue the deparaffinization, antigen retrieval, washing, blocking and primary antibody incubation steps were done on 5μm paraffin sections the same way as described above. The H₂O₂/MeOH incubation step was omitted. After incubation in primary antibody solution (anti-NeuN, anti-GFAP, anti-Iba1, biotinylated anti-GA, anti-HA – 1:500; anti-Myc – 1:250) in 10% BS in PBS at 4° C and careful washing with washing buffer, the sections were incubated in secondary antibody solution of Alexa Fluor antibodies in 10% BS in PBS (Alexa Fluor 488 Mouse anti-rat, Alexa Fluor 555 Mouse anti-rabbit or Alexa Fluor anti-streptavidin 488) in 1:250 dilution for 1 hour at room temperature. The samples were then mounted with Fluoromount G mounting medium and incubated overnight at 4° C.

3.11.3 HE stains

Sections were deparaffinized the same way as described above. All incubation steps were done at room temperature. Sections were incubated for 5 min in hematoxylin solution and then washed for 10 minutes under warm tap water. Sections were then rinsed in 70% ethanol and incubated for 3 minutes in alcoholic eosin solution. After that they were rinsed in 70% and then in 96% ethanol and incubated for 5 minutes in 100% Xylol. Finally, each slide was covered with cover-glass by means of Eukitt mounting medium.

3.11.4 Nissl stains

Sections were deparaffinized the same as described above. Sections were incubated in 70% ethanol at 40° C overnight. On the next day, sections were rinsed in distilled water and incubated for 30 minutes in cresyl violet. Afterwards, they were carefully rinsed one solution after another in distilled water, 96% ethanol, 4% glacial acetic acid in ethanol, 100% ethanol and incubated in 100% isopropanol for 10 minutes. The sections were then transferred to 100% xylol from which they were taken out, dried and covered with a cover-glass by means of Eukitt mounting medium.

3.11.5 Automatic poly-GA aggregate quantification

To investigate the therapeutic effect of the AAV-mediated anti-GA antibody therapy, I quantified poly-GA aggregates in immunofluorescent stains of brain and spinal cord sections. Biotinylated anti-GA and anti-HA primary antibodies in 1:500 dilutions were used to stain the poly-GA aggregates and the antibody respectively as described above. Imaging of frontal cortex, hippocampus and of spinal cord was done with help of confocal microscopy with 40x magnification objective and the images were saved as 1080x1080 pixel RGB files. The green channel represented the poly-GA aggregates and the red channel the recombinant HA-tagged antibody. A Python script with implementation of scikit-image library was used to automatically process the green channel signal and to unravel and count the aggregates. The scikit-image library functionality enabled representation of each pixel as a value of signal intensity. Moreover, it provided necessary tools to turn off pixels – set their intensity value to 0, which did not reach an arbitrarily set minimum intensity value. On the other hand, pixels' intensity value meeting the minimum intensity value were set to 1. Afterwards, it was possible to identify the represented by 1, neighbouring pixel-groups and to define them as objects. For those objects an arbitrary minimum size was set. Pixels of objects smaller than the arbitrary minimum size were also turned off. In this way the final, processed image emerged. The minimum intensity value of 70 and minimum object size of 400 pixels were applied, which allowed to specifically mark compact aggregates. The minimum values were determined empirically and considered which value pair resulted in possibly closest to zero aggregate count in the green channel signal of healthy individuals.

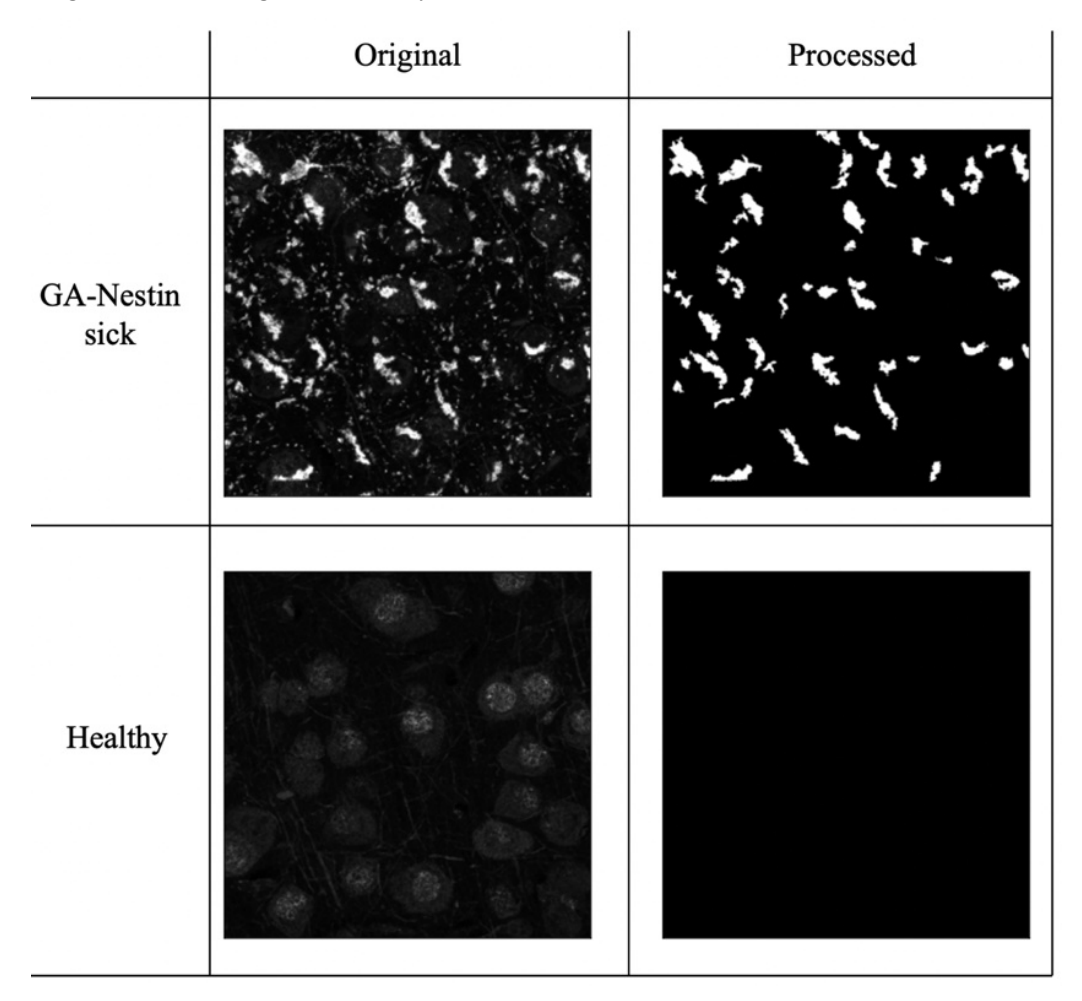


Figure 11: Automated quantification of the poly-GA aggregates from the green channel of immunofluorescent nervous tissue stains

To investigate whether AAV-mediated anti-GA antibody therapy shows therapeutic effect in GA-Nestin mice, poly-GA aggregate number of the treatment group was compared with control group. Automatic quantification with use of scikit-image library was implemented. After filtering out the pixels with lower intensity than 70 and then filtering the objects of smaller size than 400 pixels from the green channel of an 1080x1080 RGB image a processed image emerged.

3.11.6 NMJ staining of muscle tissue

The innervation in neuromuscular junction (NMJ) was compared between the experimental groups in GA-Nestin to assess the effectiveness of the AAV-mediated anti-GA therapy. Quadriceps femoris muscle of mice was harvested as described above and was fixated in 4 % PFA for 2 hours on ice. Samples were then transferred to 4°C PBS and from there embedded in 3% agarose in PBS. 50-100 μm slices were cut on a vibratome and placed on a microscopy slide. Samples were then incubated in 100 μl droplet of blocking buffer. Alexa Fluor 555 Mouse anti-β-Tubulin III in 1:100 dilution and Alexa Fluor 647 labelled Bungarotoxin in 1:250 dilution in BB were used to incubate samples for 72 hours at 4°C. Slides were then washed with PBS on a shaker for 30 minutes. The slides were finally mounted with Fluoromount G. The imaging was done with the confocal microscope for each sample at 5 multiple sites where NMJ was visible. Connection of β-Tubulin III labelled axons to Bungarotoxin labelled endplates was investigated and the ratio of NMJs with full connection to those with lacking connection was established.

3.12 ELISA

Concentrations of the antibody expressed in different parts of the mice's nervous system after the ultrasound-guided ICV AAV injection (see 3.8) was determined by enzyme-linked immunosorbent assay (ELISA).

3.12.1 Sample preparation

Nervous tissue obtained after the PBS perfusion (see 3.10) was divided into four regions: forebrain – the cortex of the brain, hindbrain – the thalamus, the cerebellum and the brainstem, cervical spinal cord – segments C3-T3 and lumbar spinal cord – segments L1-L4. Samples were placed into tubes designed for tissue homogenization. CK14 tube (Precellys) was used for brain and MK28 tube (Precellys) for spinal cord samples. 300 µl of RIPA Buffer with Protease (1:100) and Protease/Phosphatase (1:1000) Inhibitor Cocktail was added to the samples which were then homogenized with a tissue homogenizer (Precellys). Homogenized samples were centrifuged at 13000 rpm, 4° C for 10 minutes. A rich in protein supernatant was collected. The protein concentration was determined with BCA (see 3.7.2).

3.12.2 Immunodetection

ELISA was performed in 96-well plate. The plate was first coated with 100 μ l GST-(GA)₁₅ or GST-(PR)₁₅ 2 ng/ μ l overnight at 4° C. The plates were washed with washing buffer and the

plate was blocked with 300 μ l of blocking buffer for 1 hour at room temperature. Knowing the protein concentration of the samples, appropriate sample volume containing 1 μ g of protein diluted in 100 μ l blocking buffer was added to the wells and left for 1 hour at room temperature. After washing with washing buffer, anti-mouse HRP-antibody solution 1:2000 in blocking buffer was added and the plate was incubated for 1 hour at room temperature. The plate was washed with washing buffer and 100 μ l of TMB solution was pipetted to each well and incubated for 5 minutes at room temperature. To stop the chromic reaction induced by TMB, 50μ l H_2SO_4 was added to each well. The absorption at 450 nm wavelength was measured with a photometer. The antibody concentrations were determined from known concentrations of purified 1A12 or 32B3 antibody in BB by using a standard four parameter logistic curve with help of Myassays.com platform.

3.13 Barnes maze

A variation of Barnes maze was used to test learning and memory of 16 weeks old GA-Camk2A mice. Animals were trained to escape an undesirable situation of being placed in the centre of a light-exposed, circular maze containing 19 closed holes and a single open escape hole. The objective was to monitor their learning process and to measure their behaviour when the memorized escape hole was blocked. The experiment was divided into two parts. First part constituted of four days of learning sessions. During these sessions the mice were placed in the middle of the maze and left to explore freely. Due to light-exposure they were motivated to seek shelter in the predefined escape hole. Spatial visual cues were placed in the room around the maze to augment the learning process. The time to find the escape hole was used to track the learning process. If the mouse did not manage to find the escape hole in the maximum allowed time of 2 minutes, it would be gently guided by the tail to the escape hole. In the second part of the experiment – on the 5th day, the escape hole was covered and behaviour of mice on the maze was recorded for 5 minutes. An escape zone, constituting of the hole, which was available for escape route in the learning part and of two neighbouring holes, was defined. The behaviour of mice was recorded with a camera placed directly above the maze. The number of times the mice entered this zone in the testing part and the overall time they spent there were recorded and later measured with help of Anymaze software.

Following points were also considered in the experimental procedure:

- Prior to the actual experiment, mice were habituated to the experimenter. They were placed on the hand of the experimenter and were let to explore the back of the hand freely for 1 minute per day for a week.
- Before the start of any session mice were held in separate holding cages and were left for 20 minutes to acclimate to the experimental room prior to each session.
- Prior to their first recorded run, mice were placed on the maze and left to acclimate to
 the environment for 1 minute. Afterwards, they were guided by the tail to the escape
 hole.
- After every mouse run the whole maze was disinfected with 70% ethanol and allowed to dry completely before the next mouse entered the maze in order to eliminate any olfactory cues.



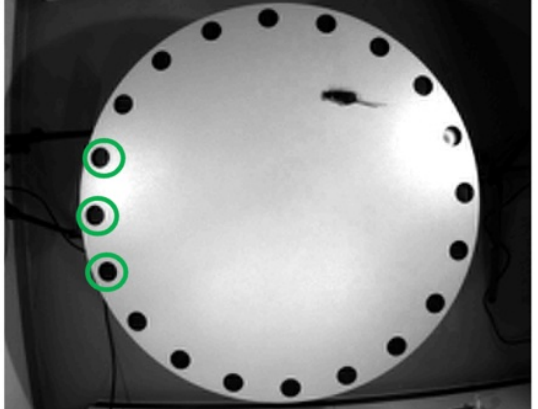


Figure 12:Barnes maze setup

On the left: the cognitive function of GA-Camk2A experimental group was investigated at 16 weeks of age by means of Barnes Maze. Strong lighting from the top motivated mice to seek shelter and escape the maze. Mice were learning how to escape the Maze with help of additional shape queues around the platform (red arrows). Prior to testing mice were kept in darkened space in the same room (blue star). On the right: the performance and cognitive function was assessed by measuring how many times the mice entered and how much time in total they spent at the escape hole and immediately neighbouring holes. Together the three holes with the escape hole in the middle constituted the escape zone (green circles).

3.14 Genotyping

3.14.1 DNA preparation

About 0.5 mm skin punch from earmarking the mouse, was incubated in 200 μl of 20 mg/ml Proteinase K in lysis buffer solution at 55° C, 700 rpm overnight. Sample was then centrifuged for 5 minutes at 13000 rpm at room temperature. 300 μl of 100% isopropanol was added to the supernatant and incubated for 10 minutes at room temperature to precipitate the DNA. The sample was centrifuged for 20 minutes, at 4°C, 13000 rpm. The pellet was washed with 300 μl of 75% ethanol and again centrifuged for 10 minutes at 4° C at 13000 rpm. The pellet containing DNA was left to dry for 15 minutes and then dissolved in 400 μl H₂O. The DNA solution was then incubated for 15 minutes at 56° C, 500 rpm on a thermoblock and polymerase chain reaction (PCR) genotyping was performed.

3.14.2 PCR

Both in case of GA-Nestin and GA-Camk2A mouse line the genotyping was done by determining the presence of Cre-Recombinase and GA-GFP sequences in the genome. 1 μ l of isolated DNA sample was mixed with 24 μ l of mix-solution made of: 18.9 μ l RNase Free H₂O, 5 μ l 5x GoGreen PCR Buffer, 0.5 μ l of 20 μ M primer solution, 0.5 μ l of dNTPs and 0.125 μ l Taq Polymerase. The PCR was carried out under following conditions:

Table 1: PCR setup for genotyping

Number of cycles	Step	Temperature	Time
1	Initialization	95°C	5 minutes
35	Denaturation	95°C	30 seconds
	Annealing	58°C	30 seconds
	Extension	72°C	45 seconds
1	Final extension	72°C	5 minutes

3.14.3 Electrophoresis

Electrophoresis was implemented to separate the proteins in the PCR samples. Samples and marker for DNA electrophoresis were placed in 1% agarose in SB gel and 120 V current was applied. The agarose gel was additionally prepared with fluorescent nucleic acid stain GelRed in 1:2000 dilution for visualization with UV camera.

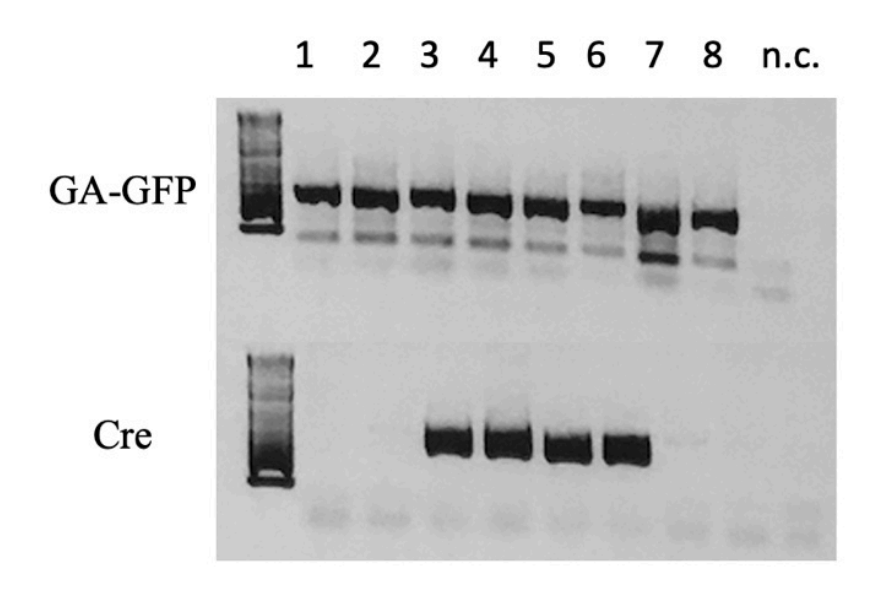


Figure 13: Example of genotyping done for GA-Nestin and GA-Camk2A mice.

Bands from the left: marker for DNA electrophoresis, exemplary samples from 1 to 8, negative control (n. c.) - water. For the top row the GA-GFP primer was used to detect GA-GFP gene, whereas on the bottom the Cre-Recombinase gene was detected. Animals positive for both genes were suffering from poly-GA aggregation and showed symptoms of C9-ALS/FTD.

4 Results

Antibody therapy directed against DPR protein aggregates has recently shown a lot of success in treatment of C9-ALS/FTD (Nguyen et al., 2020; Zhou et al., 2020). However, so far, no approach using AAV as a vector for DPR-targeted antibody expression in neurons has been tried. Here, the AAV 2/9-mediated anti-GA therapy was attempted on two poly-GA expressing mouse models. By utilizing this approach, the antibody was expressed directly in the brain and bypassed the blood-brain barrier (BBB). BBB usually constitutes a main problem in reaching high antibody titre in the nervous tissue in different forms of antibody therapy (Kouhi et al., 2021). The strategy to test the AAV-mediated anti-GA antibody therapy was to validate the AAV transduction in neuronal cell culture, observe the antibody expression *in vivo* and subsequently to test the therapy on two poly-GA expressing mouse lines: GA-Nestin and GA-Camk2A.

4.1 AAV-transduced primary rat neurons expressed functional anti-GA and anti-PR antibodies

Prior to investigating the efficacy of the AAV-mediated antibody therapy on mouse models, I tested antibody expression after AAV transduction in primary rat neurons. In addition, the antibodies' ability to bind to the corresponding DPR target proteins was investigated. To achieve these aims, I designed AAV which consisted of an AAV 2 genomic backbone with antibody transgene and AAV DJ8 capsid (see 3.5). In order to demonstrate the antibody expression in neurons, immunofluorescent stains of HA-tagged heavy chain and myc-tagged light chain were prepared and images were obtained with a confocal microscope. In the cytoplasm of some neurons, signal for HA and myc expression was detectable for anti-GA and anti-PR antibody compared to the non-transduced negative control. This indicated that the AAV transduction with the newly made AAV2/DJ8 virus led to antibody expression in neurons.

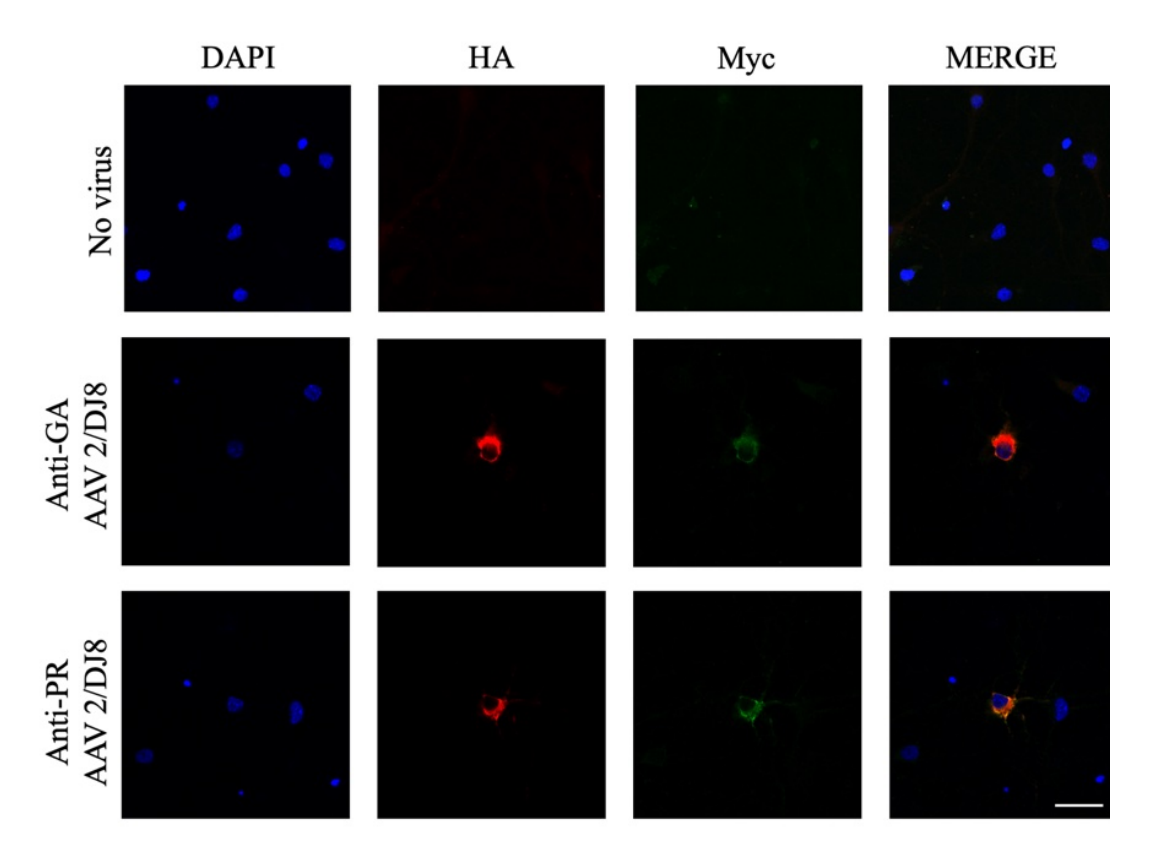


Figure 14: Immunofluorescent stains of primary rat neurons transduced with AAV 2/DJ8 showed antibody expression

To demonstrate expression of antibody in primary rat neurons immunofluorescent stains were prepared. DAPI signal represented cell nuclei. HA-tag was present on the antibody's heavy chain and myc-tag on the light chain. AAV 2/DJ8 carrying the anti-GA or anti-PR antibody transgene transduced neurons resulting in antibody expression. Scale bar = $30\mu m$.

To determine whether a functional antibody was also secreted from the neurons, I used immunoblotting. Here, supernatant from the cultured, AAV 2/DJ8 transduced neurons was used as the primary antibody for immunoblot detection of lysates of HEK293 cells transfected with GFP-(GA)₁₇₅ or GFP-(PR)₁₇₅ expression plasmids (see 3.7). As a positive control, supernatants from the original hybridoma cells expressing 1A12 anti-GA and 32B3 anti-PR were used for detection. The results from blots indicated that the antibody present in the supernatant bound to its corresponding DPR protein.

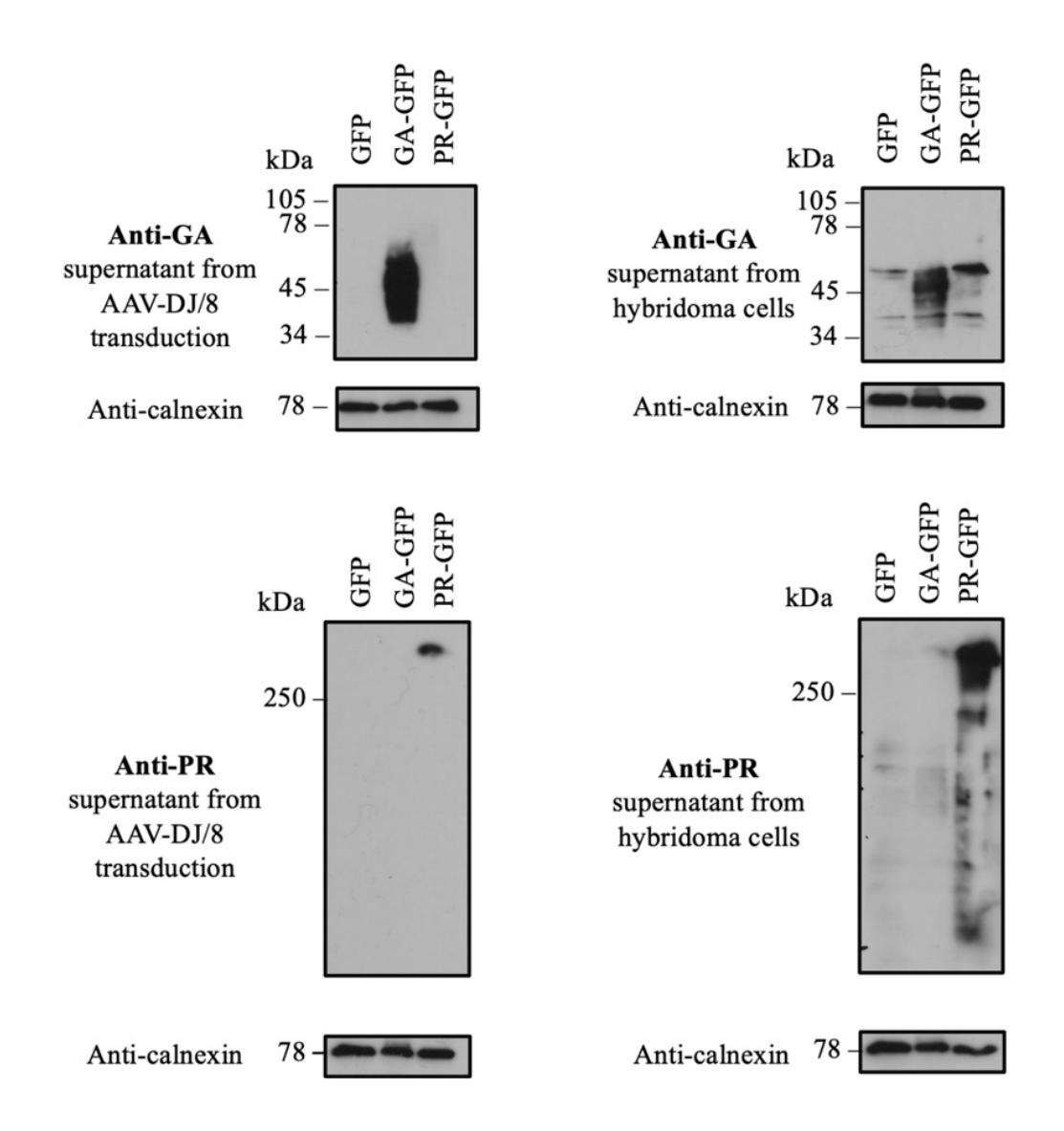


Figure 15: Immunoblots: anti-GA and anti-PR antibodies secreted from AAV2/DJ8 transduced neurons bound to corresponding DPRs

Cell culture supernatant of AAV 2/DJ8 transduced rat primary neurons was used as a source of primary antibodies for immunoblotting. The antibodies from the supernatant bound HEK293 cell-derived GFP-(GA)₁₇₅ and GFP-(PR)₁₇₅. This showed that AAV-transduced neurons secreted antibody out of the cell which then bound to aggregates. Note that poly-PR aggregates were found in the pockets of the gel. 1A12 and 32B3 hybridoma supernatants were used as positive controls.

These findings showed that neurons that have been transduced with AAV containing the monocistronic expression constructs for anti-GA or anti-PR expressed and secreted functional antibodies. Furthermore, these studies provided a foundational framework for the development and evaluation of an AAV-system with AAV 9 capsid more suitable for neuronal transduction *in vivo*.

Since capsid of AAV 9 shows very good neuronal transduction rate in neonatal mice (Chakrabarty et al., 2013), ultimately, AAV 2/9 was intended for the *in vivo* therapy. To achieve sufficient titre of the virus for *in vivo* experiments the packaging and purification was outsourced to the research group of Prof. Thomas Misgeld from TU Munich. Subsequently, the above-described experiments with the in-house packaged AAV 2/DJ8, were repeated with a concentrated AAV 2/9 (10¹² viral copies/µl). As in case of AAV 2/DJ8, neurons transduced with AAV 2/9 expressed the tagged heavy and light chains of antibody, as detected by immunofluorescent stains. The secretion of the antibody from the cell and its ability to bind the aggregates was demonstrated again with immunoblot.

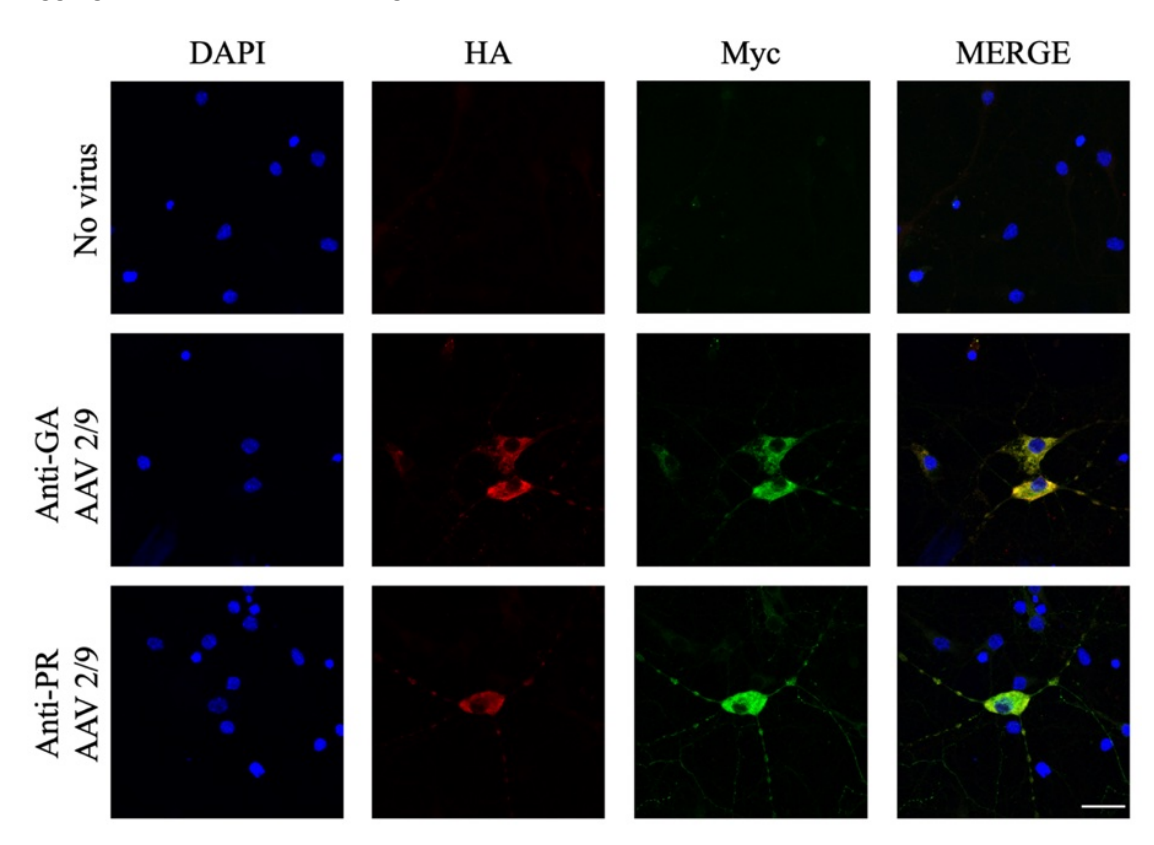


Figure 16: Immunofluorescent stains of primary rat neurons transduced with AAV 2/9 revealed antibody expression

As in visualizations for AAV 2/DJ8, DAPI signal represented cell nuclei. HA- and myc- tags were within the protein structure of the antibody on the heavy and on the light chain respectively. Signal colocalization of HA and myc in the cytoplasm of neurons indicated antibody expression after AAV 2/9 transduction for both anti-GA and anti-PR antibodies. Scale bar = 30μ m.

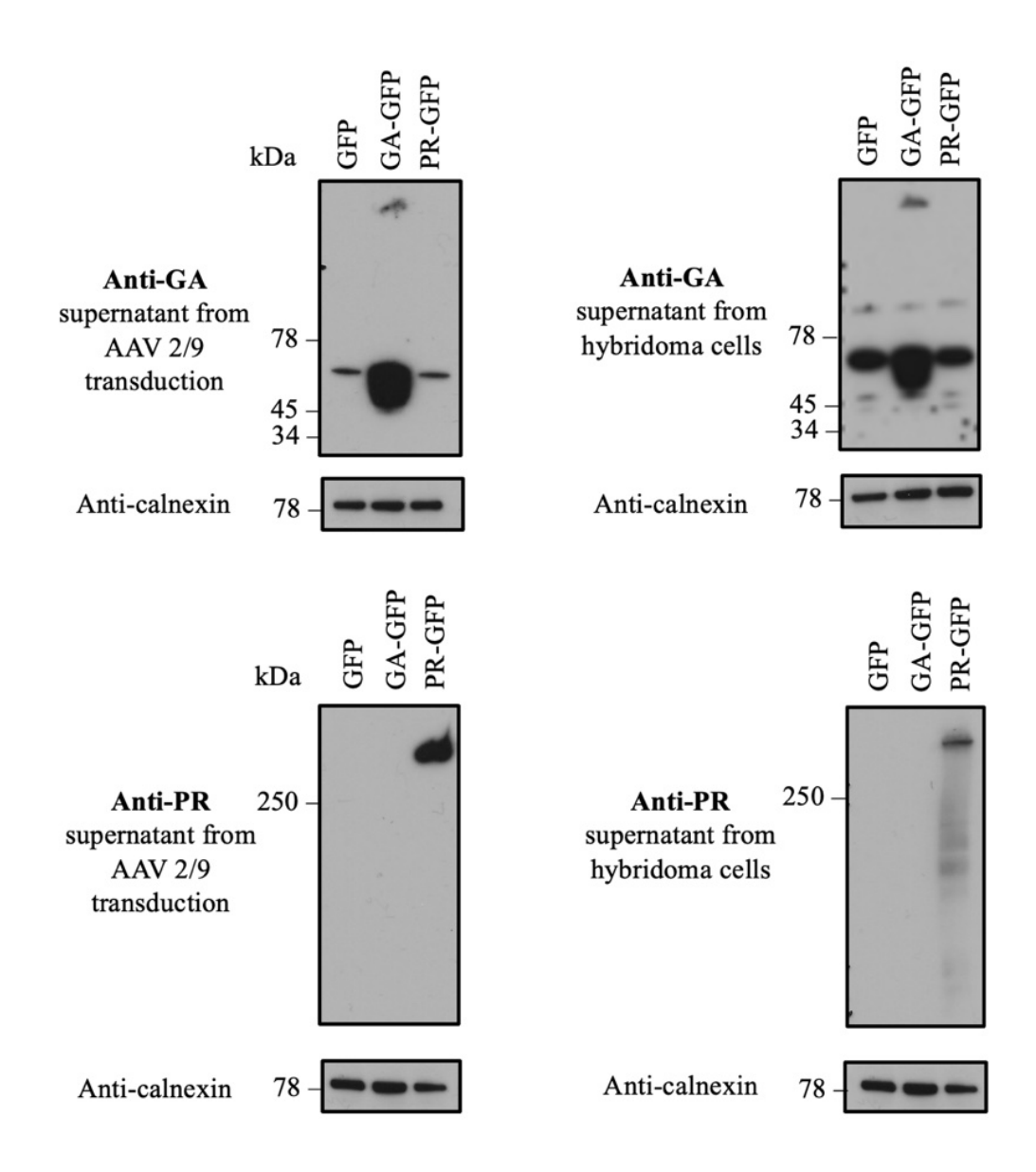


Figure 17: Immunoblots: anti-GA and anti-PR antibodies secreted from AAV 2/9 transduced neurons bound to corresponding DPRs

Capsid of AAV serotype 9 has proven to be well fitted for transduction of nervous tissue. Cell culture supernatant from AAV 2/9 transduced primary rat neurons was used for immunoblotting as primary antibody. The antibodies present in the supernatant specifically bound to the GFP-(GA)175 and GFP-(PR)175. AAV 2/9 transduced neurons expressed and secreted anti-GA or anti-PR antibodies which bound to poly-GA- and poly-PR respectively. 1A12 and 32B3 hybridoma supernatants were used as positive controls.

In summary, primary rat neurons transduced with the AAV 2/9 were expressing and secreting functional antibody binding specifically to the corresponding DPR target proteins. This demonstrated the functionality of the AAV 2/9 system and allowed its application in *in vivo* testing.

4.2 AAV injection in newborn pups led to widespread transgene expression in the nervous system

To improve the AAV transduction efficacy and the antibody expression in the brain, I used an ultrasound-guided ICV injection system (Wang et al., 2022). To investigate in which areas of the nervous system the transgene expression occurs and to establish the best timepoint for injection, C57BL/6 pups were injected with an AAV 2/9 with a Cre-GFP transgene at different postnatal timepoints. Mice were sacrificed by the age of 21 days and their brain and spinal cord were collected for immunohistochemistry stains of Cre-GFP. Since previous reports state that the timepoint of injection using conventional ICV plays an important role in the effectiveness of AAV transduction (Chakrabarty et al., 2013), pups were divided into two groups where one was injected on postnatal day one (P1, N=9) and the other on postnatal day three (P3, N=7). This allowed to estimate the best timepoint for ultrasound-guided ICV injection resulting in the most robust and widespread transgene expression. Injections at both P1 and P3 showed expression of Cre-GFP in the brain and in the spinal cord. Although both P1 and P3 groups showed robust transgene expression in the periventricular area, the P1 group showed a more prominent expression in frontotemporal cortex, which was consistent with previous reports (Chakrabarty et al., 2013). Overall, the ultrasound-guided approach for ICV injection has proven to be a viable method to test the therapeutic AAV on C9-ALS/FTD mouse models and the P1 injection timepoint appeared to have a slightly better transgene expression pattern than P3 timepoint, which is why it was used in the therapy experiments.

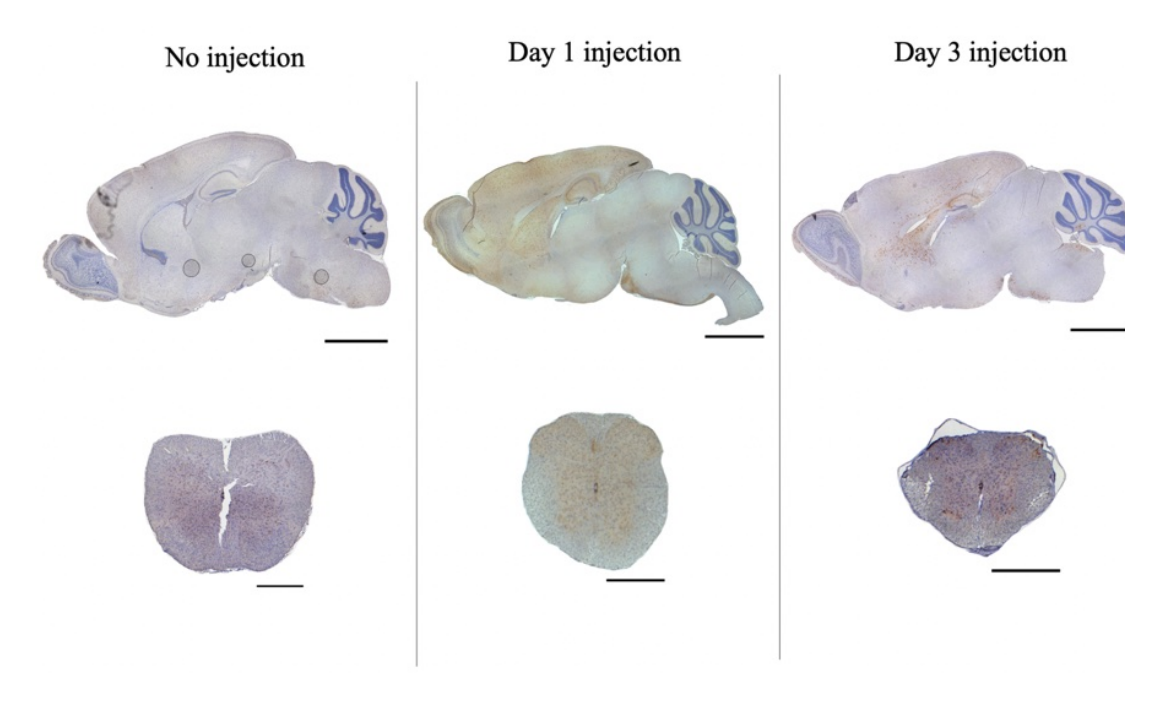


Figure 18: Immunohistochemistry stains of Cre-GFP in brains and spinal cords of 21-days old C57/BL6 mice after AAV injections done 1 and 3 days after birth

ICV injection allows for AAV application directly into cerebrospinal fluid of the lateral ventricle of the brain in neonatal mice. AAV 2/9 solution carrying a transgene for Cre-GFP protein was injected at P1 (day 1 injection) and P3 (day 3 injection) pups. At day 21 mice were sacrificed to analyse transgene expression by immunohistochemistry (brown staining) in the brain (upper row) and the spinal cord (bottom row). Both P1(middle panel) and P3 (right panel) groups showed widespread transgene expression. P1 group showed more profound Cre-GFP expression in the frontotemporal cortex and a distinct expression in spinal cord. Representative images are shown. Scalebar in brain samples=2.5 mm. Scalebar in spinal cord samples=0.5 mm.

4.3 Antibody expression was exclusive to neurons using the hSynapsin promoter

The hSynapsin promoter driving the expression of therapeutic antibodies is thought to restrict the transgene expression to neurons (McLean et al., 2014). To visualize this expression pattern for the experimental antibody, C57BL/6 pups were injected with the AAV 2/9 either with the anti-GA (N=4) or anti-PR (N=4) antibody transgene. Mice were sacrificed at 21 days of age and their brain tissue was collected for immunofluorescent staining. To demonstrate in which cells antibody expression took place the myc-tag of anti-GA or anti-PR antibody was stained together with either the neuronal marker NeuN, the astrocyte marker GFAP or the microglia marker Iba1. Both antibodies, detected with anti-myc staining, colocalized only with the NeuN⁺ neurons. Neither astrocytes, represented by GFAP signal, nor microglia showing Iba1 signal

showed colocalization of myc signal. This demonstrated that the anti-GA and anti-PR antibodies were expressed predominantly in the neurons and not in other cells.

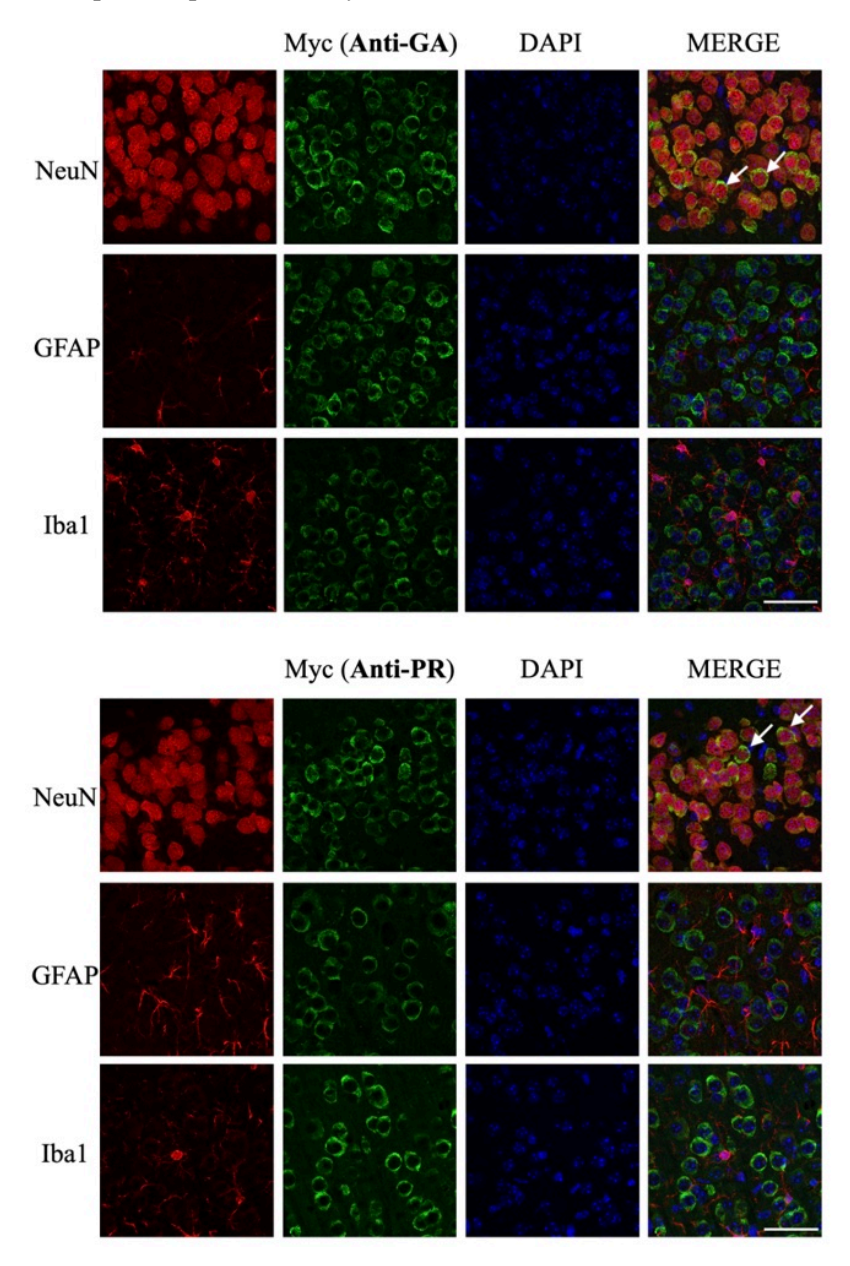


Figure 19:Anti-GA and anti-PR antibodies were expressed exclusively in neurons after AAV 2/9 ICV injection

Human Synapsin promoter, driving antibody transgene, allowed antibody expression restricted to neurons. Myc-tag staining was used to visualize antibody expressed in the cells. NeuN protein labelled neurons, GFAP astrocytes and Iba1 microglia. The myc antibody signal appeared in the cytoplasm of neurons (exemplarily indicated by white arrows), but not in astrocytes or in the microglia. Antibody expression for both anti-GA and anti-PR antibodies was restricted to neurons. Scale bar = $50 \mu m$.

4.4 GA-Nestin therapy – study design

To test AAV therapy *in vivo* I started with the fast-progressing GA-Nestin line. Mating ROSA26 GFP-GA175^{+/+} and Nestin-Cre^{+/-} resulted in a close to 1:1 ratio of affected GA-Nes⁺ and healthy GA-Nes⁻ mice without Cre recombination (Figure 5). As the experimenter, I was blind to the genotype of the mice and to the injected AAV variant. After AAV injection on postnatal day 1, three groups emerged as shown in the Table 2:

Table 2: Experimental groups in GA-Nestin mouse line experiments

	GA-Nes ⁺ /Anti-GA	GA-Nes ⁺ /Anti-PR	GA-Nes ⁻
Number of animals	6	10	15
harvested at 4 weeks of age			
Description	Affected mice which	Affected mice which	Healthy mice which
	received the	received the control	received either Anti-GA
	therapeutic Anti-GA	Anti-PR	or Anti-PR AAV
	AAV	AAV	

At 4 weeks of age mice were weighed and their nervous and muscle tissue was harvested for analysis.

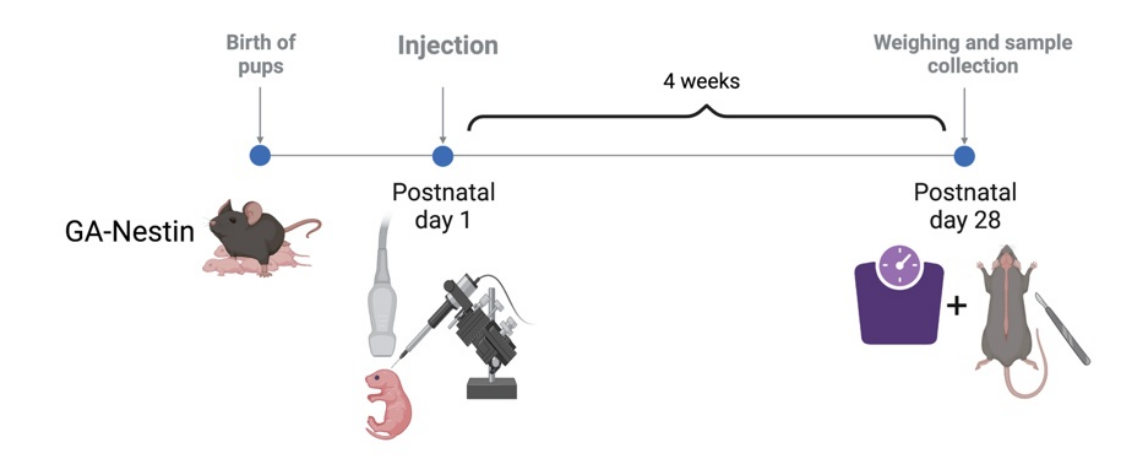


Figure 20: Experimental design for AAV therapy in GA-Nestin mouse line.

Pups of GA-Nestin mousse line underwent the ICV AAV injection at P1. 4 weeks later their final weight was measured, and the nervous tissue was harvested for antibody and poly-GA quantification. Created with BioRender.com.

4.5 Slower rate of weight gain of GA-Nes⁺ was not mitigated by the AAV-mediated anti-GA antibody therapy

It was previously described that GA-Nestin mice gain weight slower than their healthy littermates and lose weight from the fourth week on. The difference in weight between GA-Nestin mice and healthy littermates is visible already at 3 weeks of age (LaClair et al., 2020). Hence, the weight of mice at 4 weeks was taken as an indicator for therapy efficacy. GA-Nestin mice and their healthy littermates underwent an ICV AAV 2/9 injection at postnatal day 1 to express therapeutic anti-GA or the control anti-PR antibody transgene directly in the nervous system. Unfortunately, no significant difference in body weight was observed when comparing symptomatic GA-Nes⁺ mice which received the anti-GA antibody AAV treatment (GA-Nes⁺/Anti-GA) (N=12) with the ones which received the control anti-PR antibody AAV (GA-Nes⁺/Anti-PR) (N=11). Healthy littermates (GA-Nes⁻) (N=18), weighed significantly more (on average 4.5 g more) than the affected GA-Nestin mice. Data from mice not used for further biochemical and histological analysis in this work was pooled with the mice harvested for further analysis in this work, which enhanced the sample sizes.

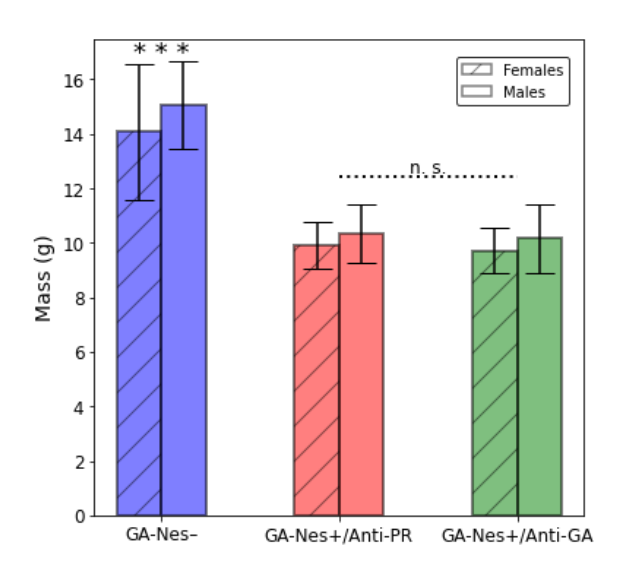


Figure 21: AAV-mediated antibody therapy did not prevent weight loss in GA-Nestin mice

GA-Nestin mice present phenotype of suppressed weight gain. Neonatal GA-Nestin and their healthy littermates underwent an ICV injection of treatment and control AAV. Body weight of the mice was measured at 4 weeks after birth. The AAV-mediated anti-GA treatment did not prevent the suppressed weight gain of GA-Nestin mice. GA-Nestin mice weighed significantly less than their unaffected littermates. Female and male mice are plotted separately, but statistical testing was performed with both genders combined, because no difference was visible between the genders.

N= [18,11,12], ANOVA: F (2,38)=45.41, p<0.001

Tukey's Post Hoc Test:

GA-Nes⁺/Anti-GA and GA-Nes⁺/Anti-PR: p=0.9.

GA-Nes- and GA-Nes+/Anti-GA: p<0.001.

GA-Nes $^-$ and GA-Nes $^+$ /Anti-PR: p < 0.001.

4.6 Antibody expression after ICV AAV injection was the most profound for anti-GA in the forebrain

To make sure that AAV ICV injection results in expression and secretion of functional anti-GA antibody *in vivo* and to better understand the expression pattern in the nervous system, I quantified the amount of antibody expressed in different parts of the nervous system of GA-Nestin mice with ELISA (see 3.12). I used recombinant DPR proteins – Glutathione S-Transferase (GST)-(GA)₁₅ and GST-(PR)₁₅ coated on 96-well plates that were incubated with tissue extracts from different regions of the nervous system. Lysates of forebrain, hindbrain, spinal cord (C3-T3) and lumbar spinal cord (L1-L4) were examined separately. The concentration of the antibody was compared to recombinant anti-GA and anti-PR standards in ELISA. Statistical analysis was done by means of one-way ANOVA and Tuckey's post-hoc test. Overall, anti-GA and anti-PR antibodies showed similar regional expression patterns

showing the greatest antibody concentration in the forebrain. Lower antibody expressions were observable in the hindbrain and in the spinal cord. Anti-GA forebrain expression was significantly greater than forebrain expression of anti-PR and higher than antibody expression in parts of the nervous system further away from the injection site. Antibody expression for all other groups did not differ from each other significantly. Altogether, the antibody expression was not homogenous between different parts of the nervous system. The highest antibody expression was detected in forebrain, which is closest to the injection site in the lateral ventricle.

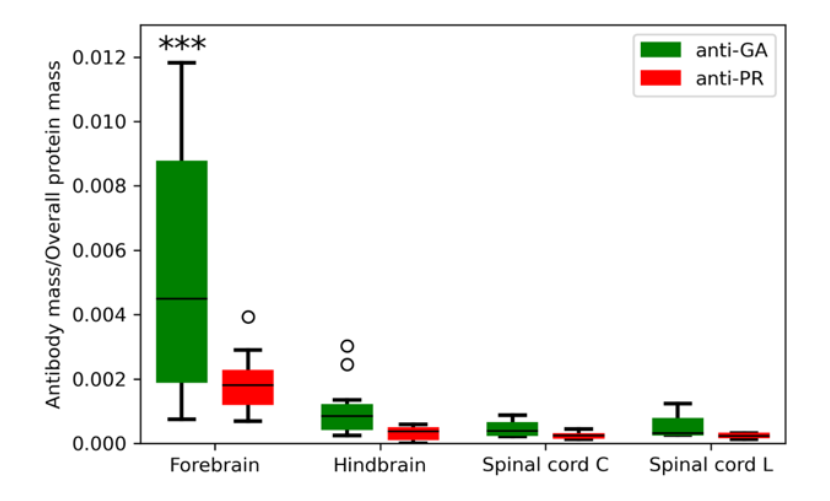


Figure 22: Antibody expression in different brain regions measured by ELISA

ICV AAV injection led to uneven antibody expression in the central nervous system of mice. ELISA was used to quantify the antibody weight per overall protein weight of sample. Anti-GA concentration in the forebrain was significantly higher than any other antibody concentration.

N = [12, 15, 14, 12, 10, 10, 9, 10], ANOVA: F(7, 84) = 14.10, p < 0.001

Tukey's Post Hoc Test: Anti-GA forebrain compared with other groups: p < 0.001. No statistically significant differences between other groups.

4.7 The AAV-mediated anti-GA therapy did not reduce neurodegeneration and inflammation in the hippocampus of GA-Nestin mice

According to previous reports GA-Nestin mice show signs of neuronal loss, especially in the hippocampus already at the age of 3 weeks (LaClair et al., 2020). The area most prone to neurodegeneration is the Cornu Ammonis (CA)-2 region of the hippocampus (LaClair et al., 2020). Thus, I tested whether the AAV-mediated anti-GA antibody therapy could potentially

slow down the neurodegeneration in this region using Hematoxylin-Eosin (HE) and Nissl stains (see 3.11) of the hippocampal region of 4-week-old GA-Nestin mice and of healthy littermates. A decrease in density of neurons in hippocampus in affected GA-Nestin animals was observed, especially in CA-2 hippocampal region. However, no recognizable difference in neurodegeneration pattern was visible between the anti-GA antibody treated group (N=4) and the control anti-PR antibody group (N=4). The therapeutic effect was also investigated by comparing poly-GA aggregation in the hippocampus by immunochemistry staining of poly-GA. In some cases of anti-GA antibody treatment, the extent of poly-GA aggregation seemed to be lower than in the control group but the difference was not profound, as exemplarily shown in the third row in the figure below. Thus, aggregates were quantified in immunofluorescent stains (see 4.8). Furthermore, LaClair et al. (2020) reported a strong microglial response in GA-Nestin mice in hippocampal region. To investigate whether this response can be changed by the therapy, immunohistochemistry stains of Iba1 were performed. In case of the affected GA-Nestin mice both the GA-Nes⁺/Anti-GA and the GA-Nes⁺/Anti-PR groups were showing signs of neuroinflammation of similar extent compared to the GA-Nes control group. Altogether, AAV-mediated anti-GA antibody expression did not show obvious positive effect on the neurodegeneration and neuroinflammation in 4-week-old GA-Nestin mice in histopathological stains.

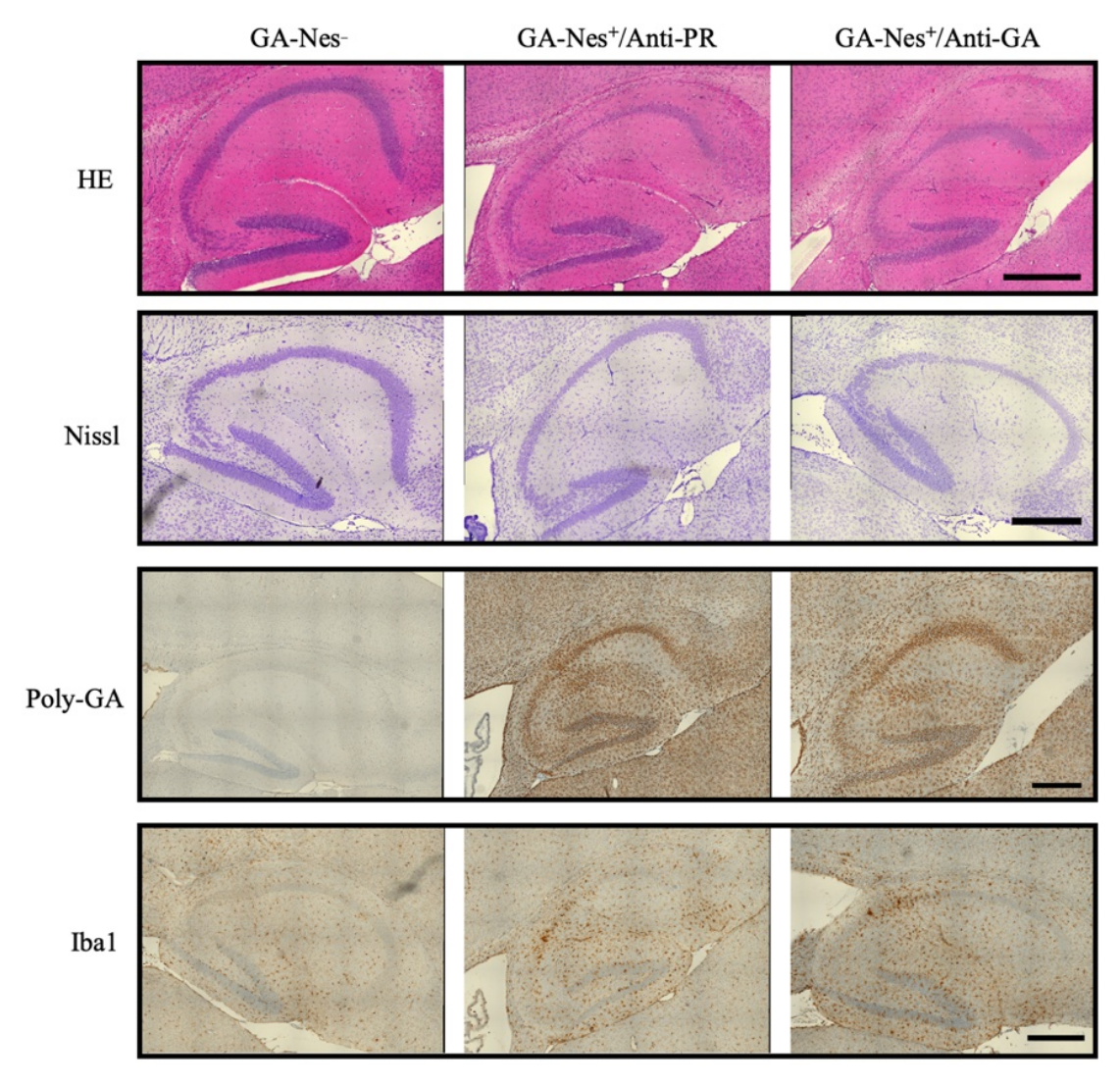


Figure 23: Neurodegeneration, poly-GA aggregation, and inflammation were not reduced by AAV-mediated anti-GA antibody expression.

GA-Nestin mice show signs of neurodegeneration in hippocampus already at 3 weeks of age. HE and Nissl stains of 4-week-old GA-Nestin mice showed neuron loss in hippocampus, with marked thinning of the Cornu Ammonis compared to healthy mice (GA-Nes')(rows one and two). Immunohistochemistry staining was used to visualize aggregates in the hippocampal region (row three). There was no visible effect of AAV-mediated anti-GA therapy on the aggregate formation in the affected mice compared to the anti-PR control group - the aggregation of poly-GA was not decreased by AAV-mediated anti-GA antibody therapy. Iba-1 staining was used to visualize the microglial response in the hippocampus (fourth row). GA-Nes*/Anti-GA and GA-Nes*/Anti-PR showed higher microglia amount than GA-Nes*. There was no difference between the microglia amount between GA-Nes*/Anti-GA and GA-Nes*/Anti-PR groups. Scalebar = 500µm.

4.8 The AAV-mediated anti-GA antibody therapy did not reduce poly-GA levels in GA-Nestin mice

To see what effect the AAV-mediated anti-GA therapy had on the poly-GA aggregation the amount of poly-GA aggregates between the treated GA-Nes⁺/Anti-GA and the control GA-Nes⁺/Anti-PR groups was compared. To quantify the poly-GA aggregates immunofluorescent stains of poly-GA in frontal cortex, hippocampus and thoracic spinal cord were prepared and imaging was done with a confocal microscope. The automated quantification was done using a self-coded Python programme (see 3.11.5). For each image two variables were analysed – the number of aggregates per number of neurons visible in the image and the overall pixel-area taken up by the aggregates per number of neurons in the image. The significance level was calculated with t-test for independent samples without assumption of equal variance. Unfortunately, no significant difference in the aggregate count or in the pixel-area taken by the aggregates was observed between GA-Nes⁺/Anti-GA and GA-Nes⁺/Anti-PR groups for any investigated part of the nervous system. This demonstrated that the AAV-mediated anti-GA antibody expression could neither prevent nor reduce poly-GA aggregation in GA-Nestin mice until the 4-week timepoint.

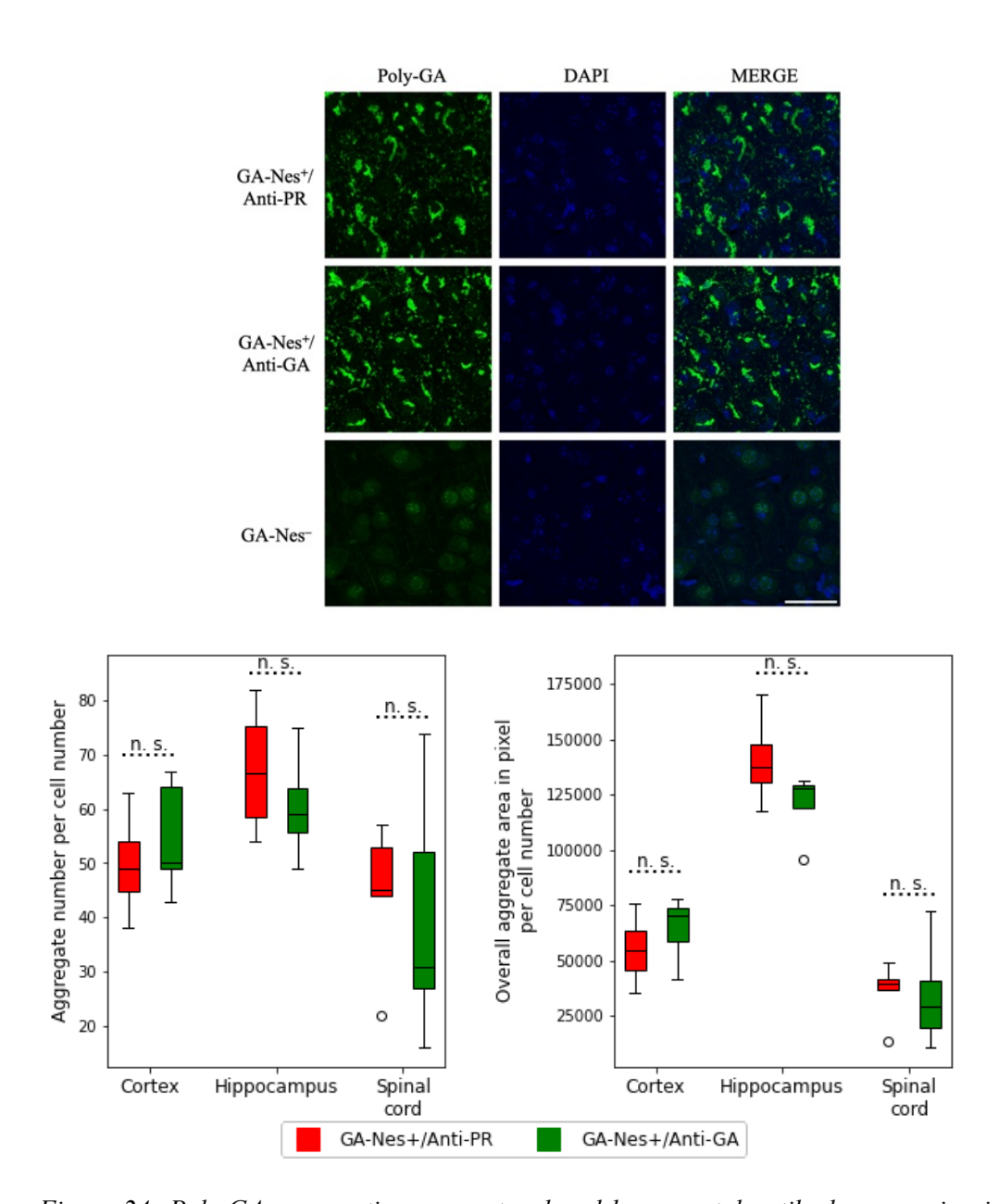


Figure 24: Poly-GA aggregation was not reduced by neonatal antibody expression in 4-week-old GA-Nestin mice

Top: Immunofluorescent stains were done to visualize abundant poly-GA aggregates in the anti-GA treated and the anti-PR control groups. Images of frontal cortex are shown as example. Scalebar=50µm.

Bottom: With help of Python programme, number and overall pixel-area of aggregates was counted. In both cases there was no significant difference between GA-Nes⁺/Anti-GA and GA-Nes⁺/Anti-PR groups.

Number of samples:

- Control group (cortex, hippocampus, spinal cord) [5,4,5].
- Treatment group: (cortex, hippocampus, spinal cord) [5,4,5].

T-test for aggregate count per cell: cortex: p=0.508, hippocampus: p=0.447, spinal cord: p=0.735.

T-test for overall pixel-area per cell: cortex: p = 0.399, hippocampus: p = 0.197, spinal cord: p = 0.905.

4.9 Anti-GA expressing GA-Nestin mice showed no signs of muscle denervation at 4 weeks of age

In the initial characterization of GA-Nestin line, we reported denervation in neuromuscular junction (NMJ) at the humane endpoint (LaClair et al., 2020). The effect of the therapy on the NMJ denervation in GA-Nestin mice was investigated at the age of 4 weeks in quadriceps femoris muscle. Immunofluorescent stains of β-tubulin III and fluorescent α-bungarotoxin was used to visualize the NMJ (see 3.11.6). α-bungarotoxin binds to the nicotinic acetylcholine receptor at the NMJ and β-tubulin is found in the axon of the innervating motor neurons. Dual staining is commonly used to show denervation as indicated by NMJs without contact to a β-tubulin-stained axon. At 4 weeks of age no difference between GA-Nes+/Anti-GA (N=2), GA-Nes-/Anti-GA (N=2) and GA-Nes-(N=4) was observed – for each sample at 5 investigated spots where NMJ was visible α-bungarotoxin was connected to tubulin III positive axons. This suggests that NMJ denervation starts only in the later stage of disease for GA-Nestin and cannot be used as a readout to quantify therapeutic benefits of anti-GA antibody expression.

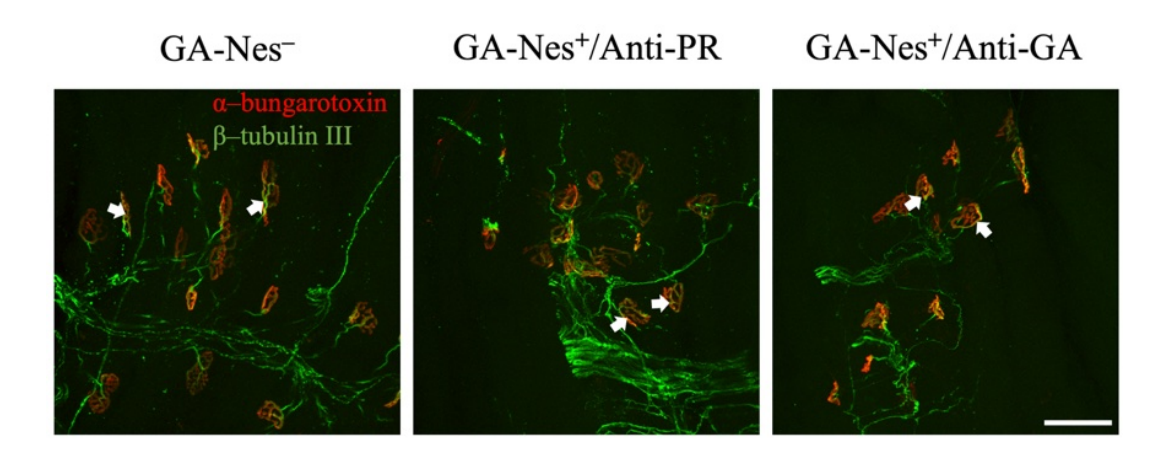


Figure 25: GA-Nestin mice did not show muscle denervation at 4 weeks of age

GA-Nestin mice suffer from muscle denervation at the survival end-stage of 6-7 weeks of age, (LaClair et al., 2020). Quadriceps femoris muscle tissue of 4-week-old GA-Nestin mice was stained with use of immunofluorescence to visualize NMJ. Connection of α -bungarotoxin to β -tubulin III was taken as a marker for healthy innervation. NMJ of neither the GA-Nes⁺ nor of the healthy littermates showed signs of denervation at 4 weeks of age indicating that the denervation happens at a later timepoint. White arrows represent exemplary healthy connections. Scale bar = 50μ m.

4.10 Study design in the GA-Camk2A mouse model

We argued that therapeutic effects might be better identified in a less severe *C9orf72* mouse model. Driving the expression of the GFP-(GA)₁₇₅ transgene using Camk2a-Cre instead of the Nestin-Cre results in less widespread aggregates, restricted to excitatory neurons and a delayed phenotype (Zhou et al, manuscript in preparation). These "GA-Camk2A" mice reach the humane end point due to 20% weight loss compared to the peak weight around 20-30 weeks of age. Moreover GA-Camk2A mice have normal motor function because the Camk2a-Cre drives aggregation of poly-GA mostly in the hippocampus and frontotemporal cortex, which only impairs learning and memory. Using the same mating strategy as in the case of GA-Nestin resulted in a close to 1:1 ratio of symptomatic GA-Camk2A⁺ and asymptomatic GA-Camk2A⁻ mice. As before, AAV injections were done blind to the genotype of the mouse and to AAV transgene. Analogous as for the GA-Nestin, three groups were analysed:

Table 3: Experimental groups in GA-Camk2A mouse line experiments

	GA-Camk2A+/Anti-GA	GA-Camk2A+/Anti-PR	GA-Camk2A ⁻
Number of	5	4	7
animals			
Description	Symptomatic mice which	Symptomatic mice which	Asymptomatic mice which
	received the therapeutic Anti-	received the control Anti-PR	received either Anti-GA or
	GA AAV	AAV	Anti-PR AAV

The evaluation of the AAV-mediated anti-GA antibody therapy on the cognitive ability of GA-Camk2A mouse line was done at 16 weeks of age using a modified Barnes Maze assay.

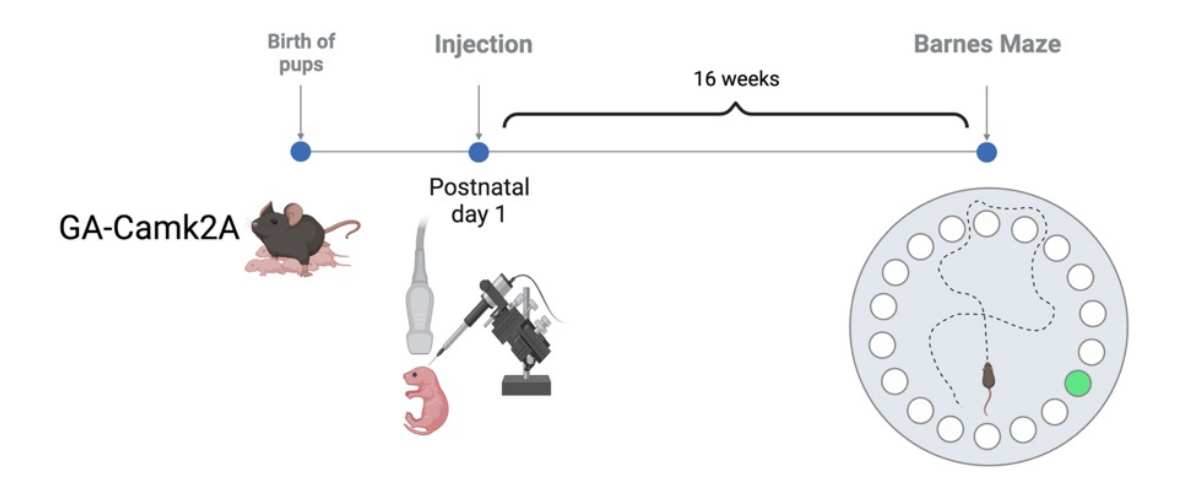


Figure 26: Experimental design for GA-Camk2A

GA-Camk2A were tested for their cognitive function. They were injected at P1 same as the GA-Nestin. Their performance at Barnes Maze was evaluated at 16 weeks post-injection. Created with BioRender.com.

4.11 The therapy did not attenuate memory impairment in GA-Camk2A

I used a modified Barnes Maze assay (see 3.13) to investigate the influence of AAV-mediated anti-GA antibody therapy on the memory function of GA-Camk2A mice. In a course of 4 days GA-Camk2A mice, together with their healthy littermates, learned to find an escape hole in the brightly lid maze arena, while tracking the required time. On the fifth day, mice were put into the same stressful maze environment, but with the escape hole covered. To investigate the memory function the number of entries into a predefined escape area, where the escape hole was previously available, was counted. Additionally, the overall time in seconds spent in this area was measured. During the four-day learning period 16-weeks old GA-Camk2A mice performed visibly worse than their healthy littermates (GA-Camk2A⁻) and for the most part could not find the escape route within the 120 second time limit. The learning period was analysed with one-way repeated measures ANOVA and Tuckey's post-hoc test. There was no significant difference in the learning effect between the anti-GA antibody AAV treated group (GA-Camk2A+/Anti-GA) and the anti-PR AAV control group (GA-Camk2A+/Anti-PR) in the four-day learning period. In this period the GA-Camk2A littermates were able to find the escape hole quicker than the GA-Camk2A⁺/Anti-GA and GA-Camk2A⁺/Anti-PR groups. The test on the fifth day was analysed with standard one-way ANOVA and Tuckey's post-hoc test. On the fifth day GA-Camk2A+/Anti-GA mice performed significantly worse than GA-Camk2A⁻, again without significant difference in performance between them and GA-

Camk2A⁺/Anti-PR. The healthy littermates of the GA-Camk2A⁻ group performed best, as they entered the escape zone most frequently and spent the most time there. These findings underline the fact that GA-Camk2A mice suffer from impaired memory function at 16 weeks of age. However, affected mice were unable to benefit from the AAV-mediated anti-GA antibody therapy in their cognitive function.

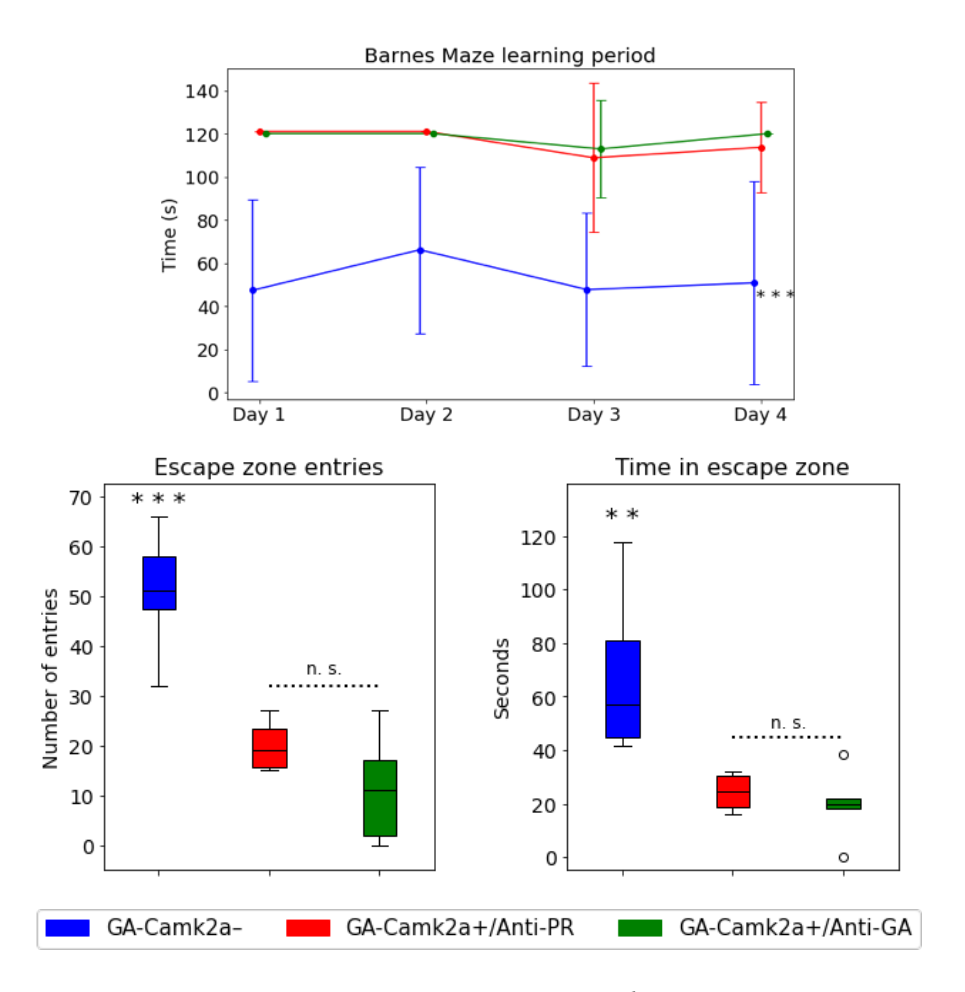


Figure 27: Barnes maze: 4-day learning period and 5th day measurements – anti-GA antibody therapy did not improve GA-Camk2A's cognitive function

GA-Camk2A mice and their healthy littermates took part in cognitive function test – Barnes Maze, at 16 weeks of age. First four days of the test were reserved as learning period, where mice were learning how to escape the maze with maximum time limit of 120 seconds.

On the fifth day of the Barnes Maze experiment the ability of mice to retrieve the learned information was investigated. There was significant difference in behaviour between GA-Camk2A mice and their healthy littermates. Both GA-Camk2A+/Anti-GA and GA-Camk2A+/Anti-PR mice have entered the escape zone much less frequently and have stayed there overall for shorter periods of time. The anti-GA antibody treatment did not prevent the cognitive regress. Statistics:

Learning period: One-way repeated measures ANOVA: F(2,9)=229.5, p<0.001. Tuckey's post-hoc test: $GA-Camk2A^{+}/Anti-GA$ and $GA-Camk2A^{+}/Anti-PR$: p=0.783. $GA-Camk2A^{+}$ comparison with other groups: p<0.001.

Escape zone entries: One-way ANOVA: F(2,13) = 25.33, p<0.001. Tuckey's post-hoc test: $GA-Camk2A^+/Anti-GA$ and $GA-Camk2A^+/Anti-PR$: p=0.446; $GA-Camk2A^-$ and $GA-Camk2A^+/Anti-GA$: p<0.001; $GA-Camk2A^-$ and $GA-Camk2A^+/Anti-PR$: p<0.001.

Escape zone time: One-way ANOVA: F(2,13)=8.14, p=0.005. Tuckey's post-hoc test: $GA-Camk2A^+/Anti-GA$ and $GA-Camk2A^+/Anti-PR$: p=0.943; $GA-Camk2A^-$ and $GA-Camk2A^+/Anti-GA$: p=0.008; $GA-Camk2A^-$ and $GA-Camk2A^+/Anti-PR$: p=0.0241.

5 Discussion

C9orf72 expansion mutation is the most common genetic cause of ALS/FTD. Patients show widespread pathognomonic aggregates of DPR proteins in central nervous system. In my thesis, I tested an AAV-mediated immunotherapy with an antibody targeting the widespread poly-GA aggregates. After establishing a monocistronic expression system in cell culture and on C57BL/6 mice the effect of the antibody expression directly in the central nervous system was tested on two poly-GA expressing C9-ALS/FTD mouse models.

5.1 The AAV system allows for successful antibody expression in neurons

In the in vitro experiments, demonstrated that AAV 2/9 can effectively transduce neurons, leading to the secretion of functional antibodies from a monocistronic expression cassette, which was required due to limiting packaging capacity of AAV. These findings align with previous research where a similar AAV was utilized to generate IgG antibodies in both HEK293T cells and rhesus fibroblast cells (Fuchs et al., 2016). Through subsequent in vivo experiments in wildtype mice, I elucidated that the timing of ultrasound-guided intracerebroventricular (ICV) injection of AAV plays an important role in achieving broad expression within the nervous system. Earlier injection at postnatal day 1 (P1) resulted in more widespread transduction compared to later injection timepoint at P3. This trend is in line with observations from stereotactic ICV AAV injections (Chakrabarty et al., 2013). As of now, only Wang et al. (2022) have described an ultrasound-guided method for ICV AAV injection. In my study, I not only corroborated the validity of this method but also showed that the expression of the anti-GA antibody was highest in the forebrain, close to the injection site, but was less prominent in the hindbrain and spinal cord. This observation suggests that this AAV application technique, could be particularly suited for testing therapeutic antibodies in disease models that primarily affect the hippocampus or cerebral cortex.

5.2 Rationale for AAV-mediated anti-GA therapy

Prior research has demonstrated the efficacy of intravenous administration of anti-GA antibodies in mitigating C9-ALS/FTD in mouse models, as demonstrated by Nguyen et al. in 2020. Encouraging outcomes have also arisen from active immunization targeting poly-GA, as

evidenced by the work of Zhou et al. in 2020. Recently, similar advancements have been made in antibody therapy against TDP-43. Active immunization with C-terminal peptide of TDP-43 resulted in decrease of serum neurofilament light chain levels in transgenic mice and have reduced aggregation of TDP-43 (Riemenschneider et al., 2023). Furthermore, monoclonal antibodies against C-terminal peptide of TDP-43 led to clearance of misfolded TDP-43 via microglia activation in a transgenic mouse model (Afroz et al., 2023).

Investigations into therapy options in neurodegenerative conditions have indicated the viability of employing AAV-mediated antibody expression. Illustratively, the AAV-mediated expression of anti-Tau antibodies exhibited a reduction in Tau pathology and in the characteristic hippocampal atrophy in mouse models (W. Liu et al., 2016). This approach is also attempted against ALS. A single-chain variable fragment antibody delivered by AAV 2/5 that targets misfolded toxic TDP-43 is in preclinical testing phase for treatment of sporadic ALS (Mead et al., 2023).

AAV-mediated antibody application directly into the CSF overcomes the obstacle of reaching high antibody titre in the nervous tissue with antibody therapies due to impermeability of BBB. BBB's composition of tight-junctions of endothelial cells, astrocyte end-feet and pericytes poses a diffusion barrier impermeable to most substances present in blood (Ballabh et al., 2004). Only very small hydrophobic molecules can pass it, while essential for nervous tissue glucose and amino acids rely on carrier-meditated transport (Kadry et al., 2020). BBB's function is to protect the homeostasis inside the CNS. Interestingly, disruption of BBB is associated with multiple neurodegenerative disorders such as multiple sclerosis (Correale & Villa, 2007), Alzheimer's or Parkinson's disease (Desai et al., 2007). The urge to overcome the problem of drug delivery to the brain parenchyma due to impermeability of BBB is big and the endeavors can be divided into increasing the BBB permeability and antibody engineering focused on increasing the trans-BBB transport (Kouhi et al., 2021). AAV-mediated expression avoids this problem altogether.

Furthermore, the utilization of monocistronic antibody expression AAV vectors are a compelling option to evaluate different antibody variants, which is a common task in drug discovery. This is because residues prone to spontaneous chemical modification need to be removed by antibody engineering to increase the shelf-life of products. Thus, from an economic standpoint, generating AAV vectors for single injection could be significantly more cost-effective compared to the resource-intensive process of producing large amounts of antibodies needed for weekly direct administration, as required in the context of passive immunization strategies.

Considering these points, it was interesting to investigate whether AAV-mediated expression of anti-GA directly in the nervous system could rescue C9-ALS/FTD poly-GA expressing mouse model.

5.3 Potential reasons for lack of therapeutical effect

The therapeutic effect of anti-GA expression was examined using biochemical and behavioural assays as well as effects on body weight. In the fast-progressing GA-Nestin line, body weight and poly-GA aggregation in brain and spinal cord were investigated at the four-week timepoint. Young GA-Nestin mice did not gain weight as effectively as their unaffected littermates and showed widespread poly-GA aggregates in the nervous tissue consistent with previous reports (LaClair et al., 2020). Unfortunately, the AAV-mediated anti-GA antibody expression had no impact on body weight or the degree of poly-GA aggregation in the GA-Nestin mouse line. In GA-Camk2A, learning and memory were assessed using Barnes Maze. Affected, GA-Camk2A mice performed significantly worse on Barnes Maze in comparison to their unaffected littermates. However, I observed no beneficial effect of anti-GA expression compared to the anti-PR control antibody. These results suggest that the AAV-mediated anti-GA expression is not a viable therapy option, which may be attributed to various reasons:

Firstly, insufficient antibody expression and concentration could have played a significant role. Although, we could see a widespread transduction of neurons in the brain and spinal cord, as detected by IHC consistent with previous reports (Ayers et al., 2015; Chakrabarty et al., 2013; McLean et al., 2014) the quantification of antibody expression in the spinal cord appeared to be considerably lower than the expression in the brain for anti-GA antibody, and lower, but not significantly, for anti-PR (see Figure 22). It is possible that AAV injection into lateral ventricles of the brain was insufficient for transduction of the spinal cord. It may have limited the expression efficacy especially in GA-Nestin mice which express poly-GA to large extent in the spinal cord (LaClair et al., 2020). Better antibody expression in the spinal cord could enhance the therapeutic efficacy.

Furthermore, the antibody/antigen ratio may have been too low. GA-Nestin mice show a very profound phenotype and a poly-GA aggregate burden far exceeding that of *C9orf72* ALS/FTD patients (LaClair et al., 2020). The poly-GA expression driven by Nestin-Cre most likely starts already prenatally and mice reach the humane endpoint at 6-7 weeks of age. They show poor weight gain after weaning, early loss of motor function and muscle denervation. The weight

loss in GA-Nestin is very remarkable, yet poorly understood. It may also be driven by poly-GA expression outside the brain, which would be less affected by anti-GA antibody expression in the brain.

Secondly, it is not clear if in case of GA-Nestin mice some therapeutic effect would have been seen at a later age stage. Their life expectancy is of 6-7 weeks without therapy, but the therapy could have influenced their survival. Furthermore, although transgene expression occurs very early after AAV injection, peak expression in rodents can be observed at first 4 weeks post injection (Reimsnider et al., 2007). On the other hand, at four weeks of age GA-Nestin mice develop a prominent ALS/FTD phenotype, making it a reasonable timepoint to address efficacy in our study (LaClair et al., 2020). Moreover, it allowed for an age-matched comparison among experimental groups. Also, a fixed time-point of 4 weeks post injection was picked for analysis, because a complete cure of the aggressive GA-Nestin model was not expected but histological and biochemical effects of the therapy could be evident already at this stage. Furthermore, allowing all animals to achieve a humane endpoint would carry an important trade-off with the biochemical and histological tests. At the humane endpoint histological and biochemical results may appear similar even for a highly effective drug that strongly extends life span. Possible biochemical and histological effects could have been missed if mice were investigated at survival endpoint. Nevertheless, it remains unclear whether some therapy effect would be visible at a later timepoint.

Finally, the impact of the poly-GA seeding mechanism on the neurodegeneration *in vivo* could be questioned considering the results. The antibody was designed to enter the endoplasmic reticulum during translation for secretion (see 3.2). and to bind to the extracellular poly-GA. Although it has been shown that DPR proteins can be transmitted from neuron to neuron in cell culture (Khosravi et al., 2020; Zhou et al., 2017) it is uncertain to what extent this process and toxicity of extracellular poly-GA are responsible for neurodegeneration *in vivo*. Even if the seeding mechanism causes neurodegeneration in neighbouring neurons in patients it is possible that it is only responsible for a small fraction of the whole neurodegenerative process in a mouse model, where poly-GA expression is more widespread. However, active vaccination conducted by Zhou (2020) in GA-CFP mice with sparse poly-GA expression showed positive results and the antibodies were active extracellularly and had to pass the blood-brain barrier to be effective. This could be caused by the fact that active vaccination against poly-GA followed by several rounds of boosting engages more suited immune response and produces more affine antibodies than mere 1A12 antibody (derived from mice receiving two immunizations) used for therapy presented here. Moreover, it is probable that active vaccination may have had

additional indirect effects on microglia response and the T cell activation. Nevertheless, more research on the seeding mechanism of DPR proteins *in vivo* would help to determine if therapies, like AAV-mediated antibody therapy, targeting the DPR seeding process could potentially be effective in the future.

5.4 Possible improvements and follow-up experiments:

Taking into consideration the findings gained through this thesis several therapy aspects could be investigated further. Firstly, different subclasses of anti-GA IgG antibody could be tried due to different characteristics and modes of function of different subclasses. There are several antibody classes: IgG, IgM, IgA, IgE and IgD. IgG is the most abundant isotype with the longest half-life and can be further divided into subclasses reflecting differences in constant region of its heavy chain (Schroeder & Cavacini, 2010). The anti-GA antibody tested in this work was a murine antibody of IgG1 subclass. Its immune effector function works via Fc gamma RIII (Hazenbos et al., 1998). In contrast murine IgG2a mediates complement activation and shows the greatest opsonophagocytic activity of all murine IgG antibodies in bacterial infections (Oishi et al., 1992). It was also highly effective in the study of Nguyen et al. (2020), where subcutaneous IgG2a anti-GA antibody injections were able to rescue the phenotype of C9-ALS/FTD mouse model depending on its effector functions. Thus, switching to the mouse IgG2a subclass could show better results also in AAV-mediated strategy.

Secondly, the use of hSynapsin promoter could be re-evaluated. Even though previous reports have shown a widespread transgene expression when hSynapsin promoter was used (McLean et al., 2014), it restricted the antibody expression to neurons. It is likely that use of a different promoter, like cytomegalovirus (CMV) promoter, which is also known for efficient expression and would allow for expression in all cells of the nervous tissue, could lead to overall greater antibody expression and possibly bigger therapeutic effect (Damdindorj et al., 2014). On the other hand, CMV promoter expression is silenced quickly by methylation (Gray et al., 2011; Prösch et al., 1996). However, this would not be of concern when testing the therapy on GA-Nestin, in which disease progression is also extremely rapid.

One of the ways of assessing the therapy efficacy was conducting the automated aggregate quantification. Different option to quantify the poly-GA aggregation in the nervous system would be concentration measurement with ELISA as used by Zhou et al. (2020). On the other hand, Jambeau et al. (2022) reported that ELISA quantification of poly-GA can lead to false

results if an antibody drug binding to poly-GA was priorly used due to competition of therapeutic and diagnostic antibodies. This effect would be caused by lack of a free binding site for antibody used for ELISA detection on the aggregated poly-GA because the binding site is already occupied by the therapeutic antibody (Jambeau et al., 2022). For this reason, image-based poly-GA quantification was probably more reliable. Another option would be to use an anti-GFP ELISA or IHC (as conducted by Zhou et al 2020), since poly-GA aggregates are GFP-tagged in GA-Nestin (LaClair et al., 2020) and GA-Camk2A.

As mentioned before the poly-GA expression in GA-Nestin was very high and exceeded the expected poly-GA burden of a C9-ALS/FTD patient. However, different forms of immunotherapy have shown positive results in mouse models with less severe poly-GA aggregation and milder phenotypes. For example, Zhou et al (2020) were able to show very promising effects in treating, a less severe, GA-CFP mouse model via active immunization. For this reason, it might be beneficial to study the therapy on a model with less extreme poly-GA expression in case the severity of GA-Nestin, did not allow for the effectiveness of antibody expression to emerge.

In case of GA-Camk2A mice, no benefit in the memory test performance was seen. Nevertheless, investigations of cognitive functions such as memory with behaviour tests can be unreliable and are prone to various sorts of bias. Although antibody expression and poly-GA load itself were not investigated in this study, it would be beneficiary to investigate the GA-Camk2A biochemically for poly-GA aggregation, similar to test of GA-Nestin. This would provide some insight into how the AAV-mediated anti-GA antibody therapy works when more time for antibody expression is given.

Finally, AAV 2/9 or AAV-PHP.eB could be applied intravenously, because they can cross the blood brain barrier (Foust et al., 2009; Mathiesen et al., 2020). Injections of AAV 2/9 to temporal vein of neonatal mice prior to postnatal day 2 lead to widespread nervous tissue transduction (Glascock et al., 2011). This way of AAV application would possibly lead to more homogenous transduction among different CNS parts benefiting the antibody expression in the spinal cord and would be more translational for future clinical trials.

5.5 Choice of the mouse model

The animal models used for therapy show mere poly-GA aggregation. Neither GA-Nestin nor GA-Camk2A mice express other DPR proteins potentially involved in C9-ALS/FTD pathology nor do they mimic other potentially crucial aspects of the C9-ALS/FTD disease like RNA

toxicity or C9orf72 protein haploinsufficiency (see 1.4). Implementation of animal models which more accurately represent the full pathophysiological spectrum of C9-ALS/FTD should be considered when investigating novel therapy strategies. However, most mouse models which carry a full *C9orf72* repeat mutation identical through introduction of a large fragment of patient DNA initially isolated in a bacterial artificial chromosome (BAC) unfortunately show only minimal symptoms (Jiang et al., 2016; Peters et al., 2015), with the exception of one highly controversial model (Y. Liu et al., 2016; Mordes et al., 2020; Nguyen et al., 2020).

5.6 AAV-mediated anti-DPR antibody therapy compared to ASO therapy

AAV-mediated antibody therapy used in this study is a unique approach potentially enabling precise antibody action at the site of risk. Other therapy approaches are also being tested for C9-ALS/FTD. One of them are antisense oligonucleotides (ASO). In C9-ALS/FTD several ASOs have been designed to trigger degradation of the low-abundance C9orf72 transcripts harbouring the expanded (G₄C₂)_n repeat without interfering with overall C9orf72 transcripts levels. This approach potentially ameliorates the neurodegenerative process at an earlier stage than anti-GA antibody does. Since poly-GA and other DPR proteins are translated from (G₄C₂)_n RNA transcripts, ASO would be able to both ameliorate the RNA toxicity and halt the DPR protein synthesis (see 1.4). On the other hand, pre-formed DPR protein aggregates and their cell-to-cell seeding cannot be addressed with this therapy strategy directly. However, recent clinical trials of two ASO drugs against C9-ALS/FTD had to be terminated due to lack of effectiveness (Biogen, 2022; Wave Life Sciences USA, 2023). Nevertheless, ASO therapy has already been successfully established for a different neurodegenerative disorder - spinal muscular atrophy (SMA) (Claborn et al., 2019). For ALS, the ASO technology has also been tested in patients with pathogenic SOD1 mutations. An ASO-based drug (Tofersen) to reduce SOD1 expression was recently approved by the FDA because it causes lower SOD1 concentration in cerebrospinal fluid and reduction of plasma neurofilament light chain indicating reduction in neuronal degeneration (Miller et al., 2022).

The AAV-meditated antibody expression presents both advantages and disadvantages when compared to ASO therapy. AAV transduction in the CNS allows continuous antibody expression over time and sidesteps the delivery bottleneck across the BBB (see 5.2). Even in the active vaccination study against poly-GA, conducted by Zhou et al. (2020), multiple vaccinations were needed to sufficiently increase the immunological response. Unfortunately, it has been shown that transgene expression after AAV application does not last infinitely and

single drug applications are not sufficient for treatment of all monogenic diseases (Brommel et al., 2020). Particularly when administered during early stages of organ development, especially in high mitotic and apoptotic activity tissue (e.g. liver), AAV-mediated transgene expression decreases substantially over short periods of time, due to loss of episomal AAV genome (Cunningham et al., 2008). However, cells in which the AAV vector is integrated into the host cell genome tend to retain the transgene expression (Cunningham et al., 2008). Liu et al. (2016) were able to show that 4 months after AAV administration the antibody levels in brain parenchyma were 50-fold greater than the levels after single systemic application (W. Liu et al., 2016). Furthermore, cell division in the nervous system is mostly restricted to glia and it is less vulnerable to episomal vector loss. This makes AAV approach particularly suitable for neurodegenerative disease treatment. Moreover, strategies which limit the transgene expression to neurons, like in this work the use of hSynapsin promoter, which are the least mitotically active cells in the nervous tissue, bypasses the mitotic vector loss problem even further. Nevertheless, research aiming at increasing the integration frequency will benefit the efficiency of AAV therapy in the future (Greig et al., 2022), also because repeated dosing of AAV in mice and patients is largely precluded by a strong antibody response (see below). On the other hand, the field of AAV gene therapy has recently encountered challenges following unfortunate demise of four patients who participated in clinical trials involving the administration of AAV 2/8, aimed at combating X-linked myotubular myopathy. Utilization of high doses of AAV resulted in hepatotoxicity which subsequently led to death of these patients (Philippidis, 2021). Despite this big setback, AAV is still considered a rather safe tool for gene therapy, demonstrating lack of acute pathogenicity for humans when small doses are applied. In total, already 4 AAV-based drugs, have been approved by agencies worldwide (see 0). However, some concerns arise regarding the possibility of long-term complications. Few findings suggest that genetic modifications stemming from AAV transduction, could heighten the susceptibility to cancer. Notably, there have been reports suggesting that the chromosomal integration of the AAV 2 genome in humans might play a role in the genesis of hepatocellular carcinoma (Russell & Grompe, 2015).

Lastly, when considering an AAV therapy it is important to acknowledge that the virus itself triggers an immunological response, which has the potential to compromise the effectiveness of the therapy. AAV prompts a humoral reaction, culminating in the production of neutralizing antibodies targeting AAV capsid proteins (Rivière et al., 2006). Such antibodies notably impede the therapeutic response, particularly in situations in which multiple administrations of the vector are necessary (Cunningham et al., 2008). Also pre-existing antibodies in a substantial

portion of potential patients presents another noteworthy concern, that may reduce therapy efficacy in those patients (Louis Jeune et al., 2013).

5.7 Outlook for AAV-mediated antibody therapy in C9-ALS/FTD and final words

Most recently, AAV-mediated antibody therapy has celebrated preclinical success for other neurodegenerative diseases. For once, a single-chain variable-fragment antibody directed against soluble oligomers of amyloid-β peptide, a protein plaque related to synaptic failure in Alzheimer's disease, was able to reverse memory deficits in disease mouse model after AAV-mediated expression (Selles et al., 2023). Another recent successful proof-of-concept of this therapy strategy was reported in the field of Parkinson's disease where application of AAV-mediated antibody expression against aggregated alpha synuclein helped in prolonging survival of a genetic mouse model (Düchs et al., 2023). Success of these studies is very promising considering the big advantage of AAV-mediated antibody expression over systemic administrations related to BBB and sheds light of encouragement for future endeavours in C9-ALS/FTD AAV-mediated antibody therapy.

The AAV system introduced in this thesis offers a valuable method to assess different antibodies against poly-GA or other DPRs in *C9orf72* mouse models. Employing the ultrasound-guided ICV injection technique proves effective for testing antibody therapies against various neurodegenerative disorders, particularly those primarily impacting the brain's cortex or hippocampus. Despite the absence of favourable outcomes from the therapy, potential benefits could emerge through optimizing the antibodies (e.g. higher affinity clones) and experimental design (e.g. mouse models).

It's worth mentioning that Prof. Edbauer's team is pursuing active vaccination based on promising data based on reduction of neurofilament light chain in several mouse studies. Preliminary, unpublished findings from Prof. Edbauer's team indicate minimal effects of the 10-week 1A12 therapy in GA-CFP mice, consistent with the data presented in this thesis. Further investigation is necessary to comprehend why active immunization against poly-GA yields more substantial results in treating poly-GA-induced disease.

In conclusion, it's crucial to emphasize that many different treatment approaches should be tested for C9-ALS/FTD, given the high failure rate of clinical trials in ALS. Distinct therapies, like AAV genetic therapy, different forms of immunotherapy, ASO or even reevaluation of drugs already in use for therapy of other disorders can uniquely address the complexity of pathophysiology of the disease. Therefore, advancing research that focuses on development of novel therapeutic approaches against C9-ALS/FTD and the synergy between these therapies is an imperative, from my perspective, to find effective help for patients suffering from C9-ALS/FTD.

6 References

- Abramzon, Y. A., Fratta, P., Traynor, B. J., & Chia, R. (2020). The Overlapping Genetics of Amyotrophic Lateral Sclerosis and Frontotemporal Dementia. *Frontiers in Neuroscience*, 14, 42. https://doi.org/10.3389/fnins.2020.00042
- Afroz, T., Chevalier, E., Audrain, M., Dumayne, C., Ziehm, T., Moser, R., Egesipe, A. L., Mottier, L., Ratnam, M., Neumann, M., Havas, D., Ollier, R., Piorkowska, K., Chauhan, M., Silva, A. B., Thapa, S., Stöhr, J., Bavdek, A., Eligert, V., . . . Seredenina, T. (2023). Immunotherapy targeting the C-terminal domain of TDP-43 decreases neuropathology and confers neuroprotection in mouse models of ALS/FTD. *Neurobiology of Disease*, 179, 106050. https://doi.org/10.1016/j.nbd.2023.106050
- Afroz, T., Hock, E. M., Ernst, P., Foglieni, C., Jambeau, M., Gilhespy, L. A. B., Laferriere, F., Maniecka, Z., Plückthun, A., Mittl, P., Paganetti, P., Allain, F. H. T., & Polymenidou, M. (2017). Functional and dynamic polymerization of the ALS-linked protein TDP-43 antagonizes its pathologic aggregation. *Nat Commun*, 8(1), 45. https://doi.org/10.1038/s41467-017-00062-0
- Agbandje-McKenna, M., & Kleinschmidt, J. (2011). AAV capsid structure and cell interactions. *Methods in Molecular Biology*, 807, 47-92. https://doi.org/10.1007/978-1-61779-370-7 3
- Al-Sarraj, S., King, A., Troakes, C., Smith, B., Maekawa, S., Bodi, I., Rogelj, B., Al-Chalabi, A., Hortobágyi, T., & Shaw, C. E. (2011). p62 positive, TDP-43 negative, neuronal cytoplasmic and intranuclear inclusions in the cerebellum and hippocampus define the pathology of C9orf72-linked FTLD and MND/ALS. *Acta Neuropathologica*, 122(6), 691-702. https://doi.org/10.1007/s00401-011-0911-2
- Amaral, J. D., Viana, R. J., Ramalho, R. M., Steer, C. J., & Rodrigues, C. M. (2009). Bile acids: regulation of apoptosis by ursodeoxycholic acid. *Journal of Lipid Research*, 50(9), 1721-1734. https://doi.org/10.1194/jlr.R900011-JLR200
- Ash, P. E., Bieniek, K. F., Gendron, T. F., Caulfield, T., Lin, W. L., Dejesus-Hernandez, M., van Blitterswijk, M. M., Jansen-West, K., Paul, J. W., 3rd, Rademakers, R., Boylan, K. B., Dickson, D. W., & Petrucelli, L. (2013). Unconventional translation of C9ORF72 GGGGCC expansion generates insoluble polypeptides specific to c9FTD/ALS. Neuron, 77(4), 639-646. https://doi.org/10.1016/j.neuron.2013.02.004
- Atchison, R. W., Casto, B. C., & Hammon, W. M. (1965). ADENOVIRUS-ASSOCIATED DEFECTIVE VIRUS PARTICLES. *Science*, 149(3685), 754-756. https://doi.org/10.1126/science.149.3685.754
- Ayers, J. I., Fromholt, S., Sinyavskaya, O., Siemienski, Z., Rosario, A. M., Li, A., Crosby, K. W., Cruz, P. E., DiNunno, N. M., Janus, C., Ceballos-Diaz, C., Borchelt, D. R., Golde, T. E., Chakrabarty, P., & Levites, Y. (2015). Widespread and efficient transduction of spinal cord and brain following neonatal AAV injection and potential disease modifying effect in ALS mice. *Molecular Therapy*, 23(1), 53-62. https://doi.org/10.1038/mt.2014.180
- Ballabh, P., Braun, A., & Nedergaard, M. (2004). The blood-brain barrier: an overview: structure, regulation, and clinical implications. *Neurobiology of Disease*, *16*(1), 1-13. https://doi.org/10.1016/j.nbd.2003.12.016
- Bañez-Coronel, M., Ayhan, F., Tarabochia, A. D., Zu, T., Perez, B. A., Tusi, S. K., Pletnikova, O., Borchelt, D. R., Ross, C. A., Margolis, R. L., Yachnis, A. T., Troncoso, J. C., & Ranum, L. P. (2015). RAN Translation in Huntington Disease. *Neuron*, 88(4), 667-677. https://doi.org/10.1016/j.neuron.2015.10.038

- Bartlett, J. S., Wilcher, R., & Samulski, R. J. (2000). Infectious entry pathway of adeno-associated virus and adeno-associated virus vectors. *Journal of Virology*, 74(6), 2777-2785. https://doi.org/10.1128/jvi.74.6.2777-2785.2000
- Benedetto Tiz, D., Bagnoli, L., Rosati, O., Marini, F., Santi, C., & Sancineto, L. (2022). FDA-Approved Small Molecules in 2022: Clinical Uses and Their Synthesis. *Pharmaceutics*, 14(11). https://doi.org/10.3390/pharmaceutics14112538
- Bensimon, G., Lacomblez, L., & Meininger, V. (1994). A controlled trial of riluzole in amyotrophic lateral sclerosis. ALS/Riluzole Study Group. *New England Journal of Medicine*, 330(9), 585-591. https://doi.org/10.1056/nejm199403033300901
- Bernaud, J., Rossi, A., Fis, A., Gardette, L., Aillot, L., Büning, H., Castelnovo, M., Salvetti, A., & Faivre-Moskalenko, C. (2018). Characterization of AAV vector particle stability at the single-capsid level. *Journal of Biological Physics*, 44(2), 181-194. https://doi.org/10.1007/s10867-018-9488-5
- Berns, K. I., & Linden, R. M. (1995). The cryptic life style of adeno-associated virus. *Bioessays*, 17(3), 237-245. https://doi.org/10.1002/bies.950170310
- Bieniek, K. F., Murray, M. E., Rutherford, N. J., Castanedes-Casey, M., DeJesus-Hernandez, M., Liesinger, A. M., Baker, M. C., Boylan, K. B., Rademakers, R., & Dickson, D. W. (2013). Tau pathology in frontotemporal lobar degeneration with C9ORF72 hexanucleotide repeat expansion. *Acta Neuropathologica*, 125(2), 289-302. https://doi.org/10.1007/s00401-012-1048-7
- Biogen. (2022, 28.03.2022). Biogen and Ionis Announce Topline Phase 1 Study Results of Investigational Drug in C9orf72 Amyotrophic Lateral Sclerosis. Retrieved Aug 7, 2023 from https://investors.biogen.com/news-releases/news-release-details/biogen-and-ionis-announce-topline-phase-1-study-results
- Blair, H. A. (2022). Onasemnogene Abeparvovec: A Review in Spinal Muscular Atrophy. *CNS Drugs*, *36*(9), 995-1005. https://doi.org/10.1007/s40263-022-00941-1
- Boeynaems, S., Bogaert, E., Kovacs, D., Konijnenberg, A., Timmerman, E., Volkov, A., Guharoy, M., De Decker, M., Jaspers, T., Ryan, V. H., Janke, A. M., Baatsen, P., Vercruysse, T., Kolaitis, R. M., Daelemans, D., Taylor, J. P., Kedersha, N., Anderson, P., Impens, F., . . . Van Den Bosch, L. (2017). Phase Separation of C9orf72 Dipeptide Repeats Perturbs Stress Granule Dynamics. *Molecular Cell*, 65(6), 1044-1055.e1045. https://doi.org/10.1016/j.molcel.2017.02.013
- Brent, J. R., Franz, C. K., Coleman, J. M., 3rd, & Ajroud-Driss, S. (2020). ALS: Management Problems. *Neurologic Clinics*, 38(3), 565-575. https://doi.org/10.1016/j.ncl.2020.03.013
- Brommel, C. M., Cooney, A. L., & Sinn, P. L. (2020). Adeno-Associated Virus-Based Gene Therapy for Lifelong Correction of Genetic Disease. *Human Gene Therapy*, *31*(17-18), 985-995. https://doi.org/10.1089/hum.2020.138
- Brotman, R. G., Moreno-Escobar, M. C., Joseph, J., & Pawar, G. (2022). Amyotrophic Lateral Sclerosis. In *StatPearls*. StatPearls Publishing
- Copyright © 2022, StatPearls Publishing LLC.
- Bryant, L. M., Christopher, D. M., Giles, A. R., Hinderer, C., Rodriguez, J. L., Smith, J. B., Traxler, E. A., Tycko, J., Wojno, A. P., & Wilson, J. M. (2013). Lessons learned from the clinical development and market authorization of Glybera. *Hum Gene Ther Clin Dev*, 24(2), 55-64. https://doi.org/10.1089/humc.2013.087
- Burnett, J. R., Hooper, A. J., & Hegele, R. A. (1993). Familial Lipoprotein Lipase Deficiency. In M. P. Adam, D. B. Everman, G. M. Mirzaa, R. A. Pagon, S. E. Wallace, L. J. H. Bean, K. W. Gripp, & A. Amemiya (Eds.), *GeneReviews*(®). University of Washington, Seattle

- Copyright © 1993-2022, University of Washington, Seattle. GeneReviews is a registered trademark of the University of Washington, Seattle. All rights reserved.
- Burrell, J. R., Kiernan, M. C., Vucic, S., & Hodges, J. R. (2011). Motor neuron dysfunction in frontotemporal dementia. *Brain*, *134*(Pt 9), 2582-2594. https://doi.org/10.1093/brain/awr195
- Byrne, S., Walsh, C., Lynch, C., Bede, P., Elamin, M., Kenna, K., McLaughlin, R., & Hardiman, O. (2011). Rate of familial amyotrophic lateral sclerosis: a systematic review and meta-analysis. *Journal of Neurology, Neurosurgery and Psychiatry*, 82(6), 623-627. https://doi.org/10.1136/jnnp.2010.224501
- Cairns, N. J., Neumann, M., Bigio, E. H., Holm, I. E., Troost, D., Hatanpaa, K. J., Foong, C., White, C. L., 3rd, Schneider, J. A., Kretzschmar, H. A., Carter, D., Taylor-Reinwald, L., Paulsmeyer, K., Strider, J., Gitcho, M., Goate, A. M., Morris, J. C., Mishra, M., Kwong, L. K., . . . Mackenzie, I. R. (2007). TDP-43 in familial and sporadic frontotemporal lobar degeneration with ubiquitin inclusions. *American Journal of Pathology*, 171(1), 227-240. https://doi.org/10.2353/ajpath.2007.070182
- Chakrabarty, P., Rosario, A., Cruz, P., Siemienski, Z., Ceballos-Diaz, C., Crosby, K., Jansen, K., Borchelt, D. R., Kim, J. Y., Jankowsky, J. L., Golde, T. E., & Levites, Y. (2013). Capsid serotype and timing of injection determines AAV transduction in the neonatal mice brain. *PloS One*, 8(6), e67680. https://doi.org/10.1371/journal.pone.0067680
- Chatterjee, D., Bhatt, M., Butler, D., De Genst, E., Dobson, C. M., Messer, A., & Kordower, J. H. (2018). Proteasome-targeted nanobodies alleviate pathology and functional decline in an α-synuclein-based Parkinson's disease model. *NPJ Parkinsons Dis*, 4, 25. https://doi.org/10.1038/s41531-018-0062-4
- Checkoway, H., Lundin, J. I., & Kelada, S. N. (2011). Neurodegenerative diseases. *IARC Scientific Publications* (163), 407-419.
- Chen, P. C., Hsieh, Y. C., Huang, C. C., & Hu, C. J. (2020). Tamoxifen for amyotrophic lateral sclerosis: A randomized double-blind clinical trial. *Medicine (Baltimore)*, 99(22), e20423. https://doi.org/10.1097/md.0000000000020423
- Cheung, A. K., Hoggan, M. D., Hauswirth, W. W., & Berns, K. I. (1980). Integration of the adeno-associated virus genome into cellular DNA in latently infected human Detroit 6 cells. *Journal of Virology*, 33(2), 739-748. https://doi.org/10.1128/jvi.33.2.739-748.1980
- Cideciyan, A. V., Aleman, T. S., Boye, S. L., Schwartz, S. B., Kaushal, S., Roman, A. J., Pang, J. J., Sumaroka, A., Windsor, E. A., Wilson, J. M., Flotte, T. R., Fishman, G. A., Heon, E., Stone, E. M., Byrne, B. J., Jacobson, S. G., & Hauswirth, W. W. (2008). Human gene therapy for RPE65 isomerase deficiency activates the retinoid cycle of vision but with slow rod kinetics. *Proceedings of the National Academy of Sciences of the United States of America*, 105(39), 15112-15117. https://doi.org/10.1073/pnas.0807027105
- Claborn, M. K., Stevens, D. L., Walker, C. K., & Gildon, B. L. (2019). Nusinersen: A Treatment for Spinal Muscular Atrophy. *Annals of Pharmacotherapy*, 53(1), 61-69. https://doi.org/10.1177/1060028018789956
- Corcia, P., Beltran, S., Bakkouche, S. E., & Couratier, P. (2021). Therapeutic news in ALS. *Revue Neurologique*, 177(5), 544-549. https://doi.org/10.1016/j.neurol.2020.12.003
- Correale, J., & Villa, A. (2007). The blood-brain-barrier in multiple sclerosis: functional roles and therapeutic targeting. *Autoimmunity*, 40(2), 148-160. https://doi.org/10.1080/08916930601183522
- Cotmore, S. F., Agbandje-McKenna, M., Chiorini, J. A., Mukha, D. V., Pintel, D. J., Qiu, J., Soderlund-Venermo, M., Tattersall, P., Tijssen, P., Gatherer, D., & Davison, A. J. (2014). The family Parvoviridae. *Archives of Virology*, 159(5), 1239-1247. https://doi.org/10.1007/s00705-013-1914-1

- Cox, B. C., Liu, Z., Lagarde, M. M., & Zuo, J. (2012). Conditional gene expression in the mouse inner ear using Cre-loxP. *J Assoc Res Otolaryngol*, 13(3), 295-322. https://doi.org/10.1007/s10162-012-0324-5
- Crooke, S. T. (2004). Progress in antisense technology. *Annual Review of Medicine*, *55*, 61-95. https://doi.org/10.1146/annurev.med.55.091902.104408
- Cunningham, S. C., Dane, A. P., Spinoulas, A., Logan, G. J., & Alexander, I. E. (2008). Gene delivery to the juvenile mouse liver using AAV2/8 vectors. *Molecular Therapy*, 16(6), 1081-1088. https://doi.org/10.1038/mt.2008.72
- Damdindorj, L., Karnan, S., Ota, A., Hossain, E., Konishi, Y., Hosokawa, Y., & Konishi, H. (2014). A comparative analysis of constitutive promoters located in adeno-associated viral vectors. *PloS One*, *9*(8), e106472. https://doi.org/10.1371/journal.pone.0106472
- Daya, S., & Berns, K. I. (2008). Gene therapy using adeno-associated virus vectors. *Clinical Microbiology Reviews*, 21(4), 583-593. https://doi.org/10.1128/cmr.00008-08
- DeJesus-Hernandez, M., Mackenzie, I. R., Boeve, B. F., Boxer, A. L., Baker, M., Rutherford, N. J., Nicholson, A. M., Finch, N. A., Flynn, H., Adamson, J., Kouri, N., Wojtas, A., Sengdy, P., Hsiung, G. Y., Karydas, A., Seeley, W. W., Josephs, K. A., Coppola, G., Geschwind, D. H., . . . Rademakers, R. (2011). Expanded GGGGCC hexanucleotide repeat in noncoding region of C9ORF72 causes chromosome 9p-linked FTD and ALS. Neuron, 72(2), 245-256. https://doi.org/10.1016/j.neuron.2011.09.011
- Desai, B. S., Monahan, A. J., Carvey, P. M., & Hendey, B. (2007). Blood-brain barrier pathology in Alzheimer's and Parkinson's disease: implications for drug therapy. *Cell Transplantation*, 16(3), 285-299. https://doi.org/10.3727/000000007783464731
- Dhillon, S. (2021). Aducanumab: First Approval. *Drugs*, 81(12), 1437-1443. https://doi.org/10.1007/s40265-021-01569-z
- Donnelly, C. J., Zhang, P. W., Pham, J. T., Haeusler, A. R., Mistry, N. A., Vidensky, S., Daley, E. L., Poth, E. M., Hoover, B., Fines, D. M., Maragakis, N., Tienari, P. J., Petrucelli, L., Traynor, B. J., Wang, J., Rigo, F., Bennett, C. F., Blackshaw, S., Sattler, R., & Rothstein, J. D. (2013). RNA toxicity from the ALS/FTD C9ORF72 expansion is mitigated by antisense intervention. *Neuron*, 80(2), 415-428. https://doi.org/10.1016/j.neuron.2013.10.015
- Doronina, V. A., Wu, C., de Felipe, P., Sachs, M. S., Ryan, M. D., & Brown, J. D. (2008). Site-specific release of nascent chains from ribosomes at a sense codon. *Molecular and Cellular Biology*, 28(13), 4227-4239. https://doi.org/10.1128/mcb.00421-08
- Dubreuil, P., Letard, S., Ciufolini, M., Gros, L., Humbert, M., Castéran, N., Borge, L., Hajem, B., Lermet, A., Sippl, W., Voisset, E., Arock, M., Auclair, C., Leventhal, P. S., Mansfield, C. D., Moussy, A., & Hermine, O. (2009). Masitinib (AB1010), a potent and selective tyrosine kinase inhibitor targeting KIT. *PloS One*, 4(9), e7258. https://doi.org/10.1371/journal.pone.0007258
- Düchs, M., Blazevic, D., Rechtsteiner, P., Kenny, C., Lamla, T., Low, S., Savistchenko, J., Neumann, M., Melki, R., Schönberger, T., Stierstorfer, B., Wyatt, D., Igney, F., & Ciossek, T. (2023). AAV-mediated expression of a new conformational anti-aggregated α-synuclein antibody prolongs survival in a genetic model of α-synucleinopathies. *NPJ Parkinsons Dis*, 9(1), 91. https://doi.org/10.1038/s41531-023-00542-9
- Fang, J., Yi, S., Simmons, A., Tu, G. H., Nguyen, M., Harding, T. C., VanRoey, M., & Jooss, K. (2007). An antibody delivery system for regulated expression of therapeutic levels of monoclonal antibodies in vivo. *Molecular Therapy*, *15*(6), 1153-1159. https://doi.org/10.1038/sj.mt.6300142
- Foust, K. D., Nurre, E., Montgomery, C. L., Hernandez, A., Chan, C. M., & Kaspar, B. K. (2009). Intravascular AAV9 preferentially targets neonatal neurons and adult astrocytes. *Nature Biotechnology*, *27*(1), 59-65. https://doi.org/10.1038/nbt.1515

- Fuchs, S. P., Martinez-Navio, J. M., Gao, G., & Desrosiers, R. C. (2016). Recombinant AAV Vectors for Enhanced Expression of Authentic IgG. *PloS One*, *11*(6), e0158009. https://doi.org/10.1371/journal.pone.0158009
- Gao, G., Alvira, M. R., Somanathan, S., Lu, Y., Vandenberghe, L. H., Rux, J. J., Calcedo, R., Sanmiguel, J., Abbas, Z., & Wilson, J. M. (2003). Adeno-associated viruses undergo substantial evolution in primates during natural infections. *Proceedings of the National Academy of Sciences of the United States of America*, 100(10), 6081-6086. https://doi.org/10.1073/pnas.0937739100
- Glascock, J. J., Osman, E. Y., Coady, T. H., Rose, F. F., Shababi, M., & Lorson, C. L. (2011). Delivery of therapeutic agents through intracerebroventricular (ICV) and intravenous (IV) injection in mice. *J Vis Exp*(56). https://doi.org/10.3791/2968
- Gorno-Tempini, M. L., Hillis, A. E., Weintraub, S., Kertesz, A., Mendez, M., Cappa, S. F., Ogar, J. M., Rohrer, J. D., Black, S., Boeve, B. F., Manes, F., Dronkers, N. F., Vandenberghe, R., Rascovsky, K., Patterson, K., Miller, B. L., Knopman, D. S., Hodges, J. R., Mesulam, M. M., & Grossman, M. (2011). Classification of primary progressive aphasia and its variants. *Neurology*, *76*(11), 1006-1014. https://doi.org/10.1212/WNL.0b013e31821103e6
- Gray, S. J., Foti, S. B., Schwartz, J. W., Bachaboina, L., Taylor-Blake, B., Coleman, J., Ehlers, M. D., Zylka, M. J., McCown, T. J., & Samulski, R. J. (2011). Optimizing promoters for recombinant adeno-associated virus-mediated gene expression in the peripheral and central nervous system using self-complementary vectors. *Human Gene Therapy*, 22(9), 1143-1153. https://doi.org/10.1089/hum.2010.245
- Greig, J. A., Breton, C., Martins, K. M., Zhu, Y., He, Z., White, J., Bell, P., Wang, L., & Wilson, J. M. (2022). Loss of transgene expression limits liver gene therapy in primates. bioRxiv, 2022.2003.2024.485675. https://doi.org/10.1101/2022.03.24.485675
- Grimm, D., Lee, J. S., Wang, L., Desai, T., Akache, B., Storm, T. A., & Kay, M. A. (2008). In vitro and in vivo gene therapy vector evolution via multispecies interbreeding and retargeting of adeno-associated viruses. *Journal of Virology*, 82(12), 5887-5911. https://doi.org/10.1128/jvi.00254-08
- Guo, Q., Lehmer, C., Martínez-Sánchez, A., Rudack, T., Beck, F., Hartmann, H., Pérez-Berlanga, M., Frottin, F., Hipp, M. S., Hartl, F. U., Edbauer, D., Baumeister, W., & Fernández-Busnadiego, R. (2018). In Situ Structure of Neuronal C9orf72 Poly-GA Aggregates Reveals Proteasome Recruitment. *Cell*, 172(4), 696-705.e612. https://doi.org/10.1016/j.cell.2017.12.030
- Hardiman, O., & van den Berg, L. H. (2017). Edaravone: a new treatment for ALS on the horizon? *Lancet Neurology*, 16(7), 490-491. https://doi.org/10.1016/s1474-4422(17)30163-1
- Hartmann, H., Hornburg, D., Czuppa, M., Bader, J., Michaelsen, M., Farny, D., Arzberger, T., Mann, M., Meissner, F., & Edbauer, D. (2018). Proteomics and C9orf72 neuropathology identify ribosomes as poly-GR/PR interactors driving toxicity. *Life Sci Alliance*, 1(2), e201800070. https://doi.org/10.26508/lsa.201800070
- Hastie, E., & Samulski, R. J. (2015). Adeno-associated virus at 50: a golden anniversary of discovery, research, and gene therapy success--a personal perspective. *Human Gene Therapy*, 26(5), 257-265. https://doi.org/10.1089/hum.2015.025
- Hazenbos, W. L., Heijnen, I. A., Meyer, D., Hofhuis, F. M., Renardel de Lavalette, C. R., Schmidt, R. E., Capel, P. J., van de Winkel, J. G., Gessner, J. E., van den Berg, T. K., & Verbeek, J. S. (1998). Murine IgG1 complexes trigger immune effector functions predominantly via Fc gamma RIII (CD16). *Journal of Immunology*, 161(6), 3026-3032.
- Hoy, S. M. (2019). Onasemnogene Abeparvovec: First Global Approval. *Drugs*, 79(11), 1255-1262. https://doi.org/10.1007/s40265-019-01162-5

- Hoy, S. M. (2023). Lecanemab: First Approval. *Drugs*, 83(4), 359-365. https://doi.org/10.1007/s40265-023-01851-2
- Jambeau, M., Meyer, K. D., Hruska-Plochan, M., Tabet, R., Lee, C. Z., Ray-Soni, A., Aguilar, C., Savage, K., Mishra, N., Cavegn, N., Borter, P., Lin, C. C., Jansen-West, K. R., Jiang, J., Freyermuth, F., Li, N., De Rossi, P., Perez-Berlanga, M., Jiang, X., . . . Lagier-Tourenne, C. (2022). Comprehensive evaluation of human-derived anti-poly-GA antibodies in cellular and animal models of C9orf72 disease. *Proc Natl Acad Sci U S A*, 119(49), e2123487119. https://doi.org/10.1073/pnas.2123487119
- Jiang, J., Zhu, Q., Gendron, T. F., Saberi, S., McAlonis-Downes, M., Seelman, A., Stauffer, J. E., Jafar-Nejad, P., Drenner, K., Schulte, D., Chun, S., Sun, S., Ling, S. C., Myers, B., Engelhardt, J., Katz, M., Baughn, M., Platoshyn, O., Marsala, M., . . . Lagier-Tourenne, C. (2016). Gain of Toxicity from ALS/FTD-Linked Repeat Expansions in C9ORF72 Is Alleviated by Antisense Oligonucleotides Targeting GGGGCC-Containing RNAs. Neuron, 90(3), 535-550. https://doi.org/10.1016/j.neuron.2016.04.006
- Johnson, J. S., Li, C., DiPrimio, N., Weinberg, M. S., McCown, T. J., & Samulski, R. J. (2010). Mutagenesis of adeno-associated virus type 2 capsid protein VP1 uncovers new roles for basic amino acids in trafficking and cell-specific transduction. *Journal of Virology*, 84(17), 8888-8902. https://doi.org/10.1128/jvi.00687-10
- Jordan, V. C. (1992). The role of tamoxifen in the treatment and prevention of breast cancer. *Current Problems in Cancer*, 16(3), 129-176. https://doi.org/10.1016/0147-0272(92)90002-6
- Kadry, H., Noorani, B., & Cucullo, L. (2020). A blood-brain barrier overview on structure, function, impairment, and biomarkers of integrity. *Fluids Barriers CNS*, 17(1), 69. https://doi.org/10.1186/s12987-020-00230-3
- Keeler, A. M., & Flotte, T. R. (2019). Recombinant Adeno-Associated Virus Gene Therapy in Light of Luxturna (and Zolgensma and Glybera): Where Are We, and How Did We Get Here? *Annu Rev Virol*, 6(1), 601-621. https://doi.org/10.1146/annurev-virology-092818-015530
- Kelich, J. M., Ma, J., Dong, B., Wang, Q., Chin, M., Magura, C. M., Xiao, W., & Yang, W. (2015). Super-resolution imaging of nuclear import of adeno-associated virus in live cells. *Mol Ther Methods Clin Dev*, 2, 15047. https://doi.org/10.1038/mtm.2015.47
- Khan, I., & De Jesus, O. (2022). Frontotemporal Lobe Dementia. In *StatPearls*. StatPearls Publishing
- Copyright © 2022, StatPearls Publishing LLC.
- Khosravi, B., Hartmann, H., May, S., Möhl, C., Ederle, H., Michaelsen, M., Schludi, M. H., Dormann, D., & Edbauer, D. (2017). Cytoplasmic poly-GA aggregates impair nuclear import of TDP-43 in C9orf72 ALS/FTLD. *Human Molecular Genetics*, *26*(4), 790-800. https://doi.org/10.1093/hmg/ddw432
- Khosravi, B., LaClair, K. D., Riemenschneider, H., Zhou, Q., Frottin, F., Mareljic, N., Czuppa, M., Farny, D., Hartmann, H., Michaelsen, M., Arzberger, T., Hartl, F. U., Hipp, M. S., & Edbauer, D. (2020). Cell-to-cell transmission of C9orf72 poly-(Gly-Ala) triggers key features of ALS/FTD. *EMBO Journal*, 39(8), e102811. https://doi.org/10.15252/embj.2019102811
- Kiernan, M. C., Vucic, S., Cheah, B. C., Turner, M. R., Eisen, A., Hardiman, O., Burrell, J. R., & Zoing, M. C. (2011). Amyotrophic lateral sclerosis. *Lancet*, 377(9769), 942-955. https://doi.org/10.1016/s0140-6736(10)61156-7
- Kim, J. Y., Grunke, S. D., Levites, Y., Golde, T. E., & Jankowsky, J. L. (2014). Intracerebroventricular viral injection of the neonatal mouse brain for persistent and widespread neuronal transduction. J Vis Exp(91), 51863. https://doi.org/10.3791/51863

- Kirshner, H. S. (2014). Frontotemporal dementia and primary progressive aphasia, a review. Neuropsychiatric Disease and Treatment, 10, 1045-1055. https://doi.org/10.2147/ndt.S38821
- Kolb, S. J., & Kissel, J. T. (2015). Spinal Muscular Atrophy. *Neurologic Clinics*, *33*(4), 831-846. https://doi.org/10.1016/j.ncl.2015.07.004
- Kouhi, A., Pachipulusu, V., Kapenstein, T., Hu, P., Epstein, A. L., & Khawli, L. A. (2021). Brain Disposition of Antibody-Based Therapeutics: Dogma, Approaches and Perspectives. *International Journal of Molecular Sciences*, 22(12). https://doi.org/10.3390/ijms22126442
- Kusaczuk, M. (2019). Tauroursodeoxycholate-Bile Acid with Chaperoning Activity: Molecular and Cellular Effects and Therapeutic Perspectives. *Cells*, 8(12). https://doi.org/10.3390/cells8121471
- Kwiatkowski, T. J., Jr., Bosco, D. A., Leclerc, A. L., Tamrazian, E., Vanderburg, C. R., Russ, C., Davis, A., Gilchrist, J., Kasarskis, E. J., Munsat, T., Valdmanis, P., Rouleau, G. A., Hosler, B. A., Cortelli, P., de Jong, P. J., Yoshinaga, Y., Haines, J. L., Pericak-Vance, M. A., Yan, J., . . . Brown, R. H., Jr. (2009). Mutations in the FUS/TLS gene on chromosome 16 cause familial amyotrophic lateral sclerosis. *Science*, *323*(5918), 1205-1208. https://doi.org/10.1126/science.1166066
- Kwon, I., Xiang, S., Kato, M., Wu, L., Theodoropoulos, P., Wang, T., Kim, J., Yun, J., Xie, Y., & McKnight, S. L. (2014). Poly-dipeptides encoded by the C9orf72 repeats bind nucleoli, impede RNA biogenesis, and kill cells. *Science*, 345(6201), 1139-1145. https://doi.org/10.1126/science.1254917
- LaClair, K. D., Zhou, Q., Michaelsen, M., Wefers, B., Brill, M. S., Janjic, A., Rathkolb, B., Farny, D., Cygan, M., de Angelis, M. H., Wurst, W., Neumann, M., Enard, W., Misgeld, T., Arzberger, T., & Edbauer, D. (2020). Congenic expression of poly-GA but not poly-PR in mice triggers selective neuron loss and interferon responses found in C9orf72 ALS. *Acta Neuropathologica*, 140(2), 121-142. https://doi.org/10.1007/s00401-020-02176-0
- Lee, Y. B., Baskaran, P., Gomez-Deza, J., Chen, H. J., Nishimura, A. L., Smith, B. N., Troakes, C., Adachi, Y., Stepto, A., Petrucelli, L., Gallo, J. M., Hirth, F., Rogelj, B., Guthrie, S., & Shaw, C. E. (2017). C9orf72 poly GA RAN-translated protein plays a key role in amyotrophic lateral sclerosis via aggregation and toxicity. *Human Molecular Genetics*, 26(24), 4765-4777. https://doi.org/10.1093/hmg/ddx350
- Lee, Y. B., Chen, H. J., Peres, J. N., Gomez-Deza, J., Attig, J., Stalekar, M., Troakes, C., Nishimura, A. L., Scotter, E. L., Vance, C., Adachi, Y., Sardone, V., Miller, J. W., Smith, B. N., Gallo, J. M., Ule, J., Hirth, F., Rogelj, B., Houart, C., & Shaw, C. E. (2013). Hexanucleotide repeats in ALS/FTD form length-dependent RNA foci, sequester RNA binding proteins, and are neurotoxic. *Cell Reports*, *5*(5), 1178-1186. https://doi.org/10.1016/j.celrep.2013.10.049
- Liu, W., Zhao, L., Blackman, B., Parmar, M., Wong, M. Y., Woo, T., Yu, F., Chiuchiolo, M. J., Sondhi, D., Kaminsky, S. M., Crystal, R. G., & Paul, S. M. (2016). Vectored Intracerebral Immunization with the Anti-Tau Monoclonal Antibody PHF1 Markedly Reduces Tau Pathology in Mutant Tau Transgenic Mice. *Journal of Neuroscience*, 36(49), 12425-12435. https://doi.org/10.1523/jneurosci.2016-16.2016
- Liu, Y., Andreucci, A., Iwamoto, N., Yin, Y., Yang, H., Liu, F., Bulychev, A., Hu, X. S., Lin, X., Lamore, S., Patil, S., Mohapatra, S., Purcell-Estabrook, E., Taborn, K., Dale, E., & Vargeese, C. (2022). Preclinical evaluation of WVE-004, aninvestigational stereopure oligonucleotide forthe treatment of C9orf72-associated ALS or FTD. *Mol Ther Nucleic Acids*, 28, 558-570. https://doi.org/10.1016/j.omtn.2022.04.007

- Liu, Y., Pattamatta, A., Zu, T., Reid, T., Bardhi, O., Borchelt, D. R., Yachnis, A. T., & Ranum, L. P. (2016). C9orf72 BAC Mouse Model with Motor Deficits and Neurodegenerative Features of ALS/FTD. *Neuron*, 90(3), 521-534. https://doi.org/10.1016/j.neuron.2016.04.005
- Liu, Y., Siriwon, N., Rohrs, J. A., & Wang, P. (2015). Generation of Targeted Adeno-Associated Virus (AAV) Vectors for Human Gene Therapy. *Current Pharmaceutical Design*, 21(22), 3248-3256. https://doi.org/10.2174/1381612821666150531171653
- Lomen-Hoerth, C., Anderson, T., & Miller, B. (2002). The overlap of amyotrophic lateral sclerosis and frontotemporal dementia. *Neurology*, *59*(7), 1077-1079. https://doi.org/10.1212/wnl.59.7.1077
- Louis Jeune, V., Joergensen, J. A., Hajjar, R. J., & Weber, T. (2013). Pre-existing anti-adeno-associated virus antibodies as a challenge in AAV gene therapy. *Hum Gene Ther Methods*, 24(2), 59-67. https://doi.org/10.1089/hgtb.2012.243
- Lusby, E., Fife, K. H., & Berns, K. I. (1980). Nucleotide sequence of the inverted terminal repetition in adeno-associated virus DNA. *Journal of Virology*, 34(2), 402-409. https://doi.org/10.1128/jvi.34.2.402-409.1980
- Lyall, R. A., Donaldson, N., Polkey, M. I., Leigh, P. N., & Moxham, J. (2001). Respiratory muscle strength and ventilatory failure in amyotrophic lateral sclerosis. *Brain*, *124*(Pt 10), 2000-2013. https://doi.org/10.1093/brain/124.10.2000
- Mackenzie, I. R., Frick, P., Grässer, F. A., Gendron, T. F., Petrucelli, L., Cashman, N. R., Edbauer, D., Kremmer, E., Prudlo, J., Troost, D., & Neumann, M. (2015). Quantitative analysis and clinico-pathological correlations of different dipeptide repeat protein pathologies in C9ORF72 mutation carriers. *Acta Neuropathologica*, 130(6), 845-861. https://doi.org/10.1007/s00401-015-1476-2
- Majounie, E., Renton, A. E., Mok, K., Dopper, E. G., Waite, A., Rollinson, S., Chiò, A., Restagno, G., Nicolaou, N., Simon-Sanchez, J., van Swieten, J. C., Abramzon, Y., Johnson, J. O., Sendtner, M., Pamphlett, R., Orrell, R. W., Mead, S., Sidle, K. C., Houlden, H., . . . Traynor, B. J. (2012). Frequency of the C9orf72 hexanucleotide repeat expansion in patients with amyotrophic lateral sclerosis and frontotemporal dementia: a cross-sectional study. *Lancet Neurology*, 11(4), 323-330. https://doi.org/10.1016/s1474-4422(12)70043-1
- Masrori, P., & Van Damme, P. (2020). Amyotrophic lateral sclerosis: a clinical review. *Eur J Neurol*, 27(10), 1918-1929. https://doi.org/10.1111/ene.14393
- Mathiesen, S. N., Lock, J. L., Schoderboeck, L., Abraham, W. C., & Hughes, S. M. (2020). CNS Transduction Benefits of AAV-PHP.eB over AAV9 Are Dependent on Administration Route and Mouse Strain. *Mol Ther Methods Clin Dev*, 19, 447-458. https://doi.org/10.1016/j.omtm.2020.10.011
- Mathis, S., Goizet, C., Soulages, A., Vallat, J. M., & Masson, G. L. (2019). Genetics of amyotrophic lateral sclerosis: A review. *Journal of the Neurological Sciences*, 399, 217-226. https://doi.org/10.1016/j.jns.2019.02.030
- May, S., Hornburg, D., Schludi, M. H., Arzberger, T., Rentzsch, K., Schwenk, B. M., Grässer, F. A., Mori, K., Kremmer, E., Banzhaf-Strathmann, J., Mann, M., Meissner, F., & Edbauer, D. (2014). C9orf72 FTLD/ALS-associated Gly-Ala dipeptide repeat proteins cause neuronal toxicity and Unc119 sequestration. *Acta Neuropathologica*, 128(4), 485-503. https://doi.org/10.1007/s00401-014-1329-4

- McCarty, D. M., Young, S. M., Jr., & Samulski, R. J. (2004). Integration of adeno-associated virus (AAV) and recombinant AAV vectors. *Annual Review of Genetics*, *38*, 819-845. https://doi.org/10.1146/annurev.genet.37.110801.143717
- McCauley, M. E., & Baloh, R. H. (2019). Inflammation in ALS/FTD pathogenesis. *Acta Neuropathologica*, *137*(5), 715-730. https://doi.org/10.1007/s00401-018-1933-9
- McLaughlin, S. K., Collis, P., Hermonat, P. L., & Muzyczka, N. (1988). Adeno-associated virus general transduction vectors: analysis of proviral structures. *Journal of Virology*, 62(6), 1963-1973. https://doi.org/10.1128/jvi.62.6.1963-1973.1988
- McLean, J. R., Smith, G. A., Rocha, E. M., Hayes, M. A., Beagan, J. A., Hallett, P. J., & Isacson, O. (2014). Widespread neuron-specific transgene expression in brain and spinal cord following synapsin promoter-driven AAV9 neonatal intracerebroventricular injection. Neuroscience Letters, 576, 73-78. https://doi.org/10.1016/j.neulet.2014.05.044
- Mead, R. J., Shan, N., Reiser, H. J., Marshall, F., & Shaw, P. J. (2023). Amyotrophic lateral sclerosis: a neurodegenerative disorder poised for successful therapeutic translation. *Nat Rev Drug Discov*, 22(3), 185-212. https://doi.org/10.1038/s41573-022-00612-2
- Meier, A. F., Fraefel, C., & Seyffert, M. (2020). The Interplay between Adeno-Associated Virus and its Helper Viruses. *Viruses*, 12(6). https://doi.org/10.3390/v12060662
- Mesulam, M. M. (2001). Primary progressive aphasia. Annals of Neurology, 49(4), 425-432.
- Mesulam, M. M., Rogalski, E. J., Wieneke, C., Hurley, R. S., Geula, C., Bigio, E. H., Thompson, C. K., & Weintraub, S. (2014). Primary progressive aphasia and the evolving neurology of the language network. *Nature Reviews: Neurology*, *10*(10), 554-569. https://doi.org/10.1038/nrneurol.2014.159
- Miller, T. M., Cudkowicz, M. E., Genge, A., Shaw, P. J., Sobue, G., Bucelli, R. C., Chiò, A., Van Damme, P., Ludolph, A. C., Glass, J. D., Andrews, J. A., Babu, S., Benatar, M., McDermott, C. J., Cochrane, T., Chary, S., Chew, S., Zhu, H., Wu, F., . . . Fradette, S. (2022). Trial of Antisense Oligonucleotide Tofersen for SOD1 ALS. New England Journal of Medicine, 387(12), 1099-1110. https://doi.org/10.1056/NEJMoa2204705
- Mitchell, J. D., & Borasio, G. D. (2007). Amyotrophic lateral sclerosis. *Lancet*, *369*(9578), 2031-2041. https://doi.org/10.1016/s0140-6736(07)60944-1
- Mizielinska, S., Grönke, S., Niccoli, T., Ridler, C. E., Clayton, E. L., Devoy, A., Moens, T., Norona, F. E., Woollacott, I. O. C., Pietrzyk, J., Cleverley, K., Nicoll, A. J., Pickering-Brown, S., Dols, J., Cabecinha, M., Hendrich, O., Fratta, P., Fisher, E. M. C., Partridge, L., & Isaacs, A. M. (2014). C9orf72 repeat expansions cause neurodegeneration in Drosophila through arginine-rich proteins. *Science*, 345(6201), 1192-1194. https://doi.org/10.1126/science.1256800
- Mora, J. S., Bradley, W. G., Chaverri, D., Hernández-Barral, M., Mascias, J., Gamez, J., Gargiulo-Monachelli, G. M., Moussy, A., Mansfield, C. D., Hermine, O., & Ludolph, A. C. (2021). Long-term survival analysis of masitinib in amyotrophic lateral sclerosis. *Therapeutic Advances in Neurological Disorders*, 14, 17562864211030365. https://doi.org/10.1177/17562864211030365
- Mordes, D. A., Morrison, B. M., Ament, X. H., Cantrell, C., Mok, J., Eggan, P., Xue, C., Wang, J. Y., Eggan, K., & Rothstein, J. D. (2020). Absence of Survival and Motor Deficits in 500 Repeat C9ORF72 BAC Mice. *Neuron*, 108(4), 775-783.e774. https://doi.org/10.1016/j.neuron.2020.08.009
- Mori, K., Weng, S. M., Arzberger, T., May, S., Rentzsch, K., Kremmer, E., Schmid, B., Kretzschmar, H. A., Cruts, M., Van Broeckhoven, C., Haass, C., & Edbauer, D. (2013). The C9orf72 GGGCC repeat is translated into aggregating dipeptide-repeat proteins in FTLD/ALS. *Science*, 339(6125), 1335-1338. https://doi.org/10.1126/science.1232927

- Naso, M. F., Tomkowicz, B., Perry, W. L., 3rd, & Strohl, W. R. (2017). Adeno-Associated Virus (AAV) as a Vector for Gene Therapy. *Biodrugs*, 31(4), 317-334. https://doi.org/10.1007/s40259-017-0234-5
- Naumer, M., Sonntag, F., Schmidt, K., Nieto, K., Panke, C., Davey, N. E., Popa-Wagner, R., & Kleinschmidt, J. A. (2012). Properties of the adeno-associated virus assembly-activating protein. *Journal of Virology*, 86(23), 13038-13048. https://doi.org/10.1128/jvi.01675-12
- Neumann, M., Sampathu, D. M., Kwong, L. K., Truax, A. C., Micsenyi, M. C., Chou, T. T., Bruce, J., Schuck, T., Grossman, M., Clark, C. M., McCluskey, L. F., Miller, B. L., Masliah, E., Mackenzie, I. R., Feldman, H., Feiden, W., Kretzschmar, H. A., Trojanowski, J. Q., & Lee, V. M. (2006). Ubiquitinated TDP-43 in frontotemporal lobar degeneration and amyotrophic lateral sclerosis. *Science*, 314(5796), 130-133. https://doi.org/10.1126/science.1134108
- Nguyen, L., Montrasio, F., Pattamatta, A., Tusi, S. K., Bardhi, O., Meyer, K. D., Hayes, L., Nakamura, K., Banez-Coronel, M., Coyne, A., Guo, S., Laboissonniere, L. A., Gu, Y., Narayanan, S., Smith, B., Nitsch, R. M., Kankel, M. W., Rushe, M., Rothstein, J., . . . Ranum, L. P. W. (2020). Antibody Therapy Targeting RAN Proteins Rescues C9 ALS/FTD Phenotypes in C9orf72 Mouse Model. *Neuron*, *105*(4), 645-662.e611. https://doi.org/10.1016/j.neuron.2019.11.007
- Oishi, K., Koles, N. L., Guelde, G., & Pollack, M. (1992). Antibacterial and protective properties of monoclonal antibodies reactive with Escherichia coli O111:B4 lipopolysaccharide: relation to antibody isotype and complement-fixing activity. *Journal of Infectious Diseases*, 165(1), 34-45. https://doi.org/10.1093/infdis/165.1.34
- Olney, N. T., Spina, S., & Miller, B. L. (2017). Frontotemporal Dementia. *Neurologic Clinics*, 35(2), 339-374. https://doi.org/10.1016/j.ncl.2017.01.008
- Olszewska, D. A., Lonergan, R., Fallon, E. M., & Lynch, T. (2016). Genetics of Frontotemporal Dementia. *Current Neurology and Neuroscience Reports*, 16(12), 107. https://doi.org/10.1007/s11910-016-0707-9
- Onyike, C. U., & Diehl-Schmid, J. (2013). The epidemiology of frontotemporal dementia. *International Review of Psychiatry*, 25(2), 130-137. https://doi.org/10.3109/09540261.2013.776523
- Peters, O. M., Cabrera, G. T., Tran, H., Gendron, T. F., McKeon, J. E., Metterville, J., Weiss, A., Wightman, N., Salameh, J., Kim, J., Sun, H., Boylan, K. B., Dickson, D., Kennedy, Z., Lin, Z., Zhang, Y. J., Daughrity, L., Jung, C., Gao, F. B., . . . Brown, R. H., Jr. (2015). Human C9ORF72 Hexanucleotide Expansion Reproduces RNA Foci and Dipeptide Repeat Proteins but Not Neurodegeneration in BAC Transgenic Mice. Neuron, 88(5), 902-909. https://doi.org/10.1016/j.neuron.2015.11.018
- Philippidis, A. (2021). Fourth Boy Dies in Trial of Astellas Gene Therapy Candidate. Retrieved Aug 8, 2023 from https://www.genengnews.com/news/fourth-boy-dies-in-trial-of-astellas-gene-therapy-candidate/
- Pillay, S., Zou, W., Cheng, F., Puschnik, A. S., Meyer, N. L., Ganaie, S. S., Deng, X., Wosen, J. E., Davulcu, O., Yan, Z., Engelhardt, J. F., Brown, K. E., Chapman, M. S., Qiu, J., & Carette, J. E. (2017). Adeno-associated Virus (AAV) Serotypes Have Distinctive Interactions with Domains of the Cellular AAV Receptor. *Journal of Virology*, 91(18). https://doi.org/10.1128/jvi.00391-17
- Pipe, S. W., Leebeek, F. W. G., Recht, M., Key, N. S., Castaman, G., Miesbach, W., Lattimore, S., Peerlinck, K., Van der Valk, P., Coppens, M., Kampmann, P., Meijer, K., O'Connell, N., Pasi, K. J., Hart, D. P., Kazmi, R., Astermark, J., Hermans, C., Klamroth, R., . . . Monahan, P. E. (2023). Gene Therapy with Etranacogene Dezaparvovec for

- Hemophilia B. *New England Journal of Medicine*, 388(8), 706-718. https://doi.org/10.1056/NEJMoa2211644
- Prösch, S., Stein, J., Staak, K., Liebenthal, C., Volk, H. D., & Krüger, D. H. (1996). Inactivation of the very strong HCMV immediate early promoter by DNA CpG methylation in vitro. *Biological Chemistry Hoppe-Seyler*, 377(3), 195-201. https://doi.org/10.1515/bchm3.1996.377.3.195
- Ramirez, C., Piemonte, M. E., Callegaro, D., & Da Silva, H. C. (2008). Fatigue in amyotrophic lateral sclerosis: frequency and associated factors. *Amyotrophic Lateral Sclerosis*, 9(2), 75-80. https://doi.org/10.1080/17482960701642502
- Rascovsky, K., Hodges, J. R., Knopman, D., Mendez, M. F., Kramer, J. H., Neuhaus, J., van Swieten, J. C., Seelaar, H., Dopper, E. G., Onyike, C. U., Hillis, A. E., Josephs, K. A., Boeve, B. F., Kertesz, A., Seeley, W. W., Rankin, K. P., Johnson, J. K., Gorno-Tempini, M. L., Rosen, H., . . . Miller, B. L. (2011). Sensitivity of revised diagnostic criteria for the behavioural variant of frontotemporal dementia. *Brain*, 134(Pt 9), 2456-2477. https://doi.org/10.1093/brain/awr179
- Reimsnider, S., Manfredsson, F. P., Muzyczka, N., & Mandel, R. J. (2007). Time course of transgene expression after intrastriatal pseudotyped rAAV2/1, rAAV2/2, rAAV2/5, and rAAV2/8 transduction in the rat. *Molecular Therapy*, 15(8), 1504-1511. https://doi.org/10.1038/sj.mt.6300227
- Renton, A. E., Majounie, E., Waite, A., Simón-Sánchez, J., Rollinson, S., Gibbs, J. R., Schymick, J. C., Laaksovirta, H., van Swieten, J. C., Myllykangas, L., Kalimo, H., Paetau, A., Abramzon, Y., Remes, A. M., Kaganovich, A., Scholz, S. W., Duckworth, J., Ding, J., Harmer, D. W., . . . Traynor, B. J. (2011). A hexanucleotide repeat expansion in C9ORF72 is the cause of chromosome 9p21-linked ALS-FTD. *Neuron*, 72(2), 257-268. https://doi.org/10.1016/j.neuron.2011.09.010
- Riemenschneider, H., Guo, Q., Bader, J., Frottin, F., Farny, D., Kleinberger, G., Haass, C., Mann, M., Hartl, F. U., Baumeister, W., Hipp, M. S., Meissner, F., Fernández-Busnadiego, R., & Edbauer, D. (2022). Gel-like inclusions of C-terminal fragments of TDP-43 sequester stalled proteasomes in neurons. *EMBO Rep*, 23(6), e53890. https://doi.org/10.15252/embr.202153890
- Riemenschneider, H., Simonetti, F., Sheth, U., Katona, E., Roth, S., Hutten, S., Farny, D., Michaelsen, M., Nuscher, B., Schmidt, M. K., Flatley, A., Schepers, A., Gruijs da Silva, L. A., Zhou, Q., Klopstock, T., Liesz, A., Arzberger, T., Herms, J., Feederle, R., . . . Edbauer, D. (2023). Targeting the glycine-rich domain of TDP-43 with antibodies prevents its aggregation in vitro and reduces neurofilament levels in vivo. *Acta Neuropathol Commun*, 11(1), 112. https://doi.org/10.1186/s40478-023-01592-z
- Rip, J., Nierman, M. C., Sierts, J. A., Petersen, W., Van den Oever, K., Van Raalte, D., Ross, C. J., Hayden, M. R., Bakker, A. C., Dijkhuizen, P., Hermens, W. T., Twisk, J., Stroes, E., Kastelein, J. J., Kuivenhoven, J. A., & Meulenberg, J. M. (2005). Gene therapy for lipoprotein lipase deficiency: working toward clinical application. *Human Gene Therapy*, 16(11), 1276-1286. https://doi.org/10.1089/hum.2005.16.1276
- Rivière, C., Danos, O., & Douar, A. M. (2006). Long-term expression and repeated administration of AAV type 1, 2 and 5 vectors in skeletal muscle of immunocompetent adult mice. *Gene Therapy*, *13*(17), 1300-1308. https://doi.org/10.1038/sj.gt.3302766
- Rose, J. A., Berns, K. I., Hoggan, M. D., & Koczot, F. J. (1969). Evidence for a single-stranded adenovirus-associated virus genome: formation of a DNA density hybrid on release of viral DNA. *Proceedings of the National Academy of Sciences of the United States of America*, 64(3), 863-869. https://doi.org/10.1073/pnas.64.3.863
- Rosen, D. R., Siddique, T., Patterson, D., Figlewicz, D. A., Sapp, P., Hentati, A., Donaldson, D., Goto, J., O'Regan, J. P., Deng, H. X., & et al. (1993). Mutations in Cu/Zn superoxide

- dismutase gene are associated with familial amyotrophic lateral sclerosis. *Nature*, 362(6415), 59-62. https://doi.org/10.1038/362059a0
- Russell, D. W., & Grompe, M. (2015). Adeno-associated virus finds its disease. *Nature Genetics*, 47(10), 1104-1105. https://doi.org/10.1038/ng.3407
- Russell, S., Bennett, J., Wellman, J. A., Chung, D. C., Yu, Z. F., Tillman, A., Wittes, J., Pappas, J., Elci, O., McCague, S., Cross, D., Marshall, K. A., Walshire, J., Kehoe, T. L., Reichert, H., Davis, M., Raffini, L., George, L. A., Hudson, F. P., . . . Maguire, A. M. (2017). Efficacy and safety of voretigene neparvovec (AAV2-hRPE65v2) in patients with RPE65-mediated inherited retinal dystrophy: a randomised, controlled, openlabel, phase 3 trial. *Lancet*, 390(10097), 849-860. https://doi.org/10.1016/s0140-6736(17)31868-8
- Ryan, S., Rollinson, S., Hobbs, E., & Pickering-Brown, S. (2022). C9orf72 dipeptides disrupt the nucleocytoplasmic transport machinery and cause TDP-43 mislocalisation to the cytoplasm. *Scientific Reports*, *12*(1), 4799. https://doi.org/10.1038/s41598-022-08724-w
- Ryu, H., Smith, K., Camelo, S. I., Carreras, I., Lee, J., Iglesias, A. H., Dangond, F., Cormier, K. A., Cudkowicz, M. E., Brown, R. H., Jr., & Ferrante, R. J. (2005). Sodium phenylbutyrate prolongs survival and regulates expression of anti-apoptotic genes in transgenic amyotrophic lateral sclerosis mice. *Journal of Neurochemistry*, *93*(5), 1087-1098. https://doi.org/10.1111/j.1471-4159.2005.03077.x
- Samulski, R. J., Zhu, X., Xiao, X., Brook, J. D., Housman, D. E., Epstein, N., & Hunter, L. A. (1991). Targeted integration of adeno-associated virus (AAV) into human chromosome 19. *EMBO Journal*, 10(12), 3941-3950. https://doi.org/10.1002/j.1460-2075.1991.tb04964.x
- Sareen, D., O'Rourke, J. G., Meera, P., Muhammad, A. K., Grant, S., Simpkinson, M., Bell, S., Carmona, S., Ornelas, L., Sahabian, A., Gendron, T., Petrucelli, L., Baughn, M., Ravits, J., Harms, M. B., Rigo, F., Bennett, C. F., Otis, T. S., Svendsen, C. N., & Baloh, R. H. (2013). Targeting RNA foci in iPSC-derived motor neurons from ALS patients with a C9ORF72 repeat expansion. *Science Translational Medicine*, *5*(208), 208ra149. https://doi.org/10.1126/scitranslmed.3007529
- Schludi, M. H., Becker, L., Garrett, L., Gendron, T. F., Zhou, Q., Schreiber, F., Popper, B., Dimou, L., Strom, T. M., Winkelmann, J., von Thaden, A., Rentzsch, K., May, S., Michaelsen, M., Schwenk, B. M., Tan, J., Schoser, B., Dieterich, M., Petrucelli, L., . . . Edbauer, D. (2017). Spinal poly-GA inclusions in a C9orf72 mouse model trigger motor deficits and inflammation without neuron loss. *Acta Neuropathologica*, *134*(2), 241-254. https://doi.org/10.1007/s00401-017-1711-0
- Schludi, M. H., May, S., Grässer, F. A., Rentzsch, K., Kremmer, E., Küpper, C., Klopstock, T., Arzberger, T., & Edbauer, D. (2015). Distribution of dipeptide repeat proteins in cellular models and C9orf72 mutation cases suggests link to transcriptional silencing. Acta Neuropathologica, 130(4), 537-555. https://doi.org/10.1007/s00401-015-1450-z
- Schmitz, A., Pinheiro Marques, J., Oertig, I., Maharjan, N., & Saxena, S. (2021). Emerging Perspectives on Dipeptide Repeat Proteins in C9ORF72 ALS/FTD. Frontiers in Cellular Neuroscience, 15, 637548. https://doi.org/10.3389/fncel.2021.637548
- Schroeder, H. W., Jr., & Cavacini, L. (2010). Structure and function of immunoglobulins. *Journal of Allergy and Clinical Immunology*, 125(2 Suppl 2), S41-52. https://doi.org/10.1016/j.jaci.2009.09.046
- Scotter, E. L., Chen, H. J., & Shaw, C. E. (2015). TDP-43 Proteinopathy and ALS: Insights into Disease Mechanisms and Therapeutic Targets. *Neurotherapeutics*, *12*(2), 352-363. https://doi.org/10.1007/s13311-015-0338-x

- Selles, M. C., Fortuna, J. T. S., Cercato, M. C., Santos, L. E., Domett, L., Bitencourt, A. L. B., Carraro, M. F., Souza, A. S., Janickova, H., Azevedo, C. V., Campos, H. C., de Souza, J. M., Alves-Leon, S., Prado, V. F., Prado, M. A. M., Epstein, A. L., Salvetti, A., Longo, B. M., Arancio, O., . . . Ferreira, S. T. (2023). AAV-mediated neuronal expression of an scFv antibody selective for Aβ oligomers protects synapses and rescues memory in Alzheimer models. *Molecular Therapy*, 31(2), 409-419. https://doi.org/10.1016/j.ymthe.2022.11.002
- Shababi, M., Lorson, C. L., & Rudnik-Schöneborn, S. S. (2014). Spinal muscular atrophy: a motor neuron disorder or a multi-organ disease? *Journal of Anatomy*, 224(1), 15-28. https://doi.org/10.1111/joa.12083
- Shao, Q., Yang, M., Liang, C., Ma, L., Zhang, W., Jiang, Z., Luo, J., Lee, J. K., Liang, C., & Chen, J. F. (2020). C9orf72 and smcr8 mutant mice reveal MTORC1 activation due to impaired lysosomal degradation and exocytosis. *Autophagy*, 16(9), 1635-1650. https://doi.org/10.1080/15548627.2019.1703353
- Shi, Y., Lin, S., Staats, K. A., Li, Y., Chang, W. H., Hung, S. T., Hendricks, E., Linares, G. R., Wang, Y., Son, E. Y., Wen, X., Kisler, K., Wilkinson, B., Menendez, L., Sugawara, T., Woolwine, P., Huang, M., Cowan, M. J., Ge, B., . . . Ichida, J. K. (2018). Haploinsufficiency leads to neurodegeneration in C9ORF72 ALS/FTD human induced motor neurons. *Nature Medicine*, 24(3), 313-325. https://doi.org/10.1038/nm.4490
- Smethurst, P., Risse, E., Tyzack, G. E., Mitchell, J. S., Taha, D. M., Chen, Y. R., Newcombe, J., Collinge, J., Sidle, K., & Patani, R. (2020). Distinct responses of neurons and astrocytes to TDP-43 proteinopathy in amyotrophic lateral sclerosis. *Brain*, *143*(2), 430-440. https://doi.org/10.1093/brain/awz419
- Sonntag, F., Bleker, S., Leuchs, B., Fischer, R., & Kleinschmidt, J. A. (2006). Adeno-associated virus type 2 capsids with externalized VP1/VP2 trafficking domains are generated prior to passage through the cytoplasm and are maintained until uncoating occurs in the nucleus. *Journal of Virology*, 80(22), 11040-11054. https://doi.org/10.1128/jvi.01056-06
- Sorenson, E. J., Crum, B., & Stevens, J. C. (2007). Incidence of aspiration pneumonia in ALS in Olmsted County, MN. *Amyotrophic Lateral Sclerosis*, 8(2), 87-89. https://doi.org/10.1080/17482960601147461
- Sreedharan, J., Blair, I. P., Tripathi, V. B., Hu, X., Vance, C., Rogelj, B., Ackerley, S., Durnall, J. C., Williams, K. L., Buratti, E., Baralle, F., de Belleroche, J., Mitchell, J. D., Leigh, P. N., Al-Chalabi, A., Miller, C. C., Nicholson, G., & Shaw, C. E. (2008). TDP-43 mutations in familial and sporadic amyotrophic lateral sclerosis. *Science*, *319*(5870), 1668-1672. https://doi.org/10.1126/science.1154584
- Statland, J. M., Barohn, R. J., McVey, A. L., Katz, J. S., & Dimachkie, M. M. (2015). Patterns of Weakness, Classification of Motor Neuron Disease, and Clinical Diagnosis of Sporadic Amyotrophic Lateral Sclerosis. *Neurologic Clinics*, 33(4), 735-748. https://doi.org/10.1016/j.ncl.2015.07.006
- Stevens, D., Claborn, M. K., Gildon, B. L., Kessler, T. L., & Walker, C. (2020). Onasemnogene Abeparvovec-xioi: Gene Therapy for Spinal Muscular Atrophy. *Annals of Pharmacotherapy*, 54(10), 1001-1009. https://doi.org/10.1177/1060028020914274
- Sugarman, E. A., Nagan, N., Zhu, H., Akmaev, V. R., Zhou, Z., Rohlfs, E. M., Flynn, K., Hendrickson, B. C., Scholl, T., Sirko-Osadsa, D. A., & Allitto, B. A. (2012). Pan-ethnic carrier screening and prenatal diagnosis for spinal muscular atrophy: clinical laboratory analysis of >72,400 specimens. *European Journal of Human Genetics*, 20(1), 27-32. https://doi.org/10.1038/ejhg.2011.134

- Tan, E., Chin, C. S. H., Lim, Z. F. S., & Ng, S. K. (2021). HEK293 Cell Line as a Platform to Produce Recombinant Proteins and Viral Vectors. *Front Bioeng Biotechnol*, *9*, 796991. https://doi.org/10.3389/fbioe.2021.796991
- Tiryaki, E., & Horak, H. A. (2014). ALS and other motor neuron diseases. *Continuum (Minneap Minn)*, 20(5 Peripheral Nervous System Disorders), 1185-1207. https://doi.org/10.1212/01.CON.0000455886.14298.a4
- Tsai, R. M., & Boxer, A. L. (2014). Treatment of frontotemporal dementia. *Current Treatment Options in Neurology*, 16(11), 319. https://doi.org/10.1007/s11940-014-0319-0
- Vachon, V. K., & Conn, G. L. (2016). Adenovirus VA RNA: An essential pro-viral non-coding RNA. *Virus Research*, 212, 39-52. https://doi.org/10.1016/j.virusres.2015.06.018
- Van Langenhove, T., van der Zee, J., & Van Broeckhoven, C. (2012). The molecular basis of the frontotemporal lobar degeneration-amyotrophic lateral sclerosis spectrum. *Annals of Medicine*, 44(8), 817-828. https://doi.org/10.3109/07853890.2012.665471
- Vieira, R. T., Caixeta, L., Machado, S., Silva, A. C., Nardi, A. E., Arias-Carrión, O., & Carta, M. G. (2013). Epidemiology of early-onset dementia: a review of the literature. *Clinical Practice and Epidemiology in Mental Health*, *9*, 88-95. https://doi.org/10.2174/1745017901309010088
- Wang, D., Tai, P. W. L., & Gao, G. (2019). Adeno-associated virus vector as a platform for gene therapy delivery. *Nat Rev Drug Discov*, 18(5), 358-378. https://doi.org/10.1038/s41573-019-0012-9
- Wang, I. F., Guo, B. S., Liu, Y. C., Wu, C. C., Yang, C. H., Tsai, K. J., & Shen, C. K. (2012). Autophagy activators rescue and alleviate pathogenesis of a mouse model with proteinopathies of the TAR DNA-binding protein 43. *Proceedings of the National Academy of Sciences of the United States of America*, 109(37), 15024-15029. https://doi.org/10.1073/pnas.1206362109
- Wang, M., Misgeld, T., & Brill, M. S. (2022). Neural labeling and manipulation by neonatal intraventricular viral injection in mice. *STAR Protoc*, 3(1), 101081. https://doi.org/10.1016/j.xpro.2021.101081
- Wave Life Sciences USA, I. (2023). Wave Life Sciences Announces Topline Results from Phase 1b/2a FOCUS-C9 Study of WVE-004 for C9orf72-associated Amyotrophic Lateral Sclerosis and Frontotemporal Dementia. Retrieved Aug 7, 2023 from https://ir.wavelifesciences.com/news-releases/news-release-details/wave-lifesciences-announces-topline-results-phase-1b2a-focus-c9
- Webster, C. P., Smith, E. F., Bauer, C. S., Moller, A., Hautbergue, G. M., Ferraiuolo, L., Myszczynska, M. A., Higginbottom, A., Walsh, M. J., Whitworth, A. J., Kaspar, B. K., Meyer, K., Shaw, P. J., Grierson, A. J., & De Vos, K. J. (2016). The C9orf72 protein interacts with Rab1a and the ULK1 complex to regulate initiation of autophagy. *EMBO Journal*, 35(15), 1656-1676. https://doi.org/10.15252/embj.201694401
- Wilmott, P., Lisowski, L., Alexander, I. E., & Logan, G. J. (2019). A User's Guide to the Inverted Terminal Repeats of Adeno-Associated Virus. *Hum Gene Ther Methods*, 30(6), 206-213. https://doi.org/10.1089/hgtb.2019.276
- Winton, M. J., Igaz, L. M., Wong, M. M., Kwong, L. K., Trojanowski, J. Q., & Lee, V. M. (2008). Disturbance of nuclear and cytoplasmic TAR DNA-binding protein (TDP-43) induces disease-like redistribution, sequestration, and aggregate formation. *Journal of Biological Chemistry*, 283(19), 13302-13309. https://doi.org/10.1074/jbc.M800342200
- Wu, J., Cai, Y., Wu, X., Ying, Y., Tai, Y., & He, M. (2021). Transcardiac Perfusion of the Mouse for Brain Tissue Dissection and Fixation. *Bio Protoc*, 11(5), e3988. https://doi.org/10.21769/BioProtoc.3988
- Wu, Z., Yang, H., & Colosi, P. (2010). Effect of genome size on AAV vector packaging. Molecular Therapy, 18(1), 80-86. https://doi.org/10.1038/mt.2009.255

- Xiao, P. J., & Samulski, R. J. (2012). Cytoplasmic trafficking, endosomal escape, and perinuclear accumulation of adeno-associated virus type 2 particles are facilitated by microtubule network. *Journal of Virology*, 86(19), 10462-10473. https://doi.org/10.1128/jvi.00935-12
- Xiao, X., Xiao, W., Li, J., & Samulski, R. J. (1997). A novel 165-base-pair terminal repeat sequence is the sole cis requirement for the adeno-associated virus life cycle. *Journal of Virology*, 71(2), 941-948. https://doi.org/10.1128/jvi.71.2.941-948.1997
- Zampatti, S., Peconi, C., Campopiano, R., Gambardella, S., Caltagirone, C., & Giardina, E. (2022). C9orf72-Related Neurodegenerative Diseases: From Clinical Diagnosis to Therapeutic Strategies. *Frontiers in Aging Neuroscience*, 14, 907122. https://doi.org/10.3389/fnagi.2022.907122
- Zarei, S., Carr, K., Reiley, L., Diaz, K., Guerra, O., Altamirano, P. F., Pagani, W., Lodin, D., Orozco, G., & Chinea, A. (2015). A comprehensive review of amyotrophic lateral sclerosis. *Surgical Neurology International*, 6, 171. https://doi.org/10.4103/2152-7806.169561
- Zhang, H., Zhan, Q., Huang, B., Wang, Y., & Wang, X. (2022). AAV-mediated gene therapy: Advancing cardiovascular disease treatment. *Front Cardiovasc Med*, *9*, 952755. https://doi.org/10.3389/fcvm.2022.952755
- Zhang, Y. J., Gendron, T. F., Ebbert, M. T. W., O'Raw, A. D., Yue, M., Jansen-West, K., Zhang, X., Prudencio, M., Chew, J., Cook, C. N., Daughrity, L. M., Tong, J., Song, Y., Pickles, S. R., Castanedes-Casey, M., Kurti, A., Rademakers, R., Oskarsson, B., Dickson, D. W., . . . Petrucelli, L. (2018). Poly(GR) impairs protein translation and stress granule dynamics in C9orf72-associated frontotemporal dementia and amyotrophic lateral sclerosis. *Nature Medicine*, *24*(8), 1136-1142. https://doi.org/10.1038/s41591-018-0071-1
- Zhang, Y. J., Gendron, T. F., Grima, J. C., Sasaguri, H., Jansen-West, K., Xu, Y. F., Katzman, R. B., Gass, J., Murray, M. E., Shinohara, M., Lin, W. L., Garrett, A., Stankowski, J. N., Daughrity, L., Tong, J., Perkerson, E. A., Yue, M., Chew, J., Castanedes-Casey, M., . . . Petrucelli, L. (2016). C9ORF72 poly(GA) aggregates sequester and impair HR23 and nucleocytoplasmic transport proteins. *Nature Neuroscience*, 19(5), 668-677. https://doi.org/10.1038/nn.4272
- Zhou, Q., Lehmer, C., Michaelsen, M., Mori, K., Alterauge, D., Baumjohann, D., Schludi, M. H., Greiling, J., Farny, D., Flatley, A., Feederle, R., May, S., Schreiber, F., Arzberger, T., Kuhm, C., Klopstock, T., Hermann, A., Haass, C., & Edbauer, D. (2017). Antibodies inhibit transmission and aggregation of C9orf72 poly-GA dipeptide repeat proteins. *EMBO Molecular Medicine*, 9(5), 687-702. https://doi.org/10.15252/emmm.201607054
- Zhou, Q., Mareljic, N., Michaelsen, M., Parhizkar, S., Heindl, S., Nuscher, B., Farny, D., Czuppa, M., Schludi, C., Graf, A., Krebs, S., Blum, H., Feederle, R., Roth, S., Haass, C., Arzberger, T., Liesz, A., & Edbauer, D. (2020). Active poly-GA vaccination prevents microglia activation and motor deficits in a C9orf72 mouse model. EMBO Molecular Medicine, 12(2), e10919. https://doi.org/10.15252/emmm.201910919
- Zu, T., Gibbens, B., Doty, N. S., Gomes-Pereira, M., Huguet, A., Stone, M. D., Margolis, J., Peterson, M., Markowski, T. W., Ingram, M. A., Nan, Z., Forster, C., Low, W. C., Schoser, B., Somia, N. V., Clark, H. B., Schmechel, S., Bitterman, P. B., Gourdon, G., . . . Ranum, L. P. (2011). Non-ATG-initiated translation directed by microsatellite expansions. *Proceedings of the National Academy of Sciences of the United States of America*, 108(1), 260-265. https://doi.org/10.1073/pnas.1013343108
- Zu, T., Guo, S., Bardhi, O., Ryskamp, D. A., Li, J., Khoramian Tusi, S., Engelbrecht, A., Klippel, K., Chakrabarty, P., Nguyen, L., Golde, T. E., Sonenberg, N., & Ranum, L. P.

- W. (2020). Metformin inhibits RAN translation through PKR pathway and mitigates disease in C9orf72 ALS/FTD mice. *Proceedings of the National Academy of Sciences of the United States of America*, 117(31), 18591-18599. https://doi.org/10.1073/pnas.2005748117
- Zu, T., Liu, Y., Bañez-Coronel, M., Reid, T., Pletnikova, O., Lewis, J., Miller, T. M., Harms, M. B., Falchook, A. E., Subramony, S. H., Ostrow, L. W., Rothstein, J. D., Troncoso, J. C., & Ranum, L. P. (2013). RAN proteins and RNA foci from antisense transcripts in C9ORF72 ALS and frontotemporal dementia. *Proceedings of the National Academy of Sciences of the United States of America*, 110(51), E4968-4977. https://doi.org/10.1073/pnas.1315438110

Acknowledgements

This was an incredible journey, which has not always been easy, but it was filled with a lot of amazing moments that have profoundly shaped me both as a researcher and as a person.

I would like to express my deepest gratitude to **Prof. Dieter Edbauer**. Your patience, guidance, and unwavering support, especially during the times I needed it most, have meant the world to me. Above all, you inspired me to explore science beyond the horizons of medical studies. I was particularly motivated by your curiosity and your ability to seamlessly integrate tools like programming into your work. Thank you for being an exceptional mentor.

I am very thankful to **Dr. rer. nat Qihui Zhou**, who supervised me throughout my experiments, teaching me essential techniques in cell culture and the animal facility. Your expertise and support were crucial for this work.

I would like to extend my sincere thanks to **Prof. Sabine Liebscher** and **Prof. Johannes Levin**, who were part of my TAC committee. I truly appreciated your input during our meetings and your support during this journey. I am grateful that you agreed to join my committee, and I am very glad I had the opportunity to benefit from your expertise.

Special thanks go to **Ali Rezaei** and **Daniel Farny** for embodying the spirit of camaraderie and teamwork both in and out of the lab. I'm grateful for your constant and unwavering support in completing this thesis. It's priceless to have such amazing friends.

To Katherine LaClair, Meike Michaelsen, Mareike Czuppa, Henrik Riemenschneider, Bahram Khosravi, and Carina Schludi, thank you for being not only wonderful colleagues but also great friends. Your willingness to help whenever I needed it made a world of difference.

A heartfelt thanks goes to **Sabine Odoy**, **Marcel Matt**, animal caretakers and everyone else who keep the lab alive and thriving from the logistical side. Your hard work behind the scenes is truly the backbone of our research.

I also want to thank **Prof. Christian Haass** and the entire **DZNE team** for fostering such a welcoming and collaborative environment. Your dedication to creating a space where passionate scientists can thrive is truly remarkable. I especially appreciated the effort you put into organizing social events like Christmas parties and Oktoberfest, which brought us all closer together.

Finally, to my family and friends: thank you for standing by me throughout this time. Your encouragement and love have been my greatest source of strength.



Dekanat Medizinische Fakultät Promotionsbüro



Cygan, Mikolaj Surname, first name I hereby declare, that the submitted thesis entitled: AAV-Mediated Anti-GA Antibody Therapy in C9orf72 ALS/FTD mouse models is my own work. I have only used the sources indicated and have not made unauthorised use of services of a third party. Where the work of others has been quoted or reproduced, the source is always given. I further declare that the dissertation presented here has not been submitted in the same or similar form to any other institution for the purpose of obtaining an academic degree. Munich, 08.10.2025 Mikolaj Cygan Place, Date Signature doctoral candidate

Affidavit Date: 27.11.2024



Dekanat Medizinische Fakultät Promotionsbüro



Confirmation of congruency between printed and electronic version of the doctoral thesis

_
_

Congruency of submitted versions

Date: 09.12.2024

Publications

Congenic expression of poly-GA but not poly-PR in mice triggers selective neuron loss and interferon responses found in C9orf72 ALS.

Published as:

LaClair, K. D., Zhou, Q., Michaelsen, M., Wefers, B., Brill, M. S., Janjic, A., Rathkolb, B., Farny, D., Cygan, M., de Angelis, M. H., Wurst, W., Neumann, M., Enard, W., Misgeld, T., Arzberger, T., & Edbauer, D. (2020). Congenic expression of poly-GA but not poly-PR in mice triggers selective neuron loss and interferon responses found in C9orf72 ALS. *Acta neuropathologica*, *140*(2), 121–142. https://doi.org/10.1007/s00401-020-02176-0